LARS Information Note 111872

Conjugate Point Determination for Multitemporal Data Overlay

by
R. A. Emmert and
C. D. McGillem

The Laboratory for Applications of Remote Sensing

Purdue University, West Lafayette, Indiana

1973

Information Note 111872

CONJUGATE POINT DETERMINATION FOR MULTITEMPORAL DATA OVERLAY

R. A. Emmert
C. D. McGillem

TR-EE 73-5
December, 1972

Published by the
Laboratory for Applications of Remote Sensing (LARS)
and the
School of Electrical Engineering
Purdue University
Lafayette, Indiana 47907

This work was sponsored by the National Aeronautics and Space Administration (NASA) under Grant No. NGL 15-005-112.

TABLE OF CONTENTS

LIST OF TABLES

LIST OF FIGURES

ABSTRACT

The machine processing of spatially variant multitemporal data such as imagery obtained at different times requires that these data be in geometrical registration such that the analysis processor may obtain the datum for a specified ground resolution element in each of the sets of imagery being utilized for analysis.

Misregistration between corresponding subsets of imagery contains both a displacement and a geometrical distortion component, and the affine transformation is postulated to characterize this misregistration between data subsets. Search techniques utilizing the moduli of the Fourier Transforms of these data are developed for estimating the coefficients of geometrical distortion components of this model.

Following the correction of these distortion components, the displacement is located by the crosscorrelation of a template obtained from one set of data, termed the reference, with the second, or background data. This template, derived for the optimum discrimination of the reference data embedded in the background, is determined by the solution of a system of equations involving the reference data and the covariance matrix of these data.

The derivation of the optimum filter includes constraints such that the maximum filter output, corresponding to the correct superposition of the reference template on the background data, is unity and the energy in the filter is finite. The filter obtained in this development is linear although it may involve a parameter requiring the solution of a nonlinear equation.

The performance of the crosscorrelation algorithm is evaluated using ideal data obtained by convolving an array of computer generated random numbers with a two-dimensional lowpass filter having a specified impulse response. The results obtained from these data generally substantiate the conclusions drawn from the analysis of this algorithm. The correlator output is then obtained for noise free and distortionless line scanner data. In these data the reference is selected as a subimage of the background data, and the data are selected to typify line scanner imagery. Multitemporal data are processed with the algorithms developed for the noise-free data to evaluate the applicability of this filter to the conjugate point problem.

It is demonstrated that the crosscorrelation of the template derived from the reference data will not yield useful results unless the geometrical correction of the data is implemented. The Fourier transform search techniques are used to estimate the distortion model coefficients, and a bilinear interpolation algorithm is utilized to correct the imagery. Results of the processor output using the corrected data are given. It is shown that the optimum filter yields a more discriminable peak of the correlation surface at the correct superposition of the reference template on the background than does the

filter chosen as a subimage of the reference data itself.

CHAPTER 1

INTRODUCTION

1.0 Processing of Remotely Sensed Data

The large scale application of remote sensing techniques to the monitoring and evaluation of the environment is rapidly becoming a reality. This realization is due to many technical and scientific advances resulting in increasing availability of multispectral photometric and radiometric instruments, aircraft and satellite instrument platforms and large data processing systems [28,42]. The data obtained by these multispectral instruments are images representing the spatial, spectral, and temporal characteristics of the area under investigation in contiguous wavelength intervals throughout the visible region of the electromagnetic spectrum as well as selected wavelength bands in the infrared and microwave portions of this spectrum.

A block diagram of a multispectral remote sensing instrumentation system is illustrated in Fig. 1-1. To analyze the large quantity of data made available by such a source, statistical pattern recognition algorithms [28] have been developed, and such pattern recognition procedures are illustrated in Fig. 1-2. The feature extractor selects from the pattern those attributes which "separate" a particular pattern as well as possible from the set of all other patterns. The output of the extractor is a k-tuple and is usually of lower dimension

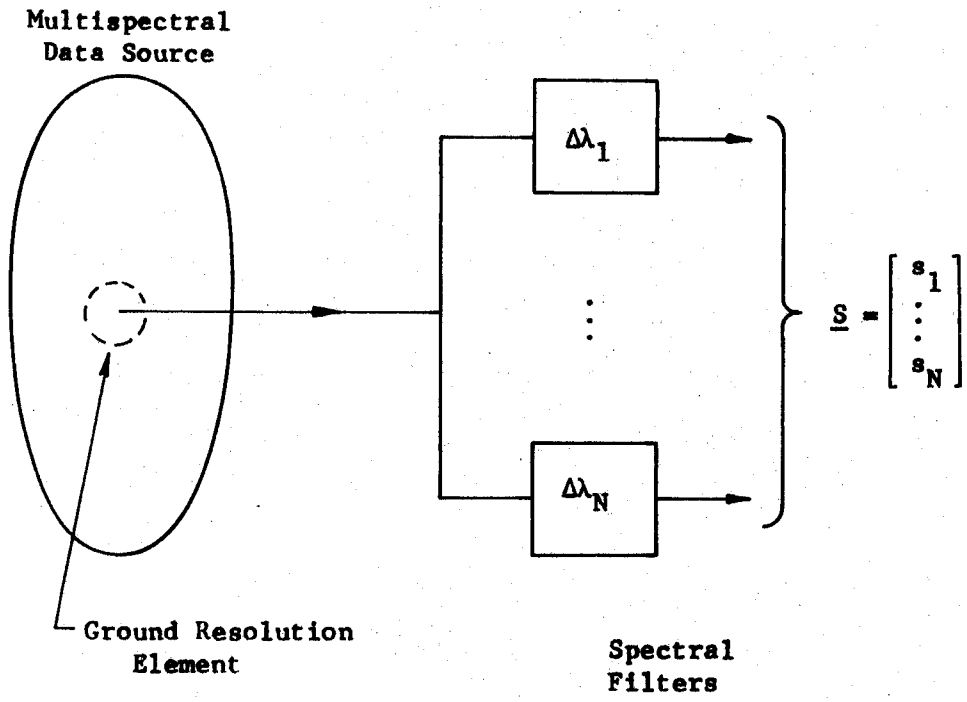

Figure 1-1 Block Diagram of a Multispectral Data System

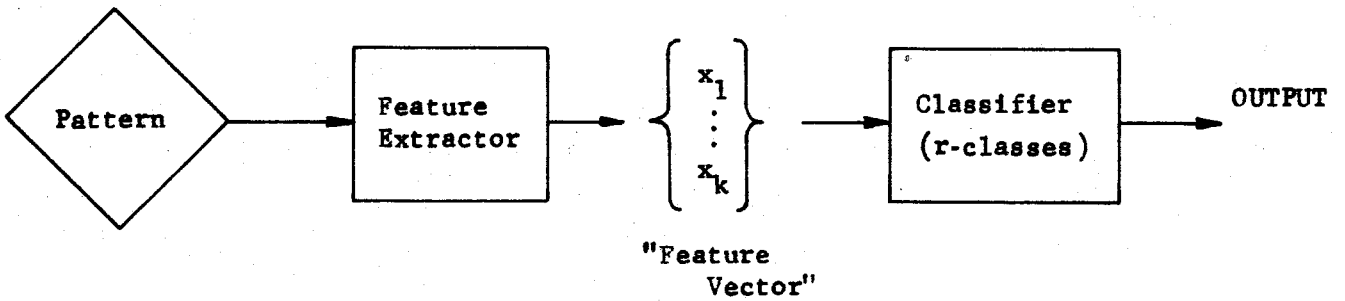

$1 \leq k \leq N$, N = number of available channels

Figure 1-2 Block Diagram of a Statistical Pattern Classifier

than the pattern vector. The pattern classifier then assigns the input vector to one of r-classes based on some predetermined decision rule.

An implicit assumption in such processors is that any one input vector is derived from a common ground resolution element. This requirement is usually satisfied if all the elements of the n-tuple are taken at time $t = t_1$ with an instrument employing a single optical path and negligible differential optical and electrical delays are introduced into the channels following the dispersion of the input optical signal.

There has been recent interest in extending the pattern classifier input vector to include a multitemporal variation. However, such data sets are generally misregistered because after obtaining the first data set, the instrument platform cannot be made to follow the same path to within a resolution element of the instrumentation system. The misregistration is a dynamic quantity and can be considered quasi-static only over that length of data defined by the dynamics of the instrument platform and the conditions of the atmosphere in the case of aircraft platforms. Therefore, for multitemporal data, a pre-processing operation must be implemented for removing this misregistration before the data analysis system can address the same spatial data element in each of the data sets being used for analysis. This requirement for addressing a data element in the various data sets is illustrated in Fig. 1-3.

1.1 Multitemporal Data Registration

A multitemporal data registration system, shown in Fig. 1-4, can

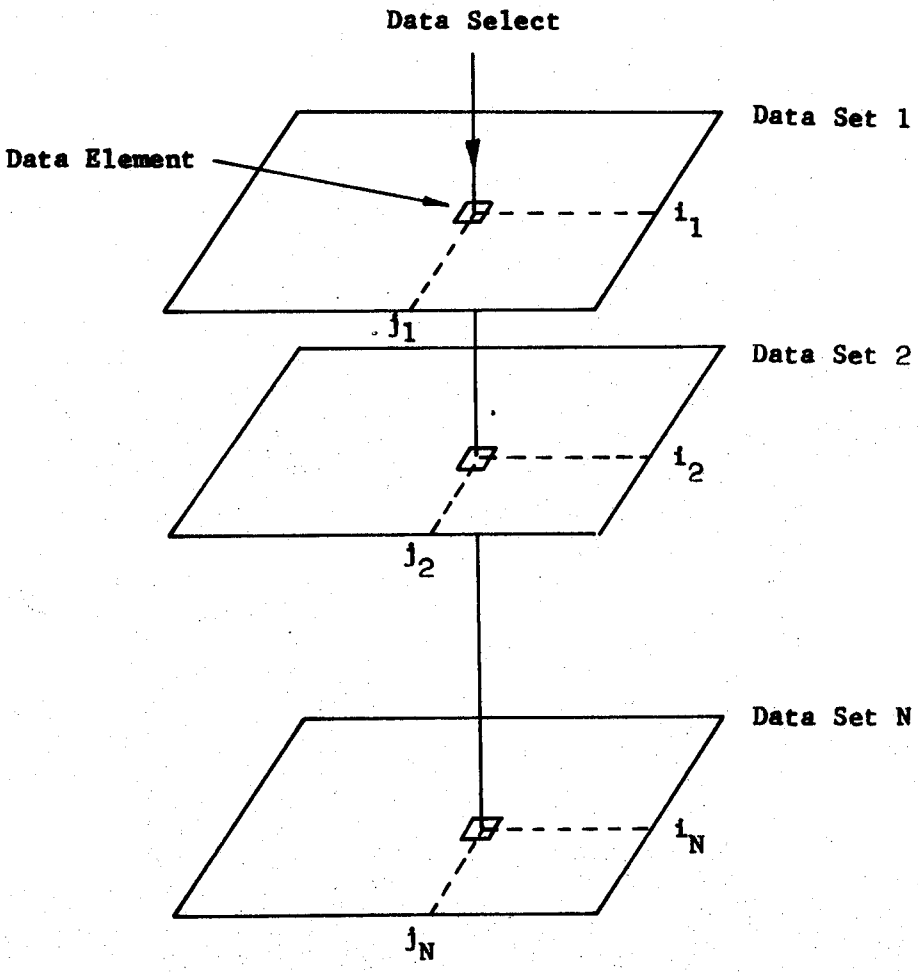

Figure 1-3 Multi-Image Registration Requirement

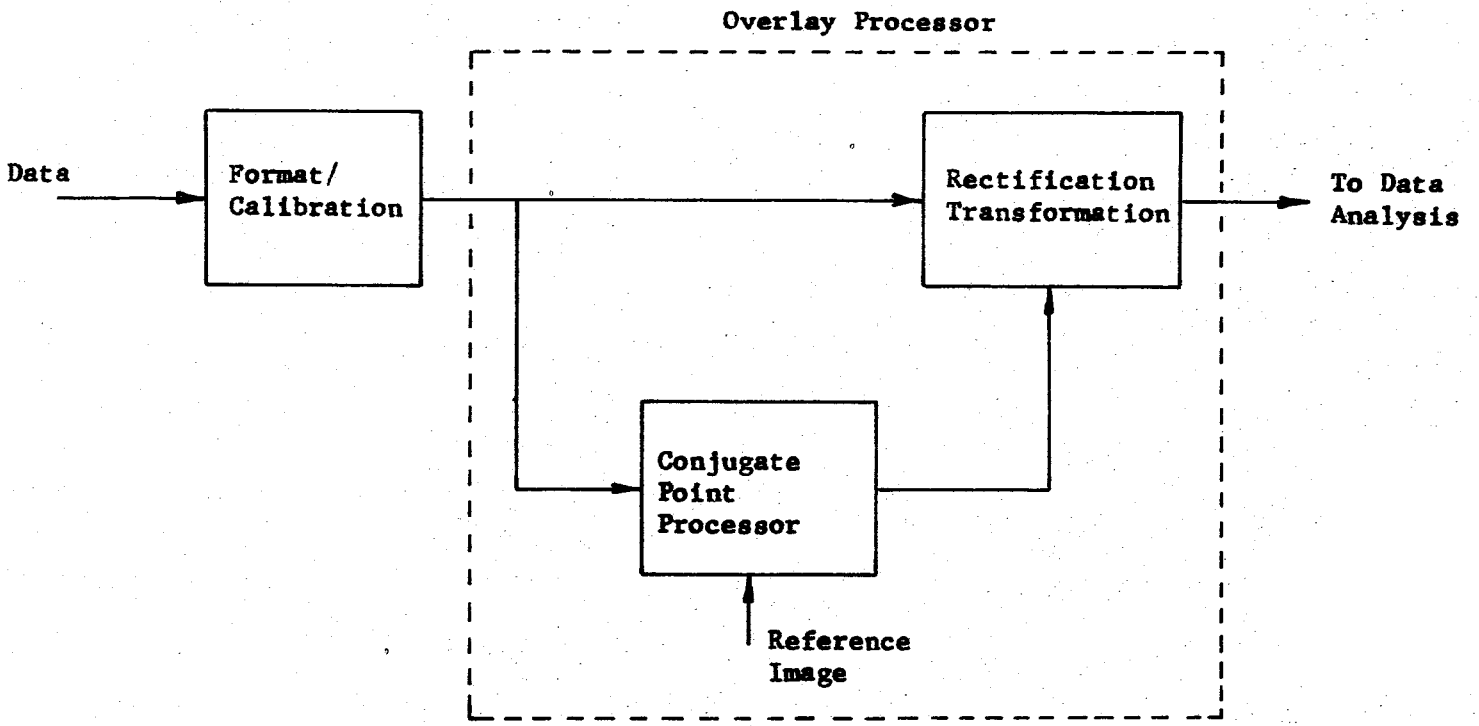

Figure 1-4 Block Diagram of Data Preprocessing

be divided into two relatively distinct parts with this dichotomy being a functional division. The ultimate objective of an overlay system, given two sets of imagery A and B, is to process set B such that its image under the transformation T is in geometrical registration with set A. Thus the first part of the overlay problem is given enough information to define the transformation T, how can the mapping be efficiently implemented for the rectification of set B under the constraints of computer memory size and data through-put requirements? This correction of a misregistered data set is illustrated in Fig. 1-5.

The solution of this part of the problem usually involves the division of the total data set into smaller images, or blocks, which are more readily handled. A transformation is derived for each of these blocks and the rectification is carried out. If it is required to have continuity of the image across the boundaries of the blocks, this condition can be approximated by making each block sufficiently small such that the differential scale factor or rotation will not alter the block size more than some fractional part of the size of an image resolution element. The alternative procedure of formulating the problem such that the blocks of set B under the transformation T are constrained to be continuous across the boundaries may be possible.

The second part of the data overlay problem is the task of determining the transformation T relating any two blocks of data. Assuming that a model has been determined for T, the parameters of this model must be estimated from the data since the misregistration is a pairwise property of the data sets and is implicitly defined

$$T: \quad y_i = \sum_{j=0}^{N-1} \sum_{k=0}^{N-1} a_{jk}^{i} \, x_1^j \, x_2^k \quad , \quad i = 1,2.$$

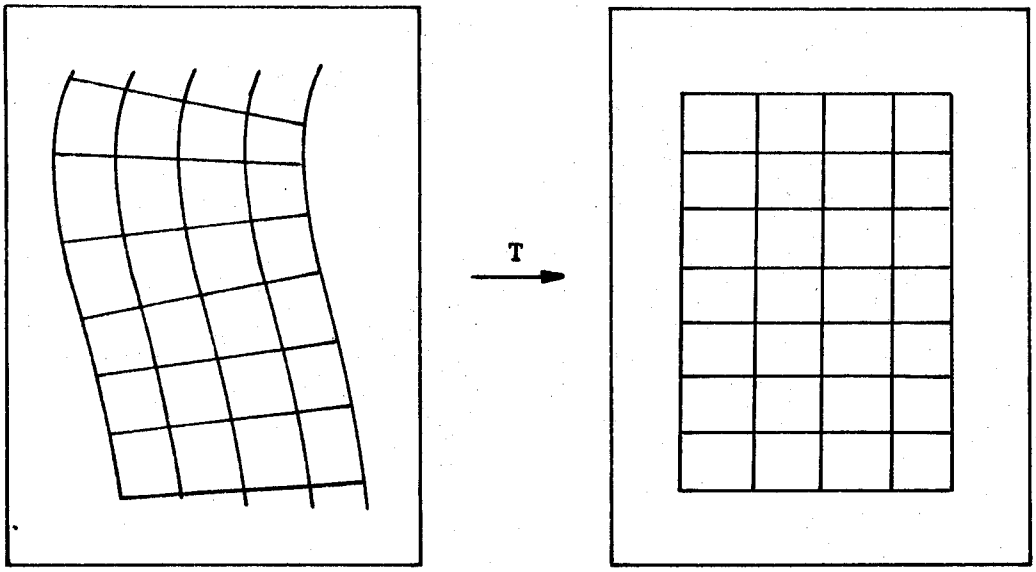

Distorted Image

Rectified Image

Figure 1-5 Rectification of Distorted Imagery

in these data.

For the unconstrained problem, a commonly used model for representing the misregistration between data blocks is the two-dimensional polynomial

$$y = \sum_{j=0}^{N-1} \sum_{k=0}^{N-1} a_{jk}^{i} x_1^j x_2^k \qquad i=1,2,. \tag{1-1}$$

The principal advantage of this polynomial model is that equation (1-1) is linear in the coefficients a_{jk}. If a set of corresponding, or "conjugate",points is known for each of the blocks constituting a set of imagery, the coefficients of the transformation for each of these blocks are readily obtained by use of a least-squares procedure. Thus the requirement arises for determining conjugate points in sets of multitemporal imagery.

Signal processing techniques used to determine conjugate points almost always use correlation between data sub-blocks as a measure of the similarity of these data subsets. To illustrate this processing, assume the data to be a discrete set obtained by sampling a continuous scene on a rectangular grid and the reference data subset $\underline{S}_r \subset A$ to be selected from data set A. A background data sub-block is chosen from data set B and the following inclusion relation is assumed

$$\underline{S}_r \overset{T}{\rightarrow} \underline{S}_r' \subset \underline{S}_b \tag{1-2}$$

where T is the transformation relating the data blocks.

The correlation surface

$$C(u,v) = \sum_i \sum_j s_r(i,j)\, s_b(u+i,\, v+j), \quad s_r \in \underline{S}_r,\ s_b \in \underline{S}_b \tag{1-3}$$

is computed for the set of indices (i,j), and the peak of this surface is assumed to be the location of the correct superposition of $\underline{S}_r$ on $\underline{S}_b$. The conjugate point pair is then taken to be the location of $\underline{S}_r$ and the corresponding subset of $\underline{S}_b$ in their respective coordinate systems for this maximum of the correlation surface.

1.2 Objective of this Investigation

This investigation is addressed to the problem of conjugate point determination in multitemporal imagery in which the task is viewed as a problem in signal theory. With conjugate points defined as in section 1.1, this problem can then be phrased as "given a reference set $\underline{S}_r$ from data set A, what signal processing operations will optimally discriminate the corresponding subimage $\underline{S}_r'$ in data set B?" This problem is treated in the sequel with consideration being given to both the noise and misregistration which exist between the data sets.

1.3 Previous Investigations

The implementation of an image registration system on a general purpose computer is a relatively new field although the roots of this task extend into antiquity. Only recently has there appeared in the literature any significant amount of work on the image registration problem. The work which has appeared as well as the experimental effort in this study have utilized digital computers.

In measuring the correlation surface, Anuta [4] used the normalized correlation coefficient, computing quanity

$$R(u,v) = \frac{\sum_{i=1}^{M}\sum_{j=1}^{N} s_b(i+u, j+v)\, s_r(i,j)}{\left[\sum_{i=1}^{M}\sum_{j=1}^{N} s_b^2(i+u, j+v) \cdot SQ\right]^{1/2}} \qquad (1\text{-}4)$$

where

$$SQ = \sum_{i=1}^{M}\sum_{j=1}^{N} s_r^2(i,j)$$

with $s_r \in \underline{S}_r$ and $s_b \in \underline{S}_b$. In a later paper Anuta [5] utilized the Fast Fourier Transform algorithm for increasing the efficiency in evaluating equation (1-4).

Rather than use the normalized correlation coefficient as a measure of image similarity, Barnea and Silverman [7] used an absolute difference metric for their similarity algorithm

$$e = \sum_{i}\sum_{j} \left| s_r(i,j) - s_b(i+u, j+v) \right| \qquad (1\text{-}5)$$

The rational for this algorithm is that if the reference data $\underline{S}_r$ are not near the correct superposition on $\underline{S}_b$, the error will increase rapidly and a threshold can be established such that if this boundary is exceeded, the checking for similarity for this observation is terminated. It is suggested that the average number of operations for testing for the correct superposition can be significantly reduced compared to the correlation algorithm.

Arcese *et al*. [6] developed a filter which maximized the ratio of the square of the filter output at the correct juxtaposition of $\underline{S}_r$ on $\underline{S}_b$. Their filter was developed for the noise free case and

with no constraints on the filter characteristics. In addition the data were assumed to be from a process having a simple exponential covariance function.

The most complete system for the overlay of large data sets was described by Lillestrand [46]. This work incorporates some of the ideas that were independently discovered during this investigation, particularly in the use of pre-processing to estimate and reduce the geometric distortion so as to increase the similarity of corresponding data sets. Hall et al. [33] discuss a method of registering cloud photographs. Their procedure employs a crosscorrelation method similar to that of Anuta for locating corresponding geographical features in the two data sets.

1.4 Outline of Investigation

The misregistration of the imagery is discussed in Chapter 2. It is observed that the geometrical components of the misregistration between these data can be considered to have been introduced by a spatially variant operator. In view of the analytical difficulties in formulating a general solution to this problem, a sequential method is proposed in which the geometrical distortion components are estimated and removed prior to determining the displacement components. It is postulated that the affine model adequately represents, for the purposes of this investigations, the misregistration between data subblocks; an algorithm utilizing the modulus of the two-dimensional Fourier transform of these data is developed for estimating the geometrical components of this model.

The optimum filter for discriminating the data set $\underline{S}_T$ embedded in the background data $\underline{S}_b$ is treated in Chapter 3. This filter is derived under constraints on both the filter output and the filter energy. Results obtained in this chapter include expressions for the filter for both noise free inputs and for inputs assumed to contain additive noise with statistical characteristics given by the covariance matrix $\underline{K}_n$.

In Chapter 4 experimental results are presented using both ideal data obtained by convolving computer generated random numbers with lowpass filters having known impulse responses and imagery obtained with a line scanning instrumentation system. Plots of the correlator outputs for various input data sets of interest are given, and the processing gains of the correlator are given for both ideal and multitemporal line scanner data.

A summary of the results obtained in this investigation is presented in Chapter 5.

CHAPTER 2

DATA MISREGISTRATION

2.0 Introduction

Misregistration of data taken at different times occurs when, after having obtained the first set of data, it is not possible to control the positioning of the instrument platform such that it will repeat the previous path to within the dimensions of the spatial resolution of the instrumentation system. For certain kinds of processing of multitemporal imagery, it is necessary to implement a data pre-processing operation such that the data are placed into registration. Following such an operation on the data, the computer or other processor is able to address (or obtain) the data from a common ground resolution element in the several data channels being used for analysis.

It is the purpose of this chapter to develop an appropriate model of the misregistration process and to investigate some methods of evaluating parameters of such a model. The first topics discussed are the characterization of the data, and definitions and nomenclature that are used subsequently. Models for regional misregistration are then discussed, and the affine transformation is proposed as a suitable representation of the misregistration process. Processors for estimating the misregistration are introduced and it is concluded

that for the data of interest in this study, the geometrical distortion and displacement parameters can be determined sequentially. The chapter concludes with the development of Fourier transform methods for estimating the coefficients of the affine model which represent the geometrical distortion components of the misregistration between an image pair.

2.1 Data Source

The data source $s(\underline{x})$ is assumed to be a real, stationary, wave-number limited, two-dimensional random field. Each realization of this process, is shown in Fig. 1-1, is obtained by impulse sampling of $s(\underline{x})$ on a bounded rectangular region R. Thus the sampled image is

$$\underline{S} = \{s_{ij}\} = s(\underline{x}) \cdot {}^{2}\pi(\underline{x}) \tag{2-1}$$

where ${}^{2}\pi$ is the two-dimensional finite sequence of impulses spaced at unit distance

$${}^{2}\pi(\underline{x}) = \sum_{n_1=-\infty}^{\infty} \sum_{n_2=-\infty}^{\infty} \delta(x_1-n_1,\ x_2-n_2)\ \text{rect}\left(\frac{x_1-p_o}{R_1}\right)\ \text{rect}\left(\frac{x_2-q_o}{R_2}\right) \tag{2-2}$$

with $\text{rect}\left(\frac{r}{R}\right) = \begin{cases} 1, & |r| \le R \\ 0, & \text{otherwise} \end{cases}$

and (p_o, q_o) is the center of the data aperture.

The set $\underline{S} = \left\{ s_{ij} : \ 1 \le i \le p,\ 1 \le j \le q \right\}$ may be represented by the column vector

$$\underline{S} = \begin{bmatrix} \underline{s}_1 \\ \vdots \\ \underline{s}_p \end{bmatrix} \tag{2-3a}$$

where the elements $\underline{s}_i$ are the column vectors

$$\underline{s}_i = \begin{bmatrix} s_{i1} \\ \vdots \\ s_{iq} \end{bmatrix} \tag{2-3b}$$

These data are also quantized; for each sample $s_{ij} \in \underline{S}$, the value is $s_{ij} = a_k$, $0 \leq k \leq K-1$ where the a_i are the quantization levels and K is the total number of levels provided by the quantizer.

Each sampled image $\underline{S}$ obtained from $s(\underline{x})$ is called a quantized picture function, or synonymously a digital picture function. Each picture function $\underline{S}$ is an element in the pq-dimensional Euclidean space, and the distance between any two digital picture functions $\underline{P}$ and $\underline{Q}$ is then

$$\begin{aligned} d(p,q) &= \|\underline{P} - \underline{Q}\| = (\underline{P},\underline{Q})^{1/2} \\ &= \left[(\underline{P} - \underline{Q})^T (\underline{P} - \underline{Q}) \right]^{1/2} \\ &= \left\{ \text{tr} \left[(\underline{P} - \underline{Q}) (\underline{P} - \underline{Q})^T \right] \right\}^{1/2} \end{aligned} \tag{2-4}$$

where tr $(\cdot)$ is the trace of the matrix. It should be noted that once a digital picture is obtained, it can be regarded as a known deterministic, discrete, two-dimensional signal. However, the statistical properties of this picture, such as variance or bandwidth, are in fact related to these same properties of $s(\underline{x})$.

Considering now the content of the picture function, an "object" is a subset of $\underline{S}$ which represents some identifiable physical entity in the object plane. The distance between two objects in a picture function is defined as the sum of their row and column distances.

Thus for two objects located at (x_1, x_2) and (y_1, y_2) respectively

$$\Delta_{row} = |x_2 - y_2| \tag{2-5a}$$

$$\Delta_{col} = |x_1 - y_1| \tag{2-5b}$$

and

$$d(\underline{x}, \underline{y}) = \Delta_{row} + \Delta_{col} \tag{2-6}$$

A "scene" is composed of a collection of objects together with their mutual geometrical relationships; the term scene is synonymous with the term imagery if the data are assumed continuous, whereas it is synonymous with digital picture function when the data are in a discrete format.

Geometrical distortion between two scenes $r(\underline{x})$ and $s(\underline{x})$ is defined to be the mapping D of one scene onto the other. Such a mapping can be expressed as

$$r(\underline{x}) = D\,[s(\underline{x})] = s[\xi(\underline{x}), \eta(\underline{x})] \tag{2-7}$$

where ξ, η are real valued functions and this mapping is one-to-one and onto. Distortion manifests itself in the differences in the distances between corresponding objects in the two digital pictures $\underline{R}$, $\underline{S}$, where

$$\underline{R} = r(\underline{x}) \cdot {}^{2}\pi(\underline{x}) \tag{2-8a}$$

$$\underline{S} = s(\underline{x}) \cdot {}^{2}\pi(\underline{x}) \tag{2-8b}$$

Translation is defined as

$$r(\underline{x}) = T[s(\underline{x})] = s(x_1 + t_1, x_2 + t_2) \tag{2-9}$$

Misregistration in general can be expressed by the product of the operators D and T as

$$r(\underline{x}) = (TD)\ s(\underline{x}) = T\{D[s(\underline{x})]\} \tag{2-10}$$

which for digital picture functions results in

$$r(\underline{x}) \cdot {}^{2}\pi(\underline{x}) = \{TD[s(\underline{x})]\} \cdot {}^{2}\pi(\underline{x}) \tag{2-11}$$

In the sequel the discussion often requires a qualification as to the size of the data set being considered. To this end the imprecisely defined terms local, global and regional will be used. The term local is used to indicate that the data set consists of an element s_{ij} together with those immediately surrounding elements $\{s_{kl}\}$ such that

$$d(s_{ij}, s_{kl}) = |i - k| + |j - \ell| \leq N \tag{2-12}$$

with N as integer.

The term global is used in the sense that the entire data set is being considered. Between these extremes, the term regional is used to define a data set for which one choice of distortion model coefficients serves to adequately represent the misregistration between the data and its conjugate image. The size of a region is very dependent on both the assumed misregistration model and on the data itself.

2.2 A Regional Misregistration Model

Remotely sensed images typical of those obtained by a line scanning instrument are shown in Fig. 2-1. As illustrated by this figure, seldom is the misregistration between two data sets characterized solely by the displacement of one image with respect

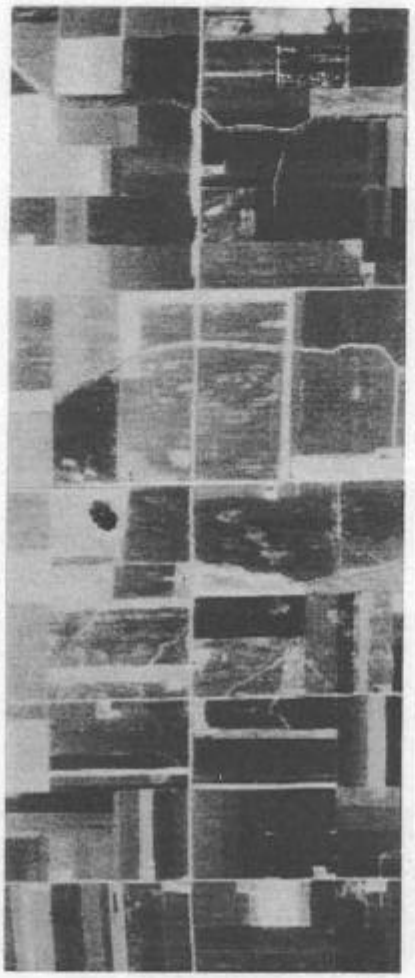

Example A

Example B

Figure 2-1 Multitemporal Imagery Exhibiting Misregistration

to the other. Rather, a geometrical component, as defined by equation (2-7) is also present. A commonly used model for characterizing this misregistration is the two-dimensional polynomial

$$y_i = \sum_{j=0}^{N-1} \sum_{k=0}^{N-1} {}^{i}a_{jk}\, x_1^j\, x_2^k, \quad i=1,2 \tag{2-13}$$

where $\underline{x}$ and $\underline{y}$ are respectively the coordinate systems of the reference and background data sets.

The utility of the polynomial model lies in the linearity of equation (2-13) as a function of the coefficients a_{jk}. Thus, this model is useful in least-squares procedures where a set of corresponding image points is given and an equation of a given order which best relates these points is desired. Table 2-1 lists several polynomials obtained from equation (2-13) for degree N-1 less than or equal to three. Also given is the number of coefficients ${}^{i}a_{jk}$, i = 1,2 which must be specified for a polynomial of a given degree. It is evident that the number of coefficients required for a model increases rapidly with the degree of the polynomial.

As a function of the coordinate variables $\underline{x}$, equation (2-13) is linear only if the coefficients ${}^{i}a_{11} \neq 0$, with i = 1,2. The terms ${}^{1}a_{00}$ and ${}^{2}a_{00}$ represent the displacement of the origins of the two coordinate systems $\underline{x}$ and $\underline{y}$. This nonlinearity is removable by the coordinate translation

$$y_i = x_i - {}^{i}a_{00}, \quad i = 1,2 \tag{2-14}$$

However, the ${}^{i}a_{00}$ are unknown and are the quantities of ultimate interest. For all indices $j,k \geq 2$, equation (2-13) describes a

Table 2-1. No. of Parameters Required for Two-Dimensional Polynomial Misregistration Models.

Common Name	Degree N-1	No. Parameters Required to Determine Model
displacement	0	2
linear	1	4
affine	1	6
projection	2	8
quadratic	2	12
cubic	3	20

nonlinear transformation.

The data of interest in this study are obtained using a mechanical line scanning instrument mounted in an aircraft and operated at an altitude of approximately 5000 feet. As illustrated in Fig. 2.2, this imagery is obtained by recording the scene radiance from an effective ground resolution element as this resolution element is moved along an approximately linear locus by the rotation of a mirror within the instrument. Adjacent scan lines are spaced by the motion of the aircraft, and the angle α between the direction of the scan lines and the aircraft ground track is

$$\alpha = \frac{\pi}{2} + \gamma \tag{2-15}$$

where γ is the crab angle of the aircraft with respect to the ground track.

In this study attention is directed toward the misregistration of subimages of data, termed regions, which are used for determining geometrically corresponding points in the two data sets. The size of a region ranges between 32 x 32 and 128 x 128 picture elements. With data sets of this size and with any changes in the aircraft attitude necessarily limited by its dynamics, it is assumed that each region of data consists of a sequence of equally spaced, linear scans of the scene. Each scan line is at an angle

$$\alpha_o = \frac{\pi}{2} + \gamma_o \tag{2-16}$$

with respect to the aircraft ground track and the ground track has the angle β with respect to a pre-assigned coordinate system. These quantities are illustrated in Fig. 2-3.

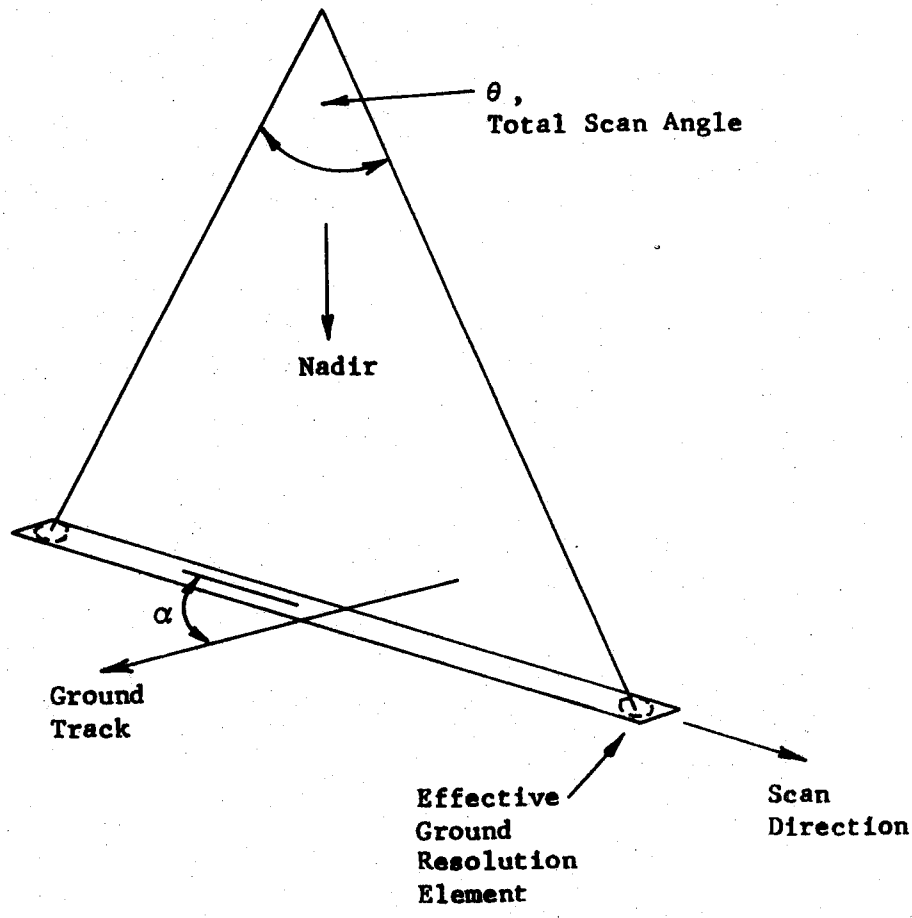

Figure 2-2 Line Scanning Geometry

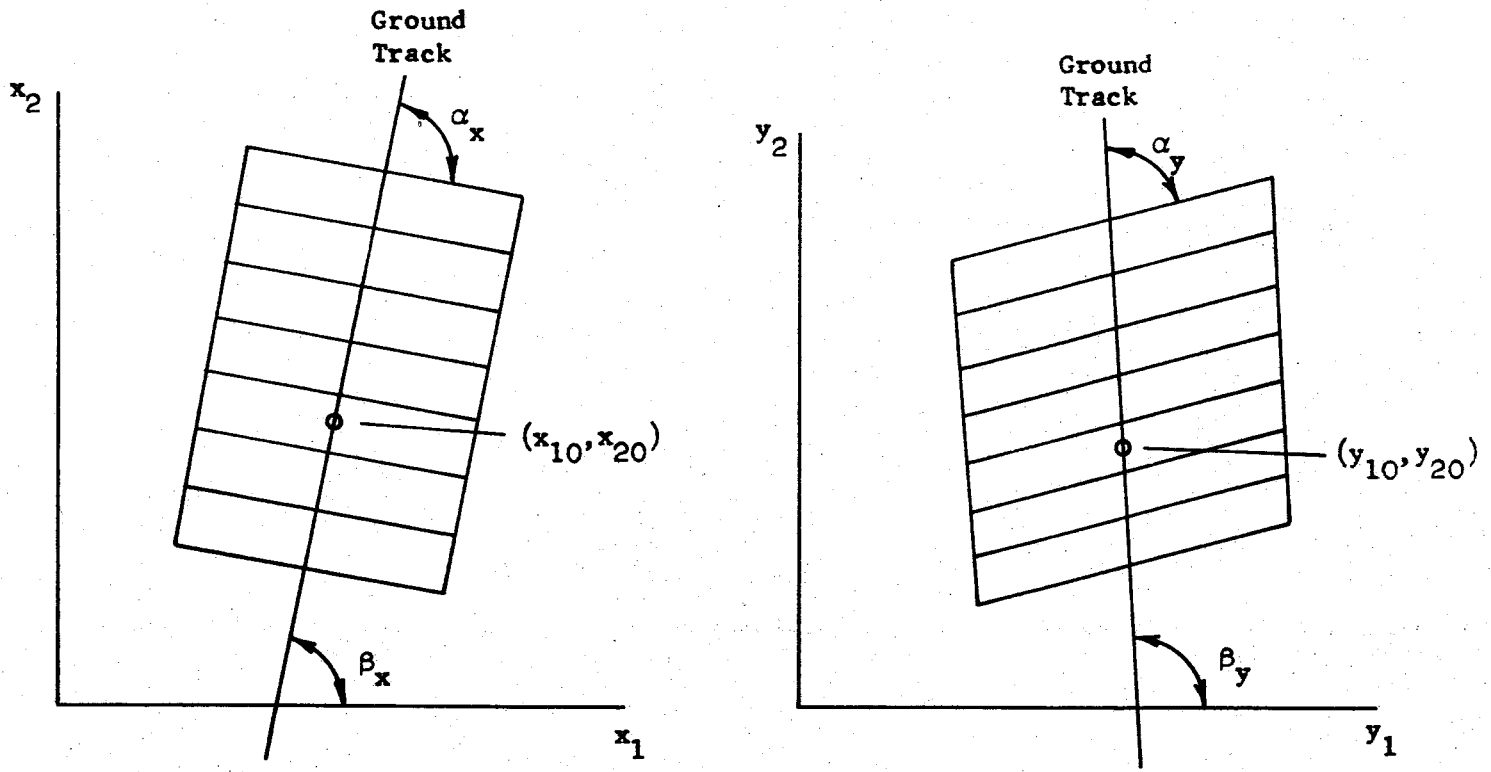

Figure 2-3 Misregistration Between Data Regions

It is observed that the regional misregistration then has the following four components:

(1) scale

(2) rotation

(3) skew

(4) displacement.

These misregistration components are assumed to be characterized by the affine transformation

$$\underline{y} = \underline{A}\,\underline{x} + \underline{t} = \underline{B}\,\underline{x} \tag{2-17}$$

where

$$\underline{y} = \begin{bmatrix} y_1 \\ y_2 \end{bmatrix}, \quad \underline{x} = \begin{bmatrix} x_1 \\ x_2 \end{bmatrix}, \quad \underline{t} = \begin{bmatrix} t_1 \\ t_2 \end{bmatrix}$$

and

$$\underline{A} = \begin{bmatrix} a_{11} & a_{12} \\ a_{21} & a_{22} \end{bmatrix}$$

is a nonsingular matrix characterizing the geometrical components of the misregistration. The quantities are illustrated in Fig. 2-3, where $\underline{x}$ and $\underline{y}$ are the coordinate systems and

$$\underline{t} = \begin{bmatrix} x_{10} - y_{10} \\ x_{20} - y_{20} \end{bmatrix} \tag{2-18}$$

is the displacement of some known point in each data set.

It is illustrative to examine the distortion matrix $\underline{A}$ in detail, identifying those coefficients which reflect the various distortions. For scaling differences along directions parallel to the coordinate axes, the distortion matrix is

$$\underline{A} = \begin{bmatrix} a_{11} & 0 \\ 0 & a_{22} \end{bmatrix} \tag{2-19}$$

where the a_{ii} are the scaling coefficients. For rotation, $\underline{A}$ becomes the orthogonal matrix

$$\underline{A} = \begin{bmatrix} \cos\beta & \sin\beta \\ -\sin\beta & \cos\beta \end{bmatrix} \tag{2-20}$$

where

$$\beta = \beta_1 = \beta_2$$

is the difference in angular orientation of the ground tracks of each data set with respect to its coordinate system.

Skew distortion is introduced by a distortion matrix of the form

$$\underline{A} = \begin{bmatrix} 1 & 1 \\ a_{21} & 1 \end{bmatrix} \tag{2-21}$$

and it is readily verified that the angle α, defined by equation (2-16a) is

$$\alpha = \alpha_1 - \alpha_2 = \tan^{-1}(a_{21}) \tag{2-22}$$

The distortion matrix $\underline{A}$ is some combination of these components distortions. The necessity to determine the elements of $\underline{A}$ from the two regional data sets and a procedure for accomplishing this task for certain classes of data are discussed in the subsequent sections.

The significance of the affine model assumption is that the misregistration can be interpreted as consisting of two components; the first is the displacement of corresponding regions and the second is the characterization of the geometrical distortion by a linear model. It will be established in the sequel that for certain classes of data and under very reasonable assumptions, Fourier transform methods may be used to separate these two misregistration components and straightforward search techniques are available for estimating these distortion parameters in the spatial frequency domain.

2.3 Misregistration Processor

The function of the misregistration processor is to identify corresponding points in the two sets of imagery being processed. Since these data are ordered by a Cartesian coordinate system, this identification requires the determination of the translational component $\underline{t}$ of the assumed misregistration model.

The general problem of conjugate point identification is illustrated by the block diagram of Fig. 2-4. The operator $\underline{D}$ introduces the misregistration; the noise $\underline{N}$ is assumed to be additive, independent of $\underline{S}$ and with a constant power spectral density. The filter $\underline{H}$ is to be determined such that with the reference data set $\underline{S}_r$ selected from $\underline{S}$, the filter output when $\underline{S}_r$ overlays its conjugate data set $\underline{S}_r'$ in $\underline{S}_b$ is maximally discriminable from the outputs at all other

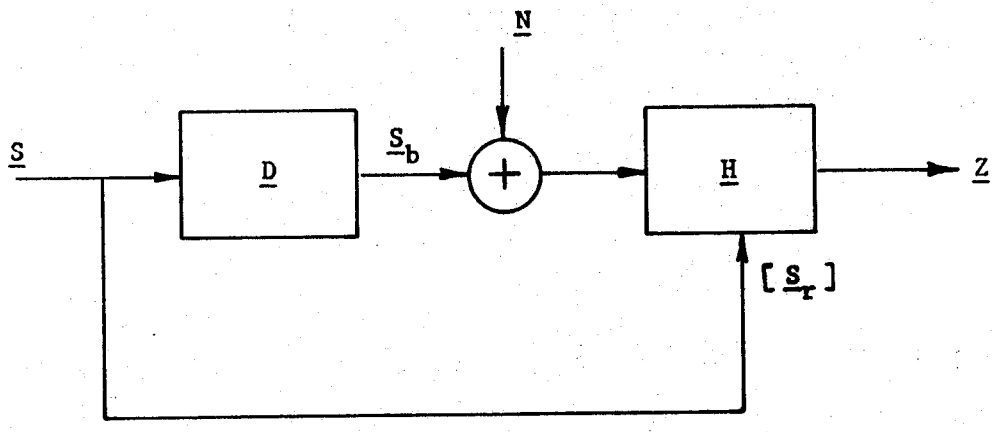

Figure 2-4 Block Diagram of a General Misregistration Processor

spatial juxtapositions of $\underline{S}_r$ on $\underline{S}_b$.

An interesting aspect of this problem is developed by examining the operator $\underline{D}$. For this operator to be spatially invariant it must have the property of commuting with the translation operator T [56]. Assuming continuous operators on $f(\underline{x})$

$$D[T\, f(\underline{x})] = T\,[D\, f(\underline{x})] \tag{2-23}$$

where T is the translation operator

$$T[f(\underline{x})] = f(x_1 + t_1,\ x_2 + t_2) \tag{2-24}$$

The operator D induces the mapping

$$D[f(\underline{x})] = f[\xi(\underline{x}),\ \eta(\underline{x})] \tag{2-25}$$

where ξ, η are real and the mapping is one-to-one and onto. Applying the criterion of equation (2-22) to the scene $s(\underline{x})$ gives

$$D\{T[s(\underline{x})]\} = s[\xi(\underline{x} - \underline{t}),\ \eta(\underline{x} - \underline{t})] \tag{2-26}$$

$$T\{D[s(\underline{x})]\} = s[\xi(\underline{x}) - t_1,\ \eta(\underline{x}) - t_2] \tag{2-27}$$

and it immediately follows from equations (2-26) and (2-27) that

$$D\{T[s(\underline{x})]\} \neq T\{D[s(\underline{x})]\} \tag{2-28}$$

From equation (2-28) it is concluded that

$$^2\pi(\underline{x}) \cdot D\{T[s(\underline{x})]\} \neq {}^2\pi(\underline{x}) \cdot T\{D[s(\underline{x})]\} \tag{2-29}$$

and $\underline{D}$ is a spatially-variant operator.

In view of the fact that the transformation D is spatially variant, the determination of $\underline{H}$ for the general misregistration is not pursued

farther. Rather a sequential procedure is developed, illustrated by Fig. 2-5, where the geometrical distortion components are estimated and removed before the signal is processed by the filter H.

For the class of data of interest in this study, additional simplifying assumptions are made for purposes of formulating the distortion estimation problem in a straightforward manner. These assumptions are as follows:

(1) neglect the earth's curvature

(2) neglect scan-line foreshortening

(3) assume uniform illumination

With the affine model assumed to describe the misregistration and these simplifying assumptions, Fourier transform techniques for estimating the geometrical distortion are discussed in the subsequent sections of this chapter.

2.4 The Two-Dimensional Fourier Transform under an Affine Transformation.

Under the assumption of an affine transformation as the model representing the distortion between two images, the expression relating the spatial frequency domains of these images is readily derived using the two-dimensional Fourier transform. The significance of this expression is that under some very reasonable assumptions, estimates of the distortion coefficients can be readily made for the class of data of interest in this study. The analysis of this section will use continuous functions, as no generality is lost and the notation is much clearer.

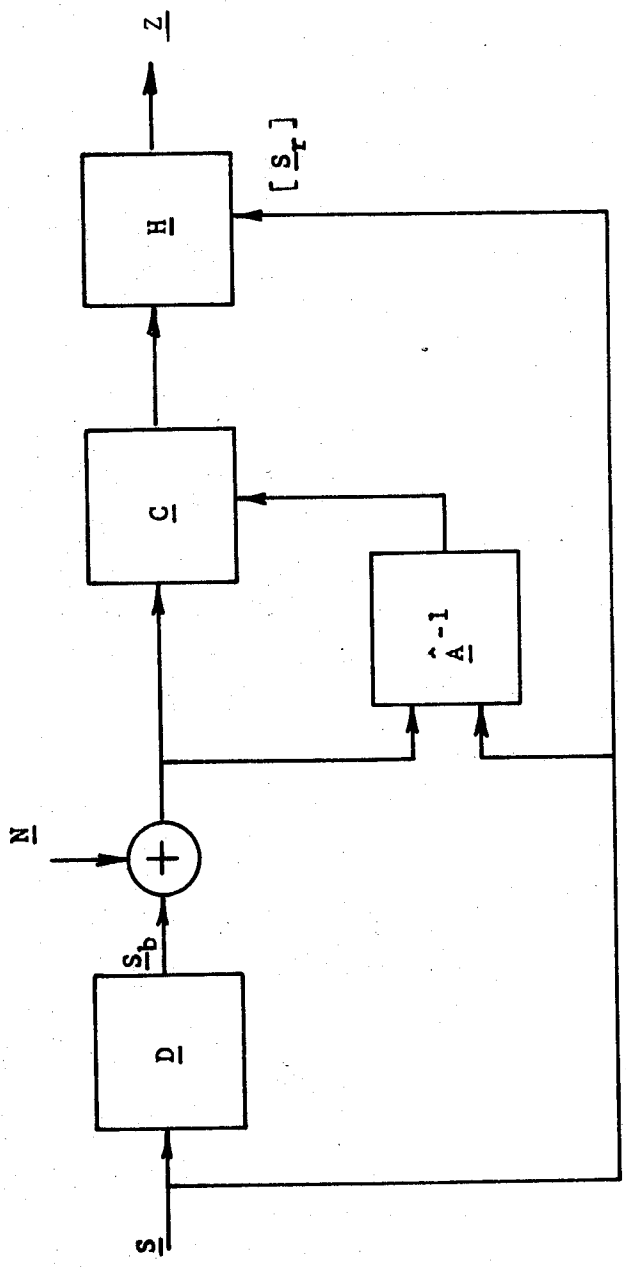

Figure 2-5 Block Diagram of a Sequential Conjugate Point Processor

The two-dimensional Fourier transform is defined as

$$F(\underline{u}) = \int_{-\infty}^{\infty} \int f(\underline{x}) \exp\left[-j2\pi(\underline{u},\underline{x})\right] d\underline{x} \tag{2-30}$$

and in polar coordinates

$$G(\rho,\phi) = \int_{o}^{\infty} \int_{o}^{2\pi} r\, g(r,\theta) \exp\left[-j2\pi r\rho \cos(\theta - \phi)\right] dr\, d\theta \tag{2-31}$$

It is shown in Appendix A that if there exists a function $\ell(\underline{x})$ such that

$$\ell(\underline{x}) = D[f(\underline{x})] = f[\underline{B}\ \underline{x}] = f(\underline{y}) \tag{2-32}$$

where $\underline{B}$ is an affine transformation, then

$$F(\underline{v}) = \frac{1}{|J|} \exp\left[-j2\pi(\underline{u},\underline{t})\right] F\left[(\underline{A}^{-1})^T\ \underline{u}\right] \tag{2-33}$$

where

$$J = \begin{bmatrix} \dfrac{\partial y_1}{\partial x_1} & \dfrac{\partial y_1}{\partial x_2} \\ \dfrac{\partial y_2}{\partial x_1} & \dfrac{\partial y_2}{\partial x_2} \end{bmatrix}$$

is the Jacobian of the transformation. It follows from (2-33) that the modulus of the transform is independent of the displacement vector $\underline{t}$.

$$M(\underline{v}) = \left[F(\underline{v})\ F^*(\underline{v})\right]^{1/2}$$

$$= \frac{1}{|J|} \left\{ \left| F[(\underline{A}^{-1})^T\ \underline{u}] \right|^2 \right\}^{1/2} \tag{2-34}$$

With proper interpretation of (2-33) and (2-34), several interesting properties of the two-dimensional Fourier transform can be emphasized.

The Fourier transform is a decomposition of $f(\underline{x})$ into a linear combination of basis functions of the form

$$\exp\left[-j2\pi\ (\underline{u},\underline{x})\right] = \exp\left[-j2\pi(u_1\ x_1 + u_2\ x_2)\right] \tag{2-35}$$

For a particular pair of coefficients (u_1,u_2), the corresponding elementary function has zero phase along the line described by

$$x_2 = -\frac{u_1}{u_2}\ x_1 + \frac{n}{u_1}\ , \quad n \text{ is integer} \tag{2-36}$$

and the wavefront has the direction

$$\theta = \tan^{-1}\frac{u_1}{u_2} \tag{2-37}$$

From Fig. 2-6 it is easily seen that the spatial period of the wavefront is

$$L = \frac{1}{u_1}\cos\theta = \frac{1}{\left[u_1^2 + u_2^2\right]^{1/2}} \tag{2-38}$$

Thus the corresponding spatial frequency is

$$u = \frac{1}{L} = \left[u_1^2 + u_2^2\right]^{1/2} \tag{2-39}$$

From (2-34) the relation between coordinates systems $\underline{u}$ and $\underline{v}$ is

$$\underline{v} = (\underline{A}^{-1})^T\ \underline{u} \tag{2-40}$$

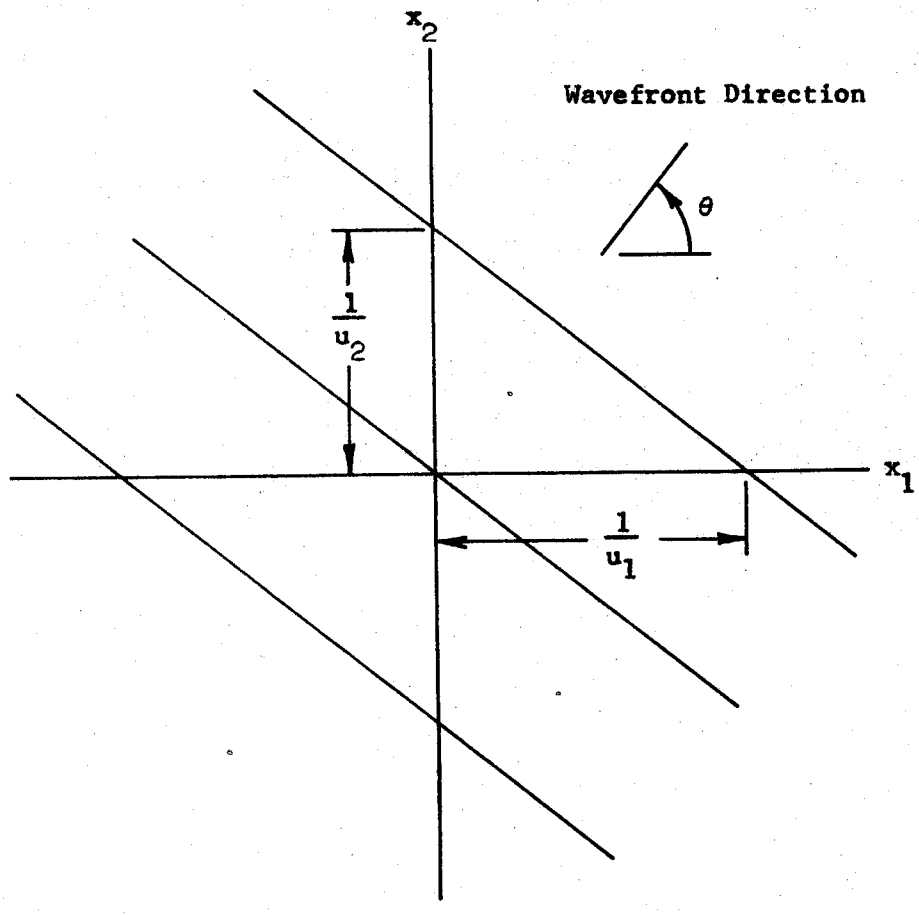

Figure 2-6 Lines of Constant Phase of Elementary Functions Associated with Spatial Frequencies (u_1, u_2)

It is illustrative to examine the effects of various geometrical distortions in the spatial and spatial-frequency domains. For scaling changes the distortion matrix is

$$\underline{A} = \begin{bmatrix} a_{11} & 0 \\ 0 & a_{22} \end{bmatrix} \tag{2-41}$$

where the scaling is assumed to be along the coordinate axes. The relationship between the spatial frequency domain coordinates is then

$$\underline{v} = (\underline{A}^{-1})^T \underline{u} = \begin{bmatrix} \frac{1}{a_{11}} & 0 \\ 0 & \frac{1}{a_{22}} \end{bmatrix} \underline{u} \tag{2-42}$$

This relation is illustrated in Fig. 2-7 where the dimensions of the rectangular blocks in the spatial domain have a width which is two times the height.

For rotation the distortion matrix is

$$\underline{A} = \begin{bmatrix} \cos\theta & \sin\theta \\ -\sin\theta & \cos\theta \end{bmatrix} \tag{2-43}$$

which is an orthogonal matrix. Thus

$$\underline{v} = (\underline{A}^{-1})^T \underline{u} = \underline{A}\,\underline{u} \tag{2-44}$$

and the transform of the distorted data is also rotated by the angle θ; this distortion is illustrated by the modulus of the transform of the ideal data shown in Fig. 2-8.

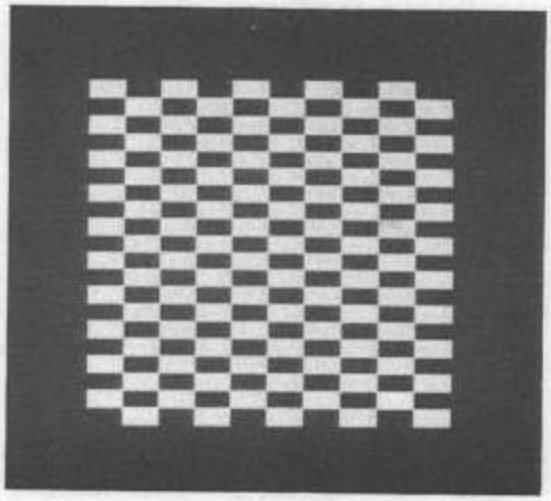

Block Pattern

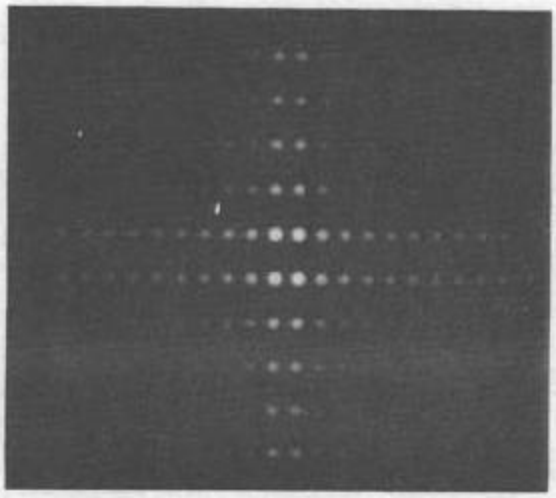

Modulus of Fourier Transform

Figure 2-7 Modulus of Fourier Transform of Block Pattern

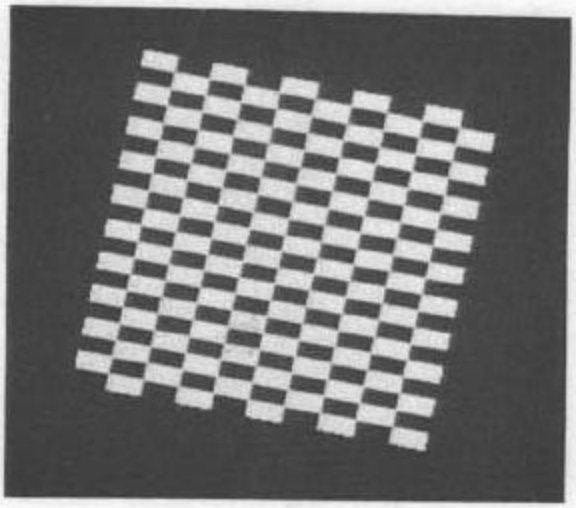

Rotated Block Pattern

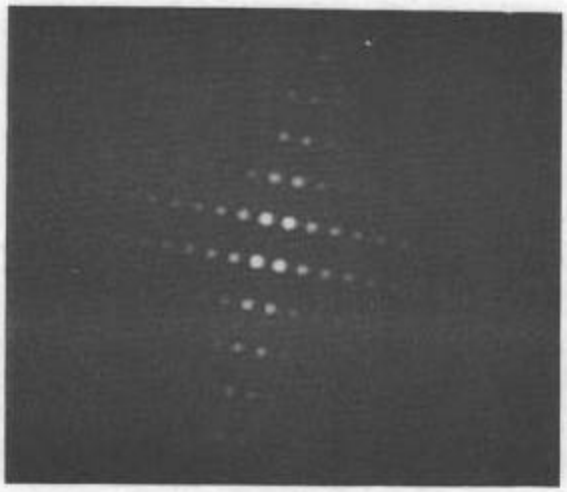

Modulus of Fourier Transform

Figure 2-8 Modulus of Fourier Transform of Rotated Block Pattern

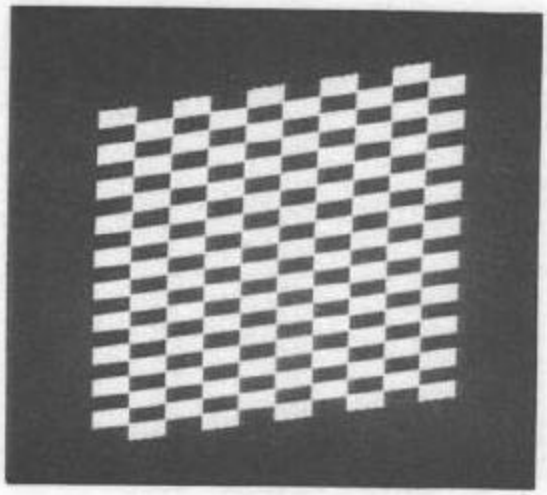

Block Pattern with Skew

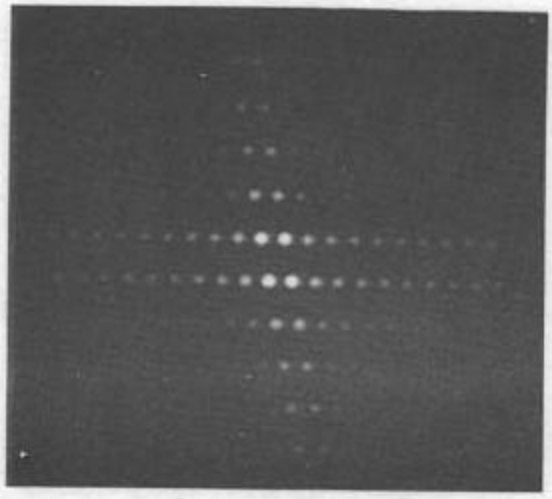

Modulus of Fourier Transform

Figure 2-9 Modulus of Fourier Transform of Skewed Block Pattern

For skew distortion the geometric distortion matrix becomes

$$\underline{A} = \begin{bmatrix} 1 & 0 \\ a_{21} & 1 \end{bmatrix} \tag{2-45}$$

and in the spatial frequency domain the coordinates are related by

$$\underline{v} = \begin{bmatrix} 1 & -a_{21} \\ 0 & 1 \end{bmatrix} \underline{u} \tag{2-46}$$

This distortion and its associated modulus of the Fourier transform are shown in Fig. 2-9.

The symmetry property of the modulus is the remaining property of the two-dimensional Fourier transform needed for this study. For real signals it readily follows from equation (2-30) that

$$F(-\underline{u}) = F^{*}(\underline{u}) \tag{2-47}$$

where the asterisk denotes the complex conjugate. Thus the modulus, equation (2-34), is symmetric about the origin, and the frequency domain search techniques need to use only one-half of the modulus.

2.5 Transform Techniques for the Correction of Regional Geometric Distortion.

For data sets with the affine model characterizing the misregistration between corresponding regions, Fourier transforms of these data may be used to advantage in determining the coefficients of the geometrical distortion components. These advantages are a result of both the property of the Fourier transform exhibiting the spatial

characteristics existing in the spatial domain and of the organization of these characteristics in the spatial frequency domain. The zero spatial frequency component is mapped into the origin of the transform domain and higher frequency components are mapped into locations proportional to both the value of their spatial frequency and in a direction from the origin characteristic of the orientation of the component in the spatial domain.

With the assumption of the affine misregistration model, equation (2-33) gives the relation between the spatial frequency domain representations of the data sets. As defined by equation (2-34) the moduli of the two-dimensional Fourier transforms of corresponding regions of data are invariant under the coordinate shift $\underline{t}$; thus the coordinate systems can be chosen arbitrarily. It is further assumed that for data of a reasonably homogenous composition, small shifts Δd of the data aperture will yield moduli which can be assumed to be unchanged for purposes of this study.

The differences between the moduli of the transforms of two corresponding regions of data provide all the information required for determining values for the coefficients of the linear distortion matrix. For the data sets employed in this study the scale factors can be estimated accurately from the flight information available. Therefore, only distortion due to skew and rotation must be estimated from the data sets.

The computation of the Fourier transforms for the data used in this study is carried out using the Fast Fourier Transform technique [5,9] since the data are in a discrete format.

2.5.1. Search Algorithms for Structured Data

The class of agricultural imagery, which is the data of principal interest in this study, typically consists of a collection of rectangular fields with each of these fields having essentially a homogenous ground cover. The data usually, but not always, are recorded such that the flight path is closely parallel to the orientation of these fields. It has been observed that the modulus of the two-dimensional Fourier transform of data sets from this class of imagery typically exhibits a simple structure with the property that a majority of the energy in the spatial frequency domain is concentrated along linear loci or rays perpendicular to these field boundaries. The moduli of transforms typical of those obtained for agriculturally related imagery are shown in Fig. 2-10(a).

The rotative and skew components of the misregistration are obtained by utilizing the geometrical differences between the moduli of the Fourier transforms of corresponding regions. This is accomplished by determining the angle between the corresponding loci of energy which are characteristic of this class of data. Assuming that the location of these loci can be determined, the distortion components are evaluated in a straightforward manner.

(1) Rotation

From equation (2-44) it is seen that rotation in the spatial domain results in the rigid body rotation of the modulus of the Fourier transform. Only the angle between the corresponding loci of the distorted and reference data transforms is required to determine the rotational distortion; this is shown in Figure 2-11. Thus

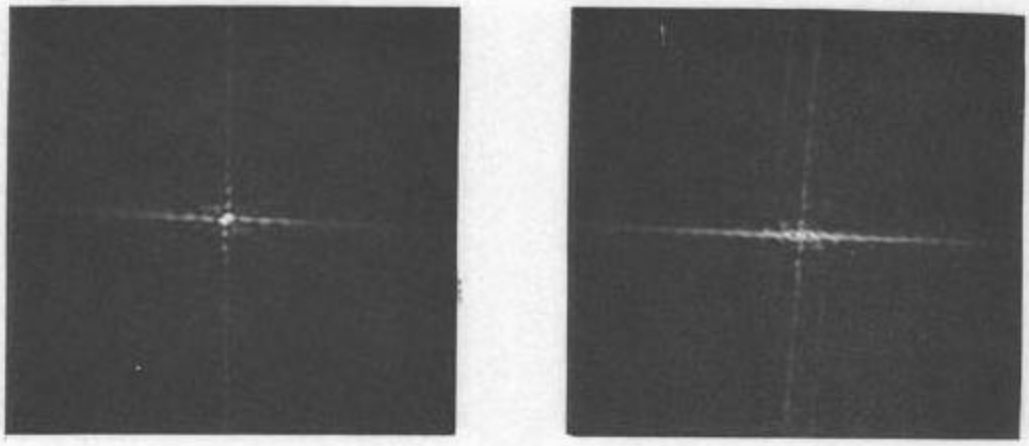

(a) Structured Data Sets

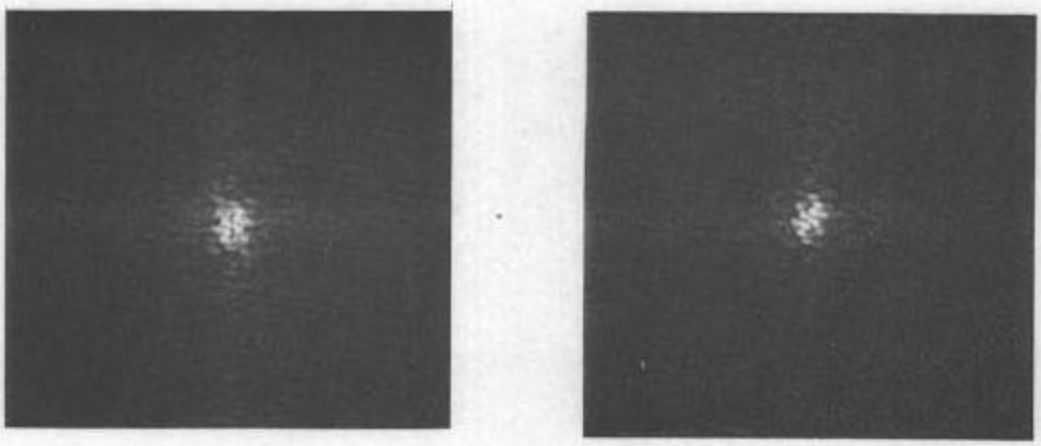

(b) Unstructured Data Sets

Figure 2-10 Examples of the Modulus of the Two-Dimensional Fourier Transform

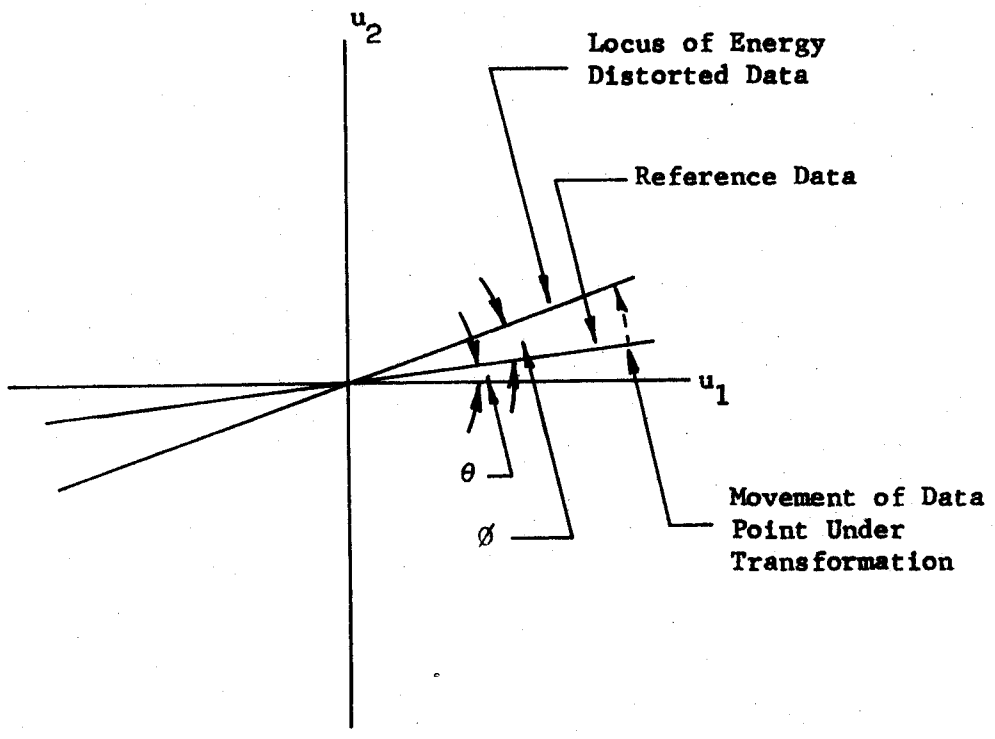

Figure 2-11 Location of Loci of Energy in the Modulus of the Two-Dimensional Fourier Transform, Rotational Distortion

the coefficients of equation (2-43) are

$$a_{11} = a_{22} = \cos \theta$$
$$a_{12} = - a_{21} = \pm \sin \theta \qquad (2\text{-}48)$$

where the sign ($\pm$) is determined by the sense of the rotation.

(2) Skew

The angular quantities related to the skew distortion component are shown in Fig. 2-12. It is assumed that a locus of energy in the modulus of the Fourier transform of the reference data is at an angle θ with respect to the u_1 axis. The corresponding locus of energy of the distorted data is at an angle ϕ with respect to the reference data locus. It then follows from equation (2-26) that these angular quantities and the skew coefficient a_{21} are related by

$$\phi = \tan^{-1}\left(\frac{\tan \theta}{1 + a_{21} \tan \theta} \right) \qquad (2\text{-}49)$$

To determine a_{21}, take the limit of ϕ as $\theta \to \pi/2$; thus

$$\phi = \lim_{\theta \to \pi/2} \tan^{-1}\left(\frac{1}{1/\tan \theta + a_{12}}\right) \qquad (2\text{-}50)$$
$$= \tan^{-1}\left(\frac{1}{a_{21}}\right)$$

The skew coefficient is obtained from the expression

$$a_{21} = \frac{1}{\tan \phi} \Bigg|_{\theta = \frac{\pi}{2}} \qquad (2\text{-}51)$$

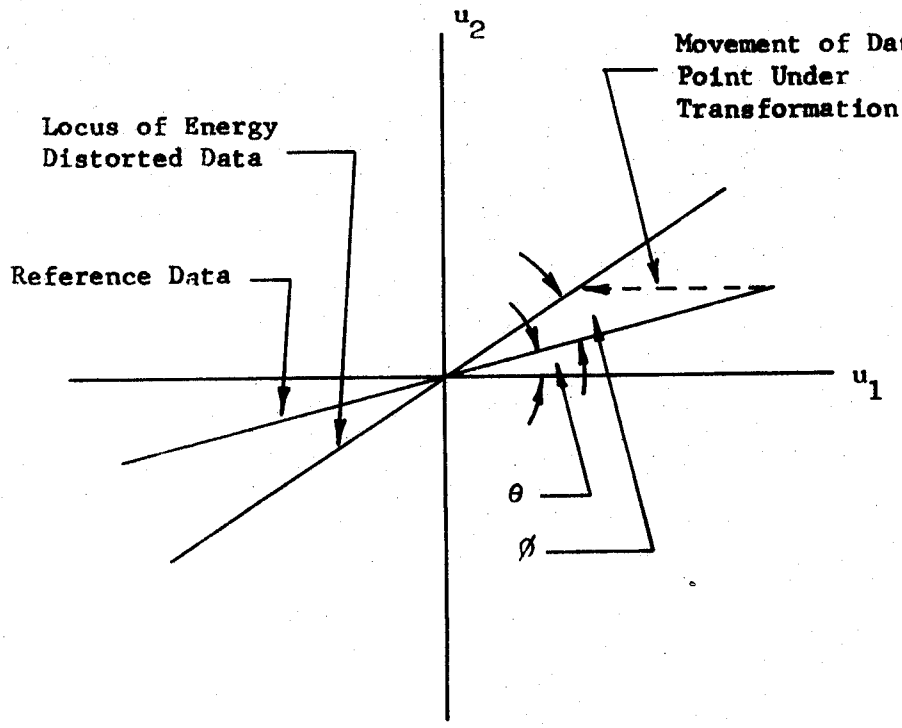

Figure 2-12 Location of Loci of Energy in the Modulus of the Two-Dimensional Fourier Transform, Skew Distortion

(3) Rotation and Skew

In the more general case of both a rotative and skew distortion component in the data, there must be at least two linear loci in each modulus of the transforms of the data sets to determine these distortion parameters. For agriculturally related data this requirement is usually satisfied with the two loci being separated by approximately $\pi/2$ radians.

With reference to Fig. 2-13 assume, without loss of generality, that one of the loci of the reference data transform is coincident with the u_1 axis. Thus from equation (2-49)

$$\theta_1 + \phi_1 = \tan^{-1}\left(\frac{\tan\theta_1}{1 + a_{21}\tan\theta_1}\right) + \alpha_1 = \alpha_1 \qquad (2\text{-}52)$$

but $\theta_1 = 0$ since the loci is assumed coincident with the u_1 axis. Thus

$$\phi_1 = \alpha_1 \qquad (2\text{-}53)$$

and the angle ϕ_1 is due only to rotational distortion as equation (2-52) demonstrates that skew and rotation are uncoupled along the u_1 axis.

Now the skew distortion component can be obtained from the expression

$$\phi_2 - \phi_1 = \tan^{-1}\left(\frac{\tan\theta_2}{1 + a_{21}\tan\theta_2}\right) \qquad (2\text{-}54)$$

and solving for a_{21}

$$a_{21} = \frac{1}{\tan\theta_2}\left(\frac{\tan\theta_2}{\tan(\theta_2 - \phi_1)} - 1\right) \qquad (2\text{-}55)$$

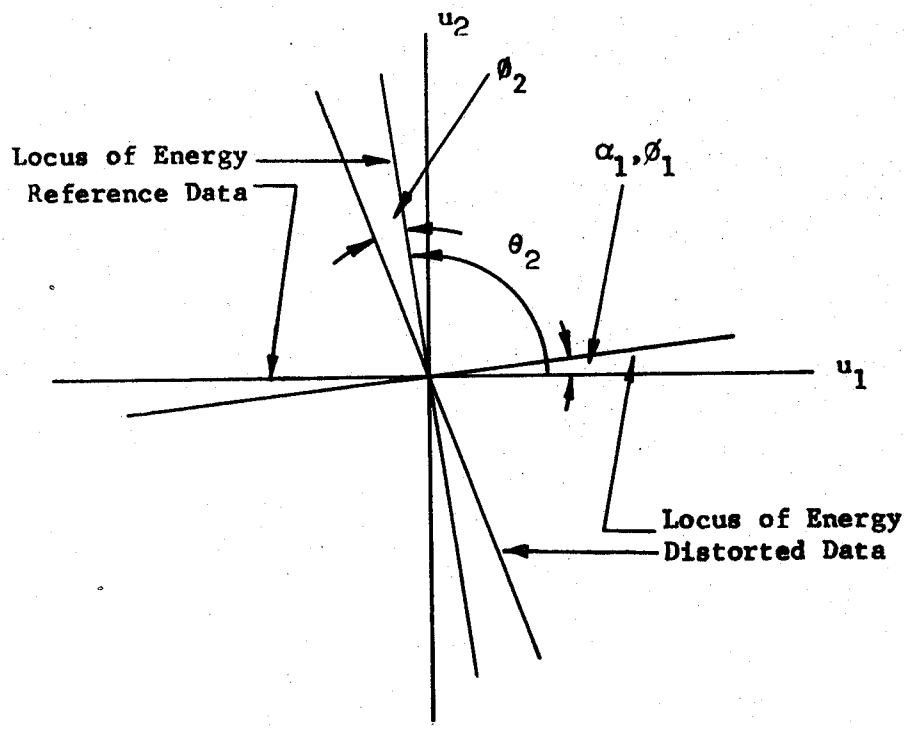

Figure 2-13 Location of Loci of Energy in the Modulus of the Two-Dimentsional Fourier Transform, Rotational and Skew Distortion

For rectangular fields for which $\theta_2 \cong \pi/2$

$$a_{21} \cong \frac{1}{\tan(\theta_2 - \phi_1)} = \frac{1}{\tan \phi_2'} \tag{2-56}$$

where $\phi_2' = \theta_2 - \phi_1$.

The distortion matrix is then the product, with attention given to the proper order of the matrices

$$\underline{A} = \begin{bmatrix} 1 & 0 \\ s_{21} & 1 \end{bmatrix} \begin{bmatrix} r_{11} & r_{12} \\ r_{21} & r_{22} \end{bmatrix} \tag{2-57a}$$

$$= \begin{bmatrix} r_{11} & r_{12} \\ s_{21}\, r_{11} + r_{21} & s_{21}\, r_{12} + r_{22} \end{bmatrix} \tag{2-57b}$$

which yields

$$\underline{A} = \begin{bmatrix} \cos \phi_1 & \pm \sin \phi_1 \\ a_{21} \cos \phi_1 \mp \sin \phi_1 & \pm a_{21} \sin \phi_1 + \cos \phi_1 \end{bmatrix} \tag{2-58}$$

The algorithm implemented in this study, for locating the loci containing the significant fraction of the energy in the spatial frequency domain, utilizes a two part procedure. The concept of the first operation is shown in Fig. 2-14(a). The wedge aperture is scanned through a total angle Γ in steps equal to the angular resolution of the aperture $\Delta\gamma$. The output of this spatial filter is the summation of those data falling within the region $(\rho_2 - \rho_1)\Delta\gamma$. The output is

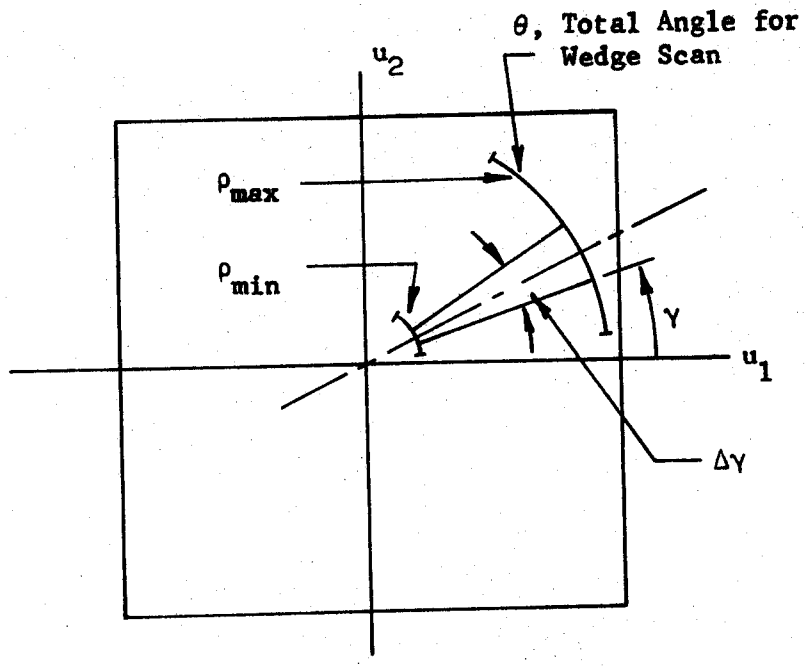

(a) Wedge Aperture

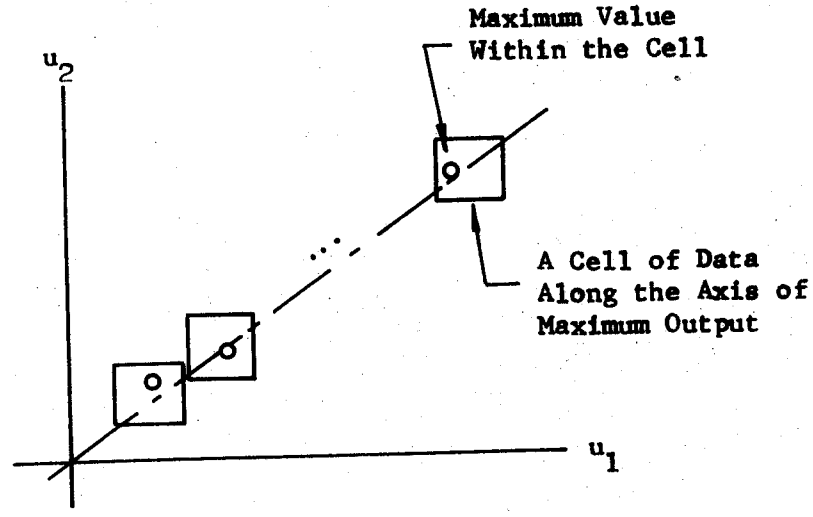

(b) Regression Line

Figure 2-14 Use of Wedge Aperture to Locate Loci in the Modulus of the Fourier Transform of Structured Data

$$w_i = \sum_{\gamma_i}^{\gamma_i + \Delta\gamma} \sum_{\rho_1}^{\rho_2} M(\rho, \gamma_i), \quad i = 1,\ldots,N \tag{2-59}$$

where $M(\rho,\gamma)$ is the modulus of the two-dimensional Fourier transform expressed in polar coordinates and N is the number of resolvable positions of the aperture within the total scan angle.

This summation necessarily involves data interpolation since the data are located on a discrete grid. The w_i are nonnegative and the largest w_i is assumed to be obtained from the segment containing the loci being sought.

The purpose of the second step is to locate the loci within this segment. A sequence of rectangular segments is selected from the data along the radial axis of the wedge giving the maximum output as shown in Fig. 2-14(b). The largest data point in each of these segments is found, and the slope β of the linear regression line through the coordinates of this set of maxima is computed. Thus

$$\beta = \frac{\sum_{i=1}^{M} (u_{1i} - \bar{u}_1)(u_{2i} - \bar{u}_2)}{\sum_{i=1}^{M} (u_{1i} - \bar{u}_1)^2} \tag{2-60}$$

with

$$\bar{u}_1 = \frac{1}{M} \sum_{i=1}^{M} u_{1i}$$

$$\bar{u}_2 = \frac{1}{M} \sum_{i=1}^{M} u_{2i}$$

and M is the number of points selected for the regression procedure. The estimated angle θ between this locus and the u_1 axis is then

$$\theta = \tan^{-1} \beta \tag{2-61}$$

2.5.2. Search Algorithms for Data with Complex Structure

The class of scenes of natural or uncultured terrian has Fourier transforms whose moduli have a more complex structure than the class considered in the previous section. The moduli of transforms typical of these obtained for this class of data are shown in Fig. 2-10(b). To identify the distortion parameters relating the transforms of two corresponding regions of data from this class of imagery necessarily involves a search procedure.

A possible search algorithm is to examine the modulus of the transform of the reference data along some locus and then search for the corresponding locus in the distorted data such that the difference between the outputs of these two spatial filters is minimized. A constant frequency search aperture, shown in Fig. 2-15, for the search locus in the transform of the reference data is appealing because it is both simply implemented and its corresponding locus under a linear transformation is readily related to the distortion matrix parameters.

The output of the constant frequency spatial filter is the sequence of numbers w_i

$$w_i = \sum_{\phi_i}^{\phi_i + \Delta\phi} \sum_{\rho_1}^{\rho_2} M(\rho, \phi_i), \qquad i = 1, \ldots, N \tag{2-62}$$

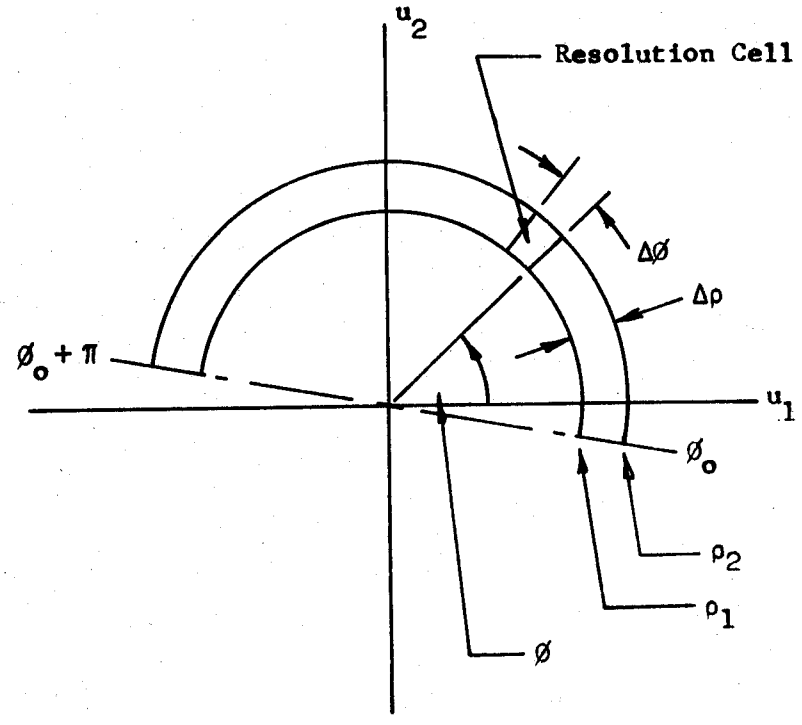

Figure 2-15 A Constant Frequency Search Aperture

where $M(\rho,\emptyset)$ is the modulus of the two-dimensional Fourier transform expressed in polar coordinates and N is the number of resolvable positions of the filter with the π radian search extent.

(1) Rotation

For rotation the search procedure is particularly simple because from equation (2-44) it is seen that a rotational distortion introduces only a rigid body rotation of the transform modulus. Thus the function to be minimized is

$$e = \sum_{i=1}^{N} \left| w_{ri}(\emptyset) - w_{bi}(\emptyset + \emptyset_o) \right|^2 \qquad (2\text{-}63)$$

where the subscripts r and b refer to the reference and background data sets repectively, and $\emptyset_o$ is the variable for which the minimum is sought. It then follows that the parameters of the distortion matrix $\underline{A}$ are

$$a_{11} = a_{22} = \cos \emptyset_o$$

$$a_{12} = - a_{21} = \pm \sin \emptyset_o \qquad (2\text{-}64)$$

where the sign is dependent on the sense of rotation.

(2) Skew

For a constant spatial frequency search locus in the reference data, the corresponding locus in the distorted data domain under a skew transformation is an ellipse. This is shown in the following development. Let the circular locus be given by

$$u_1^2 + u_2^2 = u_o^2 \qquad (2\text{-}65a)$$

From equation (2-46) the transformation of coordinates is given by

$$u_1 = v_1 + a_{21}\, v_2 \tag{2-65b}$$

$$u_2 = v_2 \tag{2-65c}$$

where unity scale factors are being assumed. Combining equations (2-65) yields

$$v_1^2 + 2\, a_{21}\, v_1\, v_2 + (1 + a_{21}^2)\, v_2^2 = u_o^2 \tag{2-66}$$

which is recognized to be the equation of an ellipse. To express (2-66) in polar coordinates, let

$$v_1 = \rho \cos \phi \tag{2-67a}$$

$$v_2 = \rho \sin \phi \tag{2-67b}$$

Then

$$\rho^2 \left[\cos^2 \phi + 2\, a_{21} \cos \phi \sin \phi + (1 + a_{21}^2) \sin^2 \phi\right] = u_o^2 \tag{2-68}$$

solving for ρ^2

$$\rho^2 = \frac{u_o^2}{1 + a_{21} \sin 2\phi + a_{21}^2 \sin^2 \phi} \tag{2-69}$$

To find the extreme values of ρ, noting that $\rho \geq 0$,

$$\frac{d\rho^2}{d\phi} = \frac{u_o^2(2\, a_{21} \cos 2\phi + 2a_{21}^2 \sin \phi \cos \phi)}{(1 + a_{21} \sin 2\phi + a_{21}^2 \sin^2 \phi)^2} = 0 \tag{2-70}$$

The stationary points of (2-70) are

$$\phi = -\frac{1}{2} \tan^{-1}\left(\frac{2}{a_{21}}\right) + \frac{n\pi}{2}, \quad n = 0,1,2,3 \tag{2-71}$$

where the principle values have been taken. Evaluating the equation of $\frac{d^2\rho^2}{d\phi^2}$ for the values of ϕ which are solutions of equation (2-71), it is found that the maxima of ρ correspond to n even and the minima to n odd.

Thus if the transform of the reference data scene is scanned by a constant frequency aperture, the corresponding search aperture on the transform of the distorted data must necessarily be elliptical. Thus the function to be minimized is

$$e = \sum_{i=1}^{N} | w_{ri}(\rho) - w_{bi}(\rho') |^2 \qquad (2\text{-}72)$$

where

$$\rho' = \left[\frac{\rho^2}{1 + a_{21} \sin 2\phi + a_{21}^2 \sin^2 \phi} \right]^{1/2} \qquad (2\text{-}73)$$

for the coefficient a_{21}.

(3) Rotation and Skew

These distortions are coupled in the sense that it is not possible to solve for each individually. Thus the equation that must be minimized is

$$e = \sum_{i=1}^{N} |w_{ri}(\rho,\phi) - w_{bi}(\rho',\phi')|^2 \qquad (2\text{-}74)$$

where

$$\rho' = \left[\frac{\rho^2}{1 + a_{21} \sin 2\phi' + a_{21} \sin^2 \phi'} \right]^{1/2}$$

$$\phi' = \phi + \phi_o$$

This is a two parameter search in which the loci are ellipses and the initial starting points are displaced by ϕ_o. As the data is experimental there always exists the possibility of local minima which will prevent the algorithm from reaching the true regional minima.

CHAPTER 3

CORRELATION PROCESSORS

3.0 Introduction

In this chapter equations are developed for the optimum spatially invariant filter for the detection of a two-dimensional discrete data set $\underline{S}_r$ embedded in the background data $\underline{S}_b$. This filter, or processor, is linear although it may contain parameters which are determined by the solution of a set of nonlinear equations. These processor equations are interpreted as a crosscorrelation of the background data set $\underline{S}_b$ with a reference template obtained from the solution of a system of equations involving the reference data covariance matrix and the reference data $\underline{S}_r$.

The processor is derived for both noise free data and for data containing uncorrelated additive noise. All data are assumed distortionless since the geometrical distortion is to be removed by the previous data pre-processing algorithm.

Following the derivation of the equations for this optimum filter several algorithms for implementing the processor are developed. These algorithms reflect the varying assumptions regarding the form of the covariance matrix of both the reference data $\underline{S}_r$ and of the noise process $\underline{N}$. The chapter concludes with a discussion of the processing gain given by the correlator processor.

3.1 Noise Model for Multitemporal Data

A model for the noise components in the remotely sensed data is shown in Fig. 3-1. It is assumed that the noise, which is taken to be the differences between the reference data set $\underline{S}_r$ and its corresponding subimage in the background data $\underline{S}_b$, can be modeled as an uncorrelated additive source $\underline{N}$. This source consists of two components; the first, $\underline{N}(\underline{x})$, is postulated to characterize such effects as sensor noise, non-zero background temperature and video signal quantization noise. The second term, $\underline{D}(\Delta t, \lambda, \underline{x})$, is assumed to represent the changes in the scene due to natural processes such as the growth and maturing of vegetation. This latter term is of little significance in areas typified by the desert and mountainous regions of the southwestern United States. However, for areas engaged in agricultural activities, the changes induced by this term can be significant over a period of a few weeks. Thus the $\underline{D}$ component contains the information made available by the multitemporal data to the scientists concerned with the ground cover changes as a function of both the time between measurements and the period within the growing season that these measurements were taken.

When amplitude correlation is used to measure similarity for the detection of two corresponding subregions of data, these temporally induced changes in the scene decrease the correlation between subimages which are known to be geometrically corresponding. In this study the time between observations will be limited such that it is reasonable to assume that the two data sets remain partially coherent. This loss of correlation, however, leads to the requirement of processing a

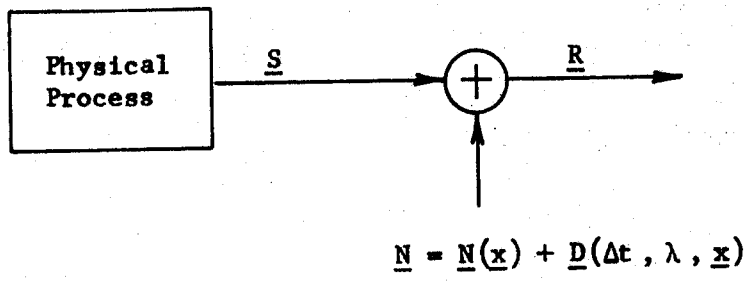

Figure 3-1 A Model of Noise Processes

larger set of data to maintain a specified average correlator output signal-to-noise ratio. That these assumptions are indeed reasonable rests with the experimental results presented in the sequel.

3.2 Processor Development

In detection theory literature the binary detection problem is most often developed in terms of simple hypothesis testing; the likelihood ratio is selected as the sufficient statistic and some criterion of optimal performance, typically the Neyman-Pearson or Bayes criterion, is stated. Under the assumption of additive, uncorrelated Gaussian noise, the resulting analytical expressions can be interpreted as a correlation processor.

For the problem considered in this investigation, however, it is not straightforward to state the two alternative hypotheses. Rather the approach taken in this study is to maximize a performance index subject to certain constraints. The resulting analytical expressions again are of a form to admit a correlation implementation.

The essential idea embodied in this performance index is the desire to process the background data $\underline{S}_b$ such that the processor output corresponding to the correct superposition of $\underline{S}_r$ on $\underline{S}'_r \subset \underline{S}_b$ is maximally discriminable from the output at all other spatial juxtapositions of the reference template on the background data. The desired processor output, therefore, consists of a large central peak, corresponding to the correct superposition of the template, surrounded by a non-zero pedestal. The filter output in the pedestal region is due to the interaction of the template with the background data for juxtapositions of the template spatially separated from the location

of the central peak by distances greater than the reciprocal of the spatial frequency bandwidth of the scene. Such a desirable output is shown in Fig. 3-2.

The discrimination between peak and pedestal is made by a comparison of amplitudes. Thus for maximum discrimination, assuming this central peak to be normalized to unit value, the peak amplitude of the filter output in the pedestal region must be minimized. Peak values are in general not useful for analytical purposes since such a value may not having meaning.

The peak values of the processor output can be probabilistically related to the variance of the process. If the output in the pedestal region is modeled as a Gaussian process, then the fraction of the time that a specified output value is exceeded is the area in the tail of the Gaussian probability density function; thus, if $p(x) = N(0,1)$,

$$\text{Prob}\ [X > x] = \frac{1}{2}\ \text{erfc}(x) \tag{3-1}$$

where erfc(x) is the complementary error function.

If the Gaussian assumption cannot be made but the random variable X has a finite second moment, then the Chebychev inequality may be used. Thus if

$$E[X^2] < \infty\ , \tag{3-2}$$

then

$$\text{Prob}\left[\ |X - E[X]| \geq \varepsilon\ \right] \leq \frac{\text{Var}(X)}{\varepsilon^2} \tag{3-3}$$

for any $\varepsilon > 0$.

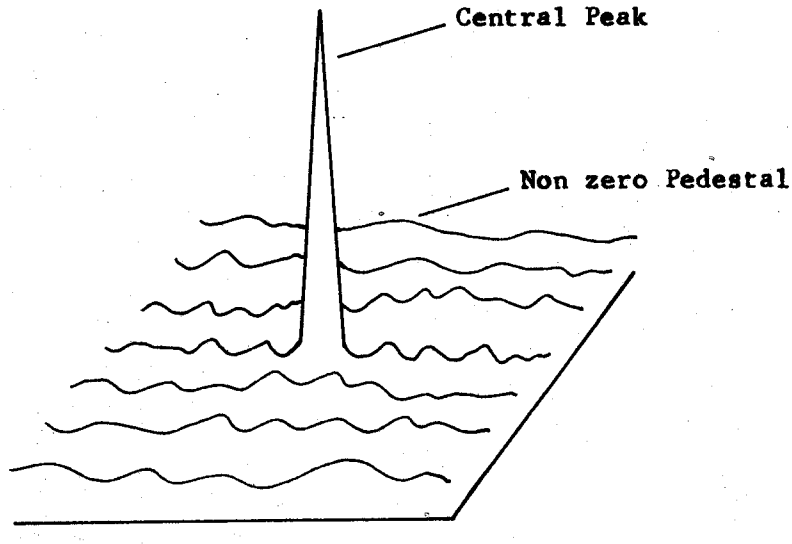

Figure 3-2 A Desired Processor Output

The thrust of this argument is that if a linear processor is derived such that the variance in the pedestal region is minimized, then it follows that the fractional time that the output exceeds the specified value $x = x_o$, will also be minimized.

To obtain an expression for this optimal processor, the quantity to be maximized is the ratio of the output at the point of correct superposition of $\underline{S}_r$ on $\underline{S}_b$ to the variance at all other juxtapositions. In the actual implementation of this filter, this operation corresponds to maximizing the ratio of the peak of the correlation surface to the variance of this surface in the pedestal region. The correlation surface is obtained by the crosscorrelation of the background data $\underline{S}_b$ with the template generated from the reference data $\underline{S}_r$.

3.3 Noise Free Processor

For noise free data the reference data $\underline{S}_r$ is a subregion of the background data $\underline{S}_b$. It is assumed that the background data are a discrete set obtained from the product of a sample function from a real, wavenumber limited, two-dimensional random process with the finite impulse grid $^2\pi$ defined by equation (2-2). The statistical properties of the reference data set are assumed to be characterized by the covariance matrix $\underline{K}$.

Using $\underline{S}_r$ the linear spatially invariant filter $\underline{H}$ is derived such that when the background data are convolved with $\underline{H}$

$$z(u,v) = \underline{H} * \underline{S}_b \tag{3-4a}$$

$$= \sum_i \sum_j s(u - i + 1, v - j + 1)\, h(i,j) \tag{3-4b}$$

the ratio

$$\gamma = \frac{z^2(u_r, v_r)}{\text{Var}\,[z(u,v)]} \tag{3-5}$$

is maximized. The quantity $z(u_r, v_r)$ is the filter output when the template is positioned on the reference data $\underline{S}_r$. This filter is further subject to the following constraints. The peak output $z(u_r, v_r)$ is constrained to have the maximum value of unity. Thus

$$I_1 = z(u_r, v_r) = 1, \tag{3-6a}$$

and this constraint can be expressed alternatively as the inner product relation

$$I_1 = (\underline{H}, \underline{S}_r) = 1 \tag{3-6b}$$

The filter must have finite energy to be realizable, thus

$$I_2 = \sum_i \sum_j |\, h_{ij} \,|^2 \tag{3-7a}$$

$$= (\underline{H}, \underline{H}) \leq M < \infty. \tag{3-7b}$$

3.3.1 Filter Equations for the Noise Free Processor

The background data set $\underline{S}_b = \{s_{ij}\}$ is assumed to be an M x N digital picture function, and the detection template $\underline{H}$ is a P x Q matrix of real numbers. For this problem to have physical meaning the matrices must have the relationship $P < M$, $Q < N$. The filter output is given by the two-dimensional convolution of this picture function and the template

$$z(u,v) = \sum_i \sum_j s(u - i + 1, v - j + 1)\, h(ij) \tag{3-8}$$

where

$$1 \leq i \leq P$$

$$1 \leq j \leq Q$$

and

$$P + 1 \leq u \leq M + 1$$

$$Q + 1 \leq v \leq N + 1$$

These indices are chosen so that the two matrices are fully juxtaposed, thus deleting the need for consideration of end effects. This convolution is illustrated in Fig. 3-3.

Equation (3-8) is expressible in terms of matrix operations which allows the convolution to be written in terms of vector quantities; note there are

$$m = (M - P + 1)\ (N - Q + 1) \tag{3-9}$$

distinct juxtapositions of the template on the background scene; each of these superpositions is called an observation. The t^{th} observation is the subimage of the background data defined by the set

$$\{s_t\} = \{s_{ij}:\ \ell \leq i \leq P + \ell - 1,\ k \leq j \leq Q + k - 1\} \tag{3-10}$$

with

$$1 \leq \ell \leq M - P + 1$$

$$1 \leq k \leq N - Q + 1$$

The set $\{s_t\}$ can be written as the equivalent pxl column vector

Figure 3-3 Convolution of the Background Data Set with the Detection Template

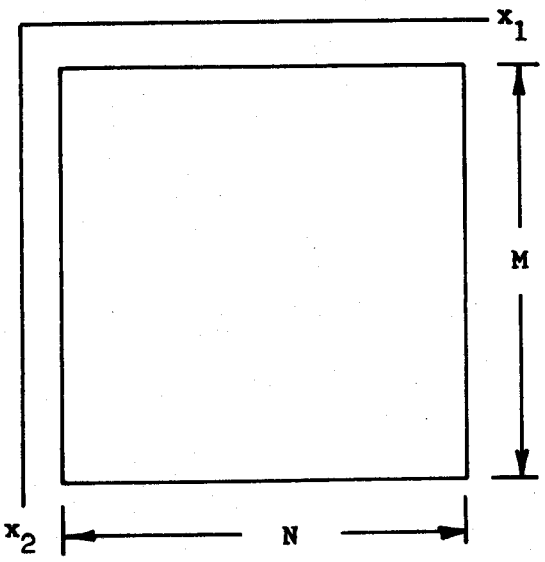

(a) Background Data Set

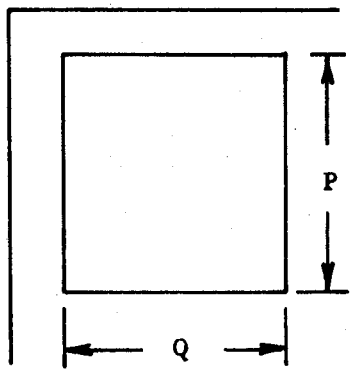

(b) Detection Template

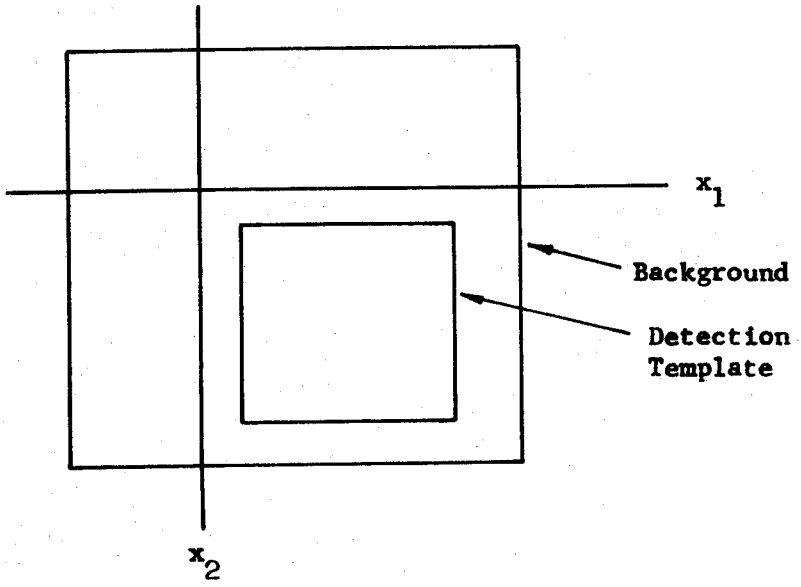

(c) Folded and Shifted Data Set

$$\{\underline{s}_t\} = \underline{s}_t = \begin{bmatrix} \underline{s}_1(t) \\ \vdots \\ \underline{s}_p(t) \end{bmatrix} \tag{3-11}$$

where each element of $\underline{s}_t$ is a q x 1 column vector

$$\underline{s}_i(t) = \begin{bmatrix} s_{i1}(t) \\ \vdots \\ s_{iq}(t) \end{bmatrix} \tag{3-12}$$

The data subimage which constitutes an observation and the organization of the elements of this observation into a vector are shown in Fig. 3-4.

From the observations defined by equation (3-10), the pq x m matrix $\underline{S}_a$ is formed

$$\underline{S}_a = \begin{bmatrix} \underline{s}_p(1) & \underline{s}_p(2) & \cdots & \underline{s}_p(m) \\ \underline{s}_{p-1}(1) & & & \\ \vdots & & & \\ \underline{s}_1(1) & & \cdots & \underline{s}_1(m) \end{bmatrix} \tag{3-13}$$

where the i^{th} column is composed of the elements of the i^{th} observation and m is the total number of observations.

Let

$$\underline{H} = \begin{bmatrix} \underline{h}_1 \\ \vdots \\ \underline{h}_p \end{bmatrix} \tag{3-14}$$

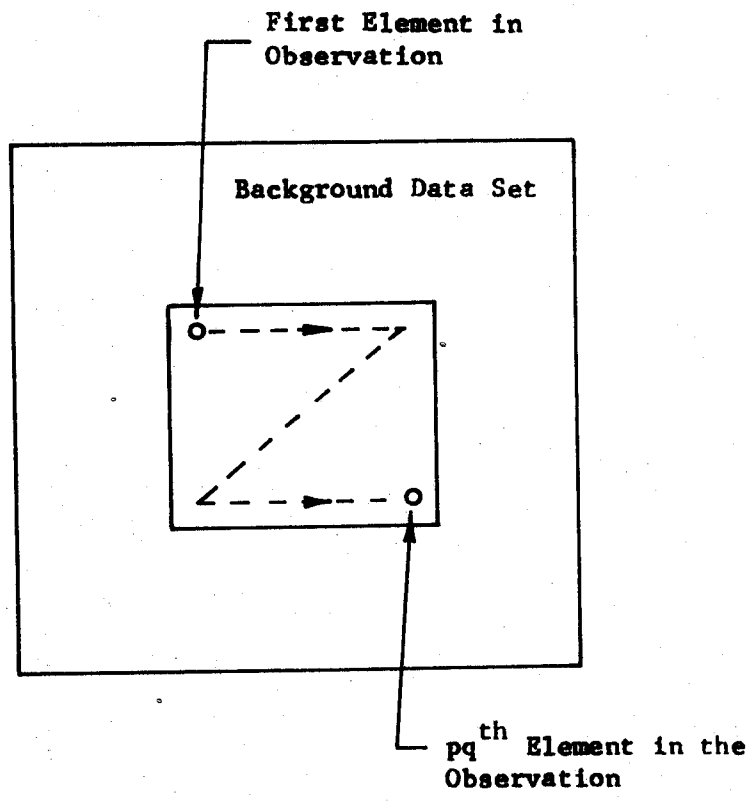

Figure 3-4 Organization of an Observation into an Equivalent Vector

be a multiple channel filter with p-input channels and one output channel. The filter coefficients for each channel $\underline{h}_i$ are given by the q x 1 column vector

$$\underline{h}_i = \begin{bmatrix} h_1(i) \\ \vdots \\ h_q(i) \end{bmatrix} \tag{3-15}$$

The filter output z(u) can be expressed as the convolution of the vector quantities

$$z(u) = \sum_{i=1}^{P} \underline{s}^T_{p-i+1}(u)\, \underline{h}_i, \quad u = 1,\ldots,m \tag{3-16}$$

Forming the m x 1 column vector

$$\underline{Z} = \begin{bmatrix} z(1) \\ \vdots \\ z(m) \end{bmatrix} \tag{3-17}$$

the convolution can be written in the matrix form as

$$\underline{Z} = \underline{S}_a^T \underline{H} \tag{3-18}$$

The ratio that is to be maximized is

$$\gamma = \frac{z^2(r)}{\text{Var}\,[\underline{Z}]} = \frac{z^2(r)}{E[(\underline{S}^T \underline{H})^T (\underline{S}^T \underline{H})]}$$

$$= \frac{z^2(r)}{E[\underline{H}^T \underline{S}\, \underline{S}^T \underline{H}]} = \frac{z^2(r)}{\underline{H}^T \underline{K}\, \underline{H}} \tag{3-19}$$

where $\underline{K} = E[\underline{S}\ \underline{S}^T]$ is the covariance matrix of the process and z(r) is the output corresponding to the correct superposition of the template and reference data set $\underline{S}_r$.

To maximize this expression, z(r) will be constrained to have a value of unity and the quadratic form $\underline{H}^T\underline{K}\underline{H}$ will be minimized. Additionally, from equation (3-7), the resulting $\underline{H}$ is constrained to have finite energy. Thus the functional relating these quantities is written as [25, 65]

$$I = \underline{H}^T\underline{K}\ \underline{H} + \lambda_1\ \underline{H}^T\underline{S}_r + \lambda_2\ \underline{H}^T\underline{H}, \qquad \lambda_2 \geq 0 \tag{3-20}$$

where λ_1 and λ_2 are the Lagrange multipliers. The extremum of this functional is found by first finding the stationary point of I with respect to $\underline{H}$. Then noting that I is convex, it follows that this stationary point is the minimum of I [47]. Thus

$$\frac{\partial I}{\partial \underline{H}} = 2\ \underline{K}\ \underline{H} + \lambda_1\ \underline{S}_r + 2\ \lambda_2\ \underline{H} = 0 \tag{3-21}$$

Solving for $\underline{H}$

$$\underline{H} = -\frac{1}{2}\ \lambda_1(\underline{K} + \lambda_2\ \underline{I})^{-1}\ \underline{S}_r \tag{3-22}$$

The values of the Lagrange multipliers λ_1 and λ_2 are obtained by solving the simultaneous set of nonlinear algebraic equations

$$\underline{H}^T\ \underline{S}_r = 1 \tag{3-23a}$$

$$\underline{H}^T\ \underline{H} = M \tag{3-23b}$$

Substituting equation (3-22) into (3-23), yields

$$-\frac{1}{2}\lambda_1 \underline{S}_r^T (\underline{K} + \lambda_2 \underline{I})^{-1} \underline{S}_r = 1 \qquad (3\text{-}24a)$$

$$\frac{1}{4}\lambda_1^2 \underline{S}_r^T \left[(\underline{K} + \lambda_2 \underline{I})^{-1}\right]^T (\underline{K} + \lambda_2 \underline{I})^{-1} \underline{S}_r = M, \ \lambda_2 \geq 0. \qquad (3\text{-}24b)$$

The solution of the equations (3-22) and (3-24) then yields the solution for the desired processor.

3.3.2 Some Observations Regarding the Noise Free Processor

Two salient points should be noted from the form of equation (3-21). First, the covariance matrix is the same for both the reference data $\underline{S}_r$ and the background data $\underline{S}_b$ since it is assumed that the process is stationary. Since there are no energy differences between the reference and background such as required for incoherent detection, this filter must be a coherent processor.

Secondly, there is a striking similarity between the filter given by equation (3-21) and the filter for detecting stationary targets in a clutter background in the radar problem [61]. In particular, for $\lambda_2 = 0$, the radar filter is the "inverse filter" which was first discussed by Urkowitz [59]. For $\lambda_2 \neq 0$, the corresponding filter is the "clutter rejection filter" [18, 61] which includes the consideration of additive receiver noise. The effect of these filters in the radar problem is to increase the bandwidth of the signal being processed; it has been shown that for the constraint of a fixed signal bandwidth, the signal spectrum for the optimum detection of targets in a clutter background is flat over this specified bandwidth [18].

The one-dimensional analog of the filter given by equation (3-21) for $\lambda_2 = 0$ is also well known in the field of seismic data processing. In this area the filter is known as the "spiking" filter.

3.4 Noise Free Algorithm Development

In this section use is made of both equation (3-22) and various assumptions regarding the form of the covariance matrix $\underline{K}$ to develop algorithms for implementing the processor on a digital computer. Care must be exercised in discussing the stationarity of the process characterized by the covariance matrix. In one-dimensional data, a result of stationarity is the requirement that the covariance depends only on the separation of the points $\tau = x_2 - x_1$. However, in two dimensions this definition is too restrictive in that it is conceivable that the covariance can depend on both the spatial separation $\underline{\tau} = \underline{x}_2 - \underline{x}_1$ and the direction of the line passing through these points.

Algorithms are developed for both cases; however, for non-isotropic covariance matrices a general covariance matrix must be considered. This in turn requires the solution of a large set of linear equations for determining the template, thus limiting the value of this procedure for reasons of computational tractability.

Major emphasis is given to algorithms for $\lambda_2 = 0$. Recall from equation (3-7) that this constraint was related to the filter energy. For finite dimensional filters this energy is finite so long as the elements of $\underline{H}$ are finite; this must be true if the covariance matrix is non-singular. In addition for the noise free processor, the variance in the output is due to the interaction of the reference template with the background signal. Thus the correlator output

signal-to-noise ratio, as defined by equation (3-19), is invariant with respect to the filter energy.

The algorithm for the general covariance matrix is considered first and, following this, study will be given to more restrictive assumptions regarding the form of the covariance matrix. In this latter case, the matrix assumes the form of a block Toplitz matrix which has much practical interest.

3.4.1 General Covariance Matrices

If the two-dimensional process from which $\underline{S}_r$ is selected has the general PQ x PQ covariance matrix $\underline{K}$, then the solution of the processor template $\underline{H}$ is given by equation (3-22)

$$\underline{H} = -\frac{1}{2}\lambda_1 \underline{K}^{-1} \underline{S}_r \tag{3-25}$$

and from equation (3-6b)

$$-\frac{1}{2}\lambda_1 \underline{S}_r^T \underline{K}^{-1} \underline{S}_r = 1 \tag{3-26a}$$

and solving for λ_1

$$\lambda_1 = \frac{-2}{\underline{S}^T \underline{K}^{-1} \underline{S}_r} \tag{3-26b}$$

Thus the template for the crosscorrelator is given by

$$\underline{H} = \frac{\underline{K}^{-1} \underline{S}_r}{\underline{S}_r^T \underline{K}^{-1} \underline{S}_r} \tag{3-27a}$$

$$= g_1 \underline{K}^{-1} \underline{S}_r \tag{3-27b}$$

where

$$g_1 = (\underline{S}_r^T \underline{K}^{-1} \underline{S}_r)^{-1} \tag{3-28}$$

is the normalization coefficient.

To estimate the covariance matrix $\underline{K}$, the data in the region surrounding $\underline{S}_r$ is partitioned into the subregions as shown in Fig. 3-5. Each subregion is called an observation and a correspondence is set up between the elements of an observation and the vector $\underline{\alpha}$ as

$$s_{ij} \leftrightarrow \alpha_j(i) \tag{3-29}$$

as illustrated in Fig. 3-5(b). Thus the i^{th} observation is mapped into the vector $\underline{\alpha}$ (i),

$$\underline{\alpha}(i) = \begin{bmatrix} s_{i1} \\ \vdots \\ s_{in} \end{bmatrix} \tag{3-30}$$

The covariance matrix is then estimated by the unbiased estimator

$$\underline{K} = \frac{1}{M-1} \begin{bmatrix} \sum_{i=1}^{M} \alpha_1(i)\,\alpha_1(i) & \cdots & \sum_{i=1}^{M} \alpha_1(i)\,\alpha_n(i) \\ \vdots & & \\ \sum_{i=1}^{M} \alpha_n(i)\,\alpha_1(i) & \cdots & \sum_{i=1}^{M} \alpha_n(i)\,\alpha_n(i) \end{bmatrix} \tag{3-31}$$

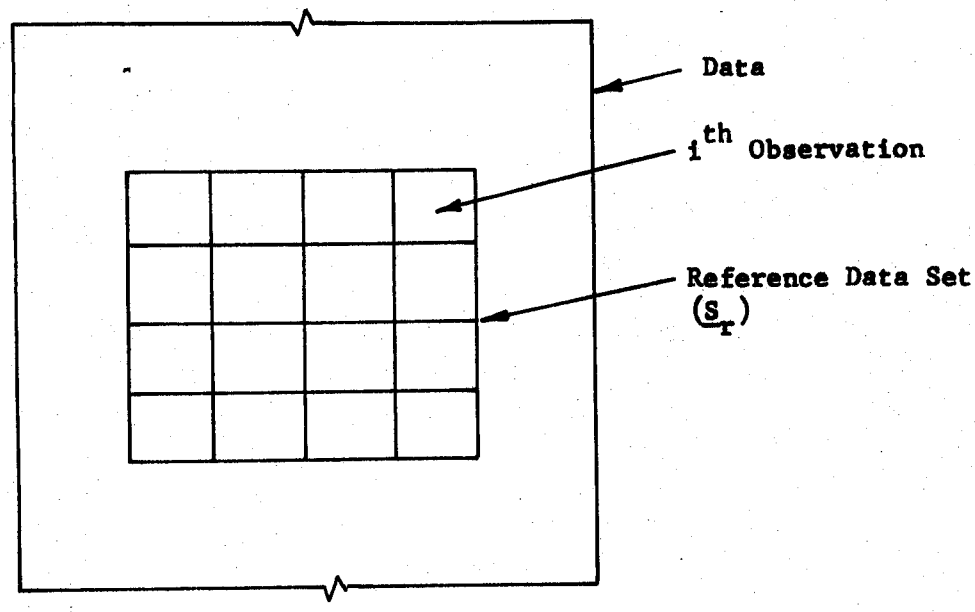

(a) Partition of Data Region into Observations for Covariance Estimation

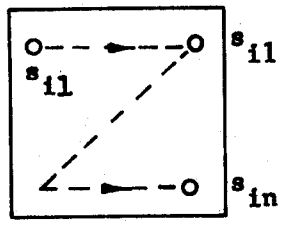

$s_{ij} \longleftrightarrow \alpha_j(i)$

$n = pq$ = No. Elements in Each Observation

(b) Packing Data Observations into a Vector

Figure 3-5 Data Format for Computing Covariance

where M is the total number of observations and n is the number of elements in $\underline{\alpha}$. If, for example, the reference data set is a subimage of 32 x 32 elements, then the resulting covariance matrix is 1024 x 1024 elements in size.

Premultiplying equation (3-27b) by $\underline{K}$ yields

$$\underline{K}\,\underline{H} = g_1\,\underline{S}_r \tag{3-32}$$

Reference data array sizes generally range between 32 x 32 to 128 x 128 elements in practical algorithms using experimental data. Thus to solve equation (3-32) for data arrays in this size range requires a computer with the capability of handling very large array sizes.

3.4.2 Covariance Matrices of the Toplitz Form

The stationary isotropic covariance matrices represent an interesting class of data for filter development; the symmetry properties of these covariance matrices can be utilized to reduce the complexity of the processor. Covariance matrices for a process of this class have the form

$$\underline{K} = \begin{bmatrix} \underline{k}_o & \underline{k}_1^T & \underline{k}_2^T & \cdots & \underline{k}_m^T \\ \underline{k}_1 & & & & \\ \vdots & & & & \\ \underline{k}_m & & & \cdots & \underline{k}_o \end{bmatrix} \tag{3-33}$$

This form of matrix is called a block Toplitz matrix and its properties have been investigated by Grenander and Szego [31]. An algorithm for inverting a matrix of this form was first given by Levinson [45] and

where a unit variance process is assumed. It is immediately evident that the matrix (3-34) has the same form as matrix (3-33) with each partitioned block of (3-34) corresponding to the data obtained from one line of the observation shown in Fig. 3-5(b).

With experimental data it is unreasonable to assume that the blocks along a diagonal will be equal. However, if the process is assumed to be of this class, then the blocks are averaged to provide a matrix of the required form. The template is again obtained from a solution of equation (3-32).

The difficulty in applying this algorithm is that a large set of data is required for estimating the covariance matrix. However, it has been observed that the correlation function for a large number of observations of remotely sensed data exhibits an approximate exponential form [52]. Thus, it is not clear that this algorithm would yield superior results to the next algorithm to be developed.

3.4.3 Isotropic Exponential Covariance Matrices

A very simple processor results if it is assumed that the statistical properties of the reference data set $\underline{S}_r$ are modeled by an isotropic exponential covariance matrix. This matrix has the block Toplitz form with the diagonal terms given by

$$\underline{k}_{ii} = \| \rho_{ij} \| \tag{3-35}$$

with

$$\rho_{ij} = \begin{cases} 1 & , \quad i = j \\ \rho^{|i-j|} & , \quad i \neq j \end{cases} \tag{3-36}$$

where ρ is equal to the average adjacent cell correlation coefficient in the reference scene. The off-diagonal terms are given by

$$\underline{k}_{ij} = \rho^{|i-j|}\,\underline{k}_{ii} \tag{3-37}$$

with ρ defined as for equation (3-35).

This covariance matrix can be written as

$$\underline{K} = \begin{bmatrix} \underline{k}_{ii} & \rho\underline{k}_{ii} & \rho^2\underline{k}_{ii} & \cdots & \rho^m\underline{k}_{ii} \\ \rho\underline{k}_{ii} & \underline{k}_{ii} & \rho\,\underline{k}_{ii} & \cdots & \rho^{m-1}\underline{k}_{ii} \\ \vdots & & & & \\ \rho^m\underline{k}_{ii} & & & \cdots & \underline{k}_{ii} \end{bmatrix} \tag{3-38}$$

The inverse of this matrix has been shown to be [6]

$$\underline{K}^{-1} = \frac{1}{1-\rho^2}\begin{bmatrix} \underline{k}_{ii}^{-1} & -\rho\underline{k}_{ii}^{-1} & 0 & \cdots & 0 \\ -\rho\underline{k}_{ii} & (1+\rho^2)\underline{k}_{ii}^{-1} & -\rho\underline{k}_{ii}^{-1} & & \\ 0 & -\rho\underline{k}_{ii}^{-1} & (1+\rho^2)\underline{k}_{ii}^{-1} & & \\ \vdots & & & & \\ 0 & & & \cdots & \underline{k}_{ii}^{-1} \end{bmatrix} \tag{3-39}$$

where

$$\underline{k}_{ii}^{-1} = \frac{1}{1-\rho^2}\begin{bmatrix} 1 & -\rho & 0 & \cdots & 0 \\ -\rho & 1+\rho^2 & -\rho & & \\ 0 & -\rho & 1+\rho^2 & & \\ \vdots & & & & \\ 0 & & & \cdots & 1 \end{bmatrix} \tag{3-40}$$

To obtain a solution for the desired template, substitute equation (3-39) into equation (3-28) and neglecting the multiplicative scalars

$$\underline{H} = \begin{bmatrix} \underline{k}_{ii}^{-1} & -\rho\underline{k}_{ii}^{-1} & 0 & \cdots & 0 \\ -\rho\underline{k}_{ii}^{-1} & (1+\rho^2)\underline{k}_{ii}^{-1} & -\rho\underline{k}_{ii}^{-1} & & \\ 0 & -\rho\underline{k}_{ii}^{-1} & (1+\rho^2)\underline{k}_{ii}^{-1} & & \\ \vdots & & & & \\ 0 & & & \cdots & \underline{k}_{ii}^{-1} \end{bmatrix} \begin{bmatrix} \underline{s}_p(r) \\ \vdots \\ \underline{s}_1(r) \end{bmatrix} \tag{3-41}$$

where the reference data set $\underline{S}_r$ has been written as an equivalent column vector as defined by equation (3-11). Expanding equation (3-41), the i^{th} filter element $\underline{h}_i$ is

$$\underline{h}_i = \left[-\rho\underline{k}_{ii}^{-1}\,\underline{s}_{i+1} + (1+\rho^2)\underline{k}_{ii}^{-1}\,\underline{s}_i - \rho\underline{k}_{ii}^{-1}\,\underline{s}_{i-1}\right] \tag{3-42}$$

where the identifier that the $\underline{s}_i$ are from the reference data has been omitted. Now substituting equation (3-40) into equation (3-42), again omitting multiplicative constants, yields the elements of the template. Thus

$$\begin{aligned} h_{ik} = &- \rho\left[-\rho\, s_{i+1,k+1} + (1+\rho^2)\, s_{i+1,k} - \rho\, s_{i+1,k-1}\right] \\ &+ (1+\rho^2)\left[-\rho s_{i,k+1} + (1+\rho^2)s_{i,k} - \rho\, s_{i,k-1}\right] \\ &- \rho\left[-\rho\, s_{i-1,k+1} + (1+\rho^2)\, s_{i-1,k} - \rho\, s_{i-1,k-1}\right] \end{aligned} \tag{3-43}$$

Expanding,

$$h_{ik} = \rho^2 s_{i+1,k+1} - \rho(1+\rho^2) s_{i+1,k} + \rho^2 s_{i+1,k-1}$$
$$- \rho(1+\rho^2) s_{i,k+1} + (1+\rho^2)^2 s_{i,k} - \rho(1+\rho^2) s_{i,k-1}$$
$$+ \rho^2 s_{i-1,k+1} - \rho(1+\rho^2) s_{i-1,k} + \rho^2 s_{i-1,k-1} \qquad (3\text{-}44)$$

Equation (3-44) is recognized as one term of the discrete convolution of the grid operator $\underline{G}$, where

$$\underline{G} = \begin{bmatrix} \rho^2 & -\rho(1+\rho^2) & \rho^2 \\ -\rho(1+\rho^2) & (1+\rho^2)^2 & -\rho(1+\rho^2) \\ \rho^2 & -\rho(1+\rho^2) & \rho^2 \end{bmatrix} \qquad (3\text{-}45)$$

with the reference data set $\underline{S}_r$. This convolution is written as

$$\underline{H} = \underline{G} * \begin{bmatrix} — & — & — & — & — \\ — & s_{i-1,k-1} & s_{i-1,k} & s_{i-1,k+1} & — \\ — & s_{i,k-1} & s_{i,k} & s_{i,k+1} & — \\ — & s_{i+1,k-1} & s_{i+1,k} & s_{i+1,k+1} & — \\ — & — & — & — & — \end{bmatrix} \qquad (3\text{-}46)$$

where

$$2 \leq i \leq P - 1$$
$$2 \leq k \leq Q - 1$$

and only the elements of $\underline{S}_r$ used for evaluating h_{ik} have been explicitly indicated. The indices have been chosen to eliminate the end effects of

the convolution; therefore, the reference data set should be two rows and two columns larger than the desired template size.

The result of the development of $\underline{G}$ is that rather than having to evaluate $\underline{H}$ using equation (3-41), $\underline{H}$ can be evaluated directly using equation (3-46). The resulting simplification is very substantial.

The grid operator $\underline{G}$ has several interesting properties. For $\rho = 0$, equation (3-46) becomes

$$\underline{G} = \begin{bmatrix} 0 & 0 & 0 \\ 0 & 1 & 0 \\ 0 & 0 & 0 \end{bmatrix} \tag{3-47}$$

Thus if the reference scene consists of a set of uncorrelated points $\underline{G}$ becomes the identity grid operator for the convolution of equation (3-46) and $h_{ik} = s_{ik}$. Thus the template is the reference data set itself.

For $\rho = 1$, the grid operator becomes

$$\underline{G} = \begin{bmatrix} 1 & -2 & 1 \\ -2 & 4 & -2 \\ 1 & -2 & 1 \end{bmatrix} \tag{3-48}$$

This is the discrete approximation to the mixed fourth partial derivative, obtained by convolving the discrete approximations to the second partial derivative along each coordinate axis. Thus

$$\underline{G} = \underline{G}_1 * \underline{G}_2 = \begin{bmatrix} 0 & 0 & 0 \\ 1 & -2 & 1 \\ 0 & 0 & 0 \end{bmatrix} * \begin{bmatrix} 0 & 1 & 0 \\ 0 & -2 & 0 \\ 0 & 1 & 0 \end{bmatrix} \tag{3-49}$$

The coefficient ρ required for determining the grid operator $\underline{G}$

is experimentally obtained from the data. A useful procedure is to re-format the reference data $\underline{S}_r$, which is represented as the P x Q matrix, into the [L x 2] matrix $\underline{S}_\rho = \{s_\rho(i,j)\}$ with

$$L = \left[\frac{P}{2} \right] Q \tag{3-50}$$

where $[\cdot]$ is read "the greatest integer less than or equal to."

The correlation coefficient ρ is then given by

$$\rho = \frac{\sum_{i=1}^{L} s_\rho(i,1)\, \underline{s}_\rho(i,2)}{\left[\sum_{i=1}^{L} s^2{}_\rho(i,1) \sum_{i=1}^{L} s^2{}_\rho(i,2) \right]^{1/2}} \tag{3-51}$$

3.4.4 Non-zero Constraints on Filter Energy

The solution for the crosscorrelation template was given by equation (3-22) as

$$\underline{H} = -\frac{1}{2} \lambda_1 \left(\underline{K} + \lambda_2 \underline{I}\right)^{-1} \underline{S}_r \tag{3-52}$$

Recall that the Lagrange multipliers λ_1 and λ_2 were introduced into the problem formulation so as to constrain the filter output amplitude and energy respectively. To solve for λ_1 and λ_2 it was found necessary to solve the simultaneous system of equations

$$-\frac{1}{2} \lambda_1 \underline{S}_r^T \left(\underline{K} + \lambda_2 \underline{I}\right)^{-1} \underline{S}_r = 1 \tag{3-53}$$

$$\frac{1}{4} \lambda_1^2 \underline{S}_r^T \left[\left(\underline{K} + \lambda_2 \underline{I}\right)^{-1}\right]^T \left(\underline{K} + \lambda_2 \underline{I}\right)^{-1} \underline{S}_r = M \tag{3-54}$$

From equation (3-53) solve for λ_1

$$\lambda_1 = \frac{-2}{\underline{S}^T (\underline{K} + \lambda_2 \underline{I}) \underline{S}_r^T} \tag{3-55}$$

and substituting equation (3-55) into equation (3-54) yields

$$\frac{\underline{S}_r^T \left[(\underline{K} + \lambda_2 \underline{I})^{-1} \right]^T (\underline{K} + \lambda_2 \underline{I})^{-1} \underline{S}_r}{\underline{S}_r^T (\underline{K} + \lambda_2 \underline{I})^{-1} \underline{S}_r} = M \tag{3-56}$$

and further

$$\underline{S}_r^T \left[(\underline{K} + \lambda_2 \underline{I})^{-1} \right]^T (\underline{K} + \lambda_2 \underline{I})^{-1} \underline{S}_r - M \underline{S}_r^T (\underline{K} + \lambda_2 \underline{I})^{-1} \underline{S}_r = 0 \tag{3-57}$$

This is a nonlinear equation in the one known λ_2. To solve this equation requires an algorithm for evaluating (3-57) which includes a nonlinear root finding program. If the value of λ_2 obtained from the solution of equation (3-57) is negative, the constraint is not active for the specified value of M and λ_2 is set equal to zero [65].

3.4.5 Signal Prewhitening

The function of the inverse covariance matrix is to prewhiten both the input scene and the stored reference picture function. A processor for the detection of $\underline{S}_r$ in the background $\underline{S}_b$ is shown in Fig. 3-6(a). In this implementation the observations $\underline{S}$ from $\underline{S}_b$ are crosscorrelated with $^{w}\underline{S}_r$ where

$$^{w}\underline{S}_r = \underline{K}^{-1} \underline{S}_r \tag{3-58}$$

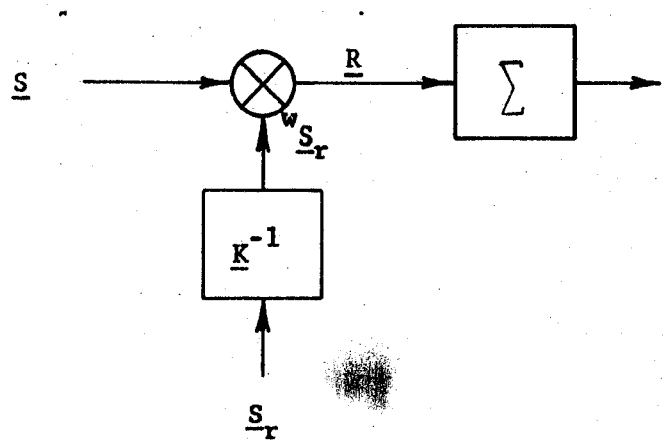

(a) Using Inverse Covariance Matrix

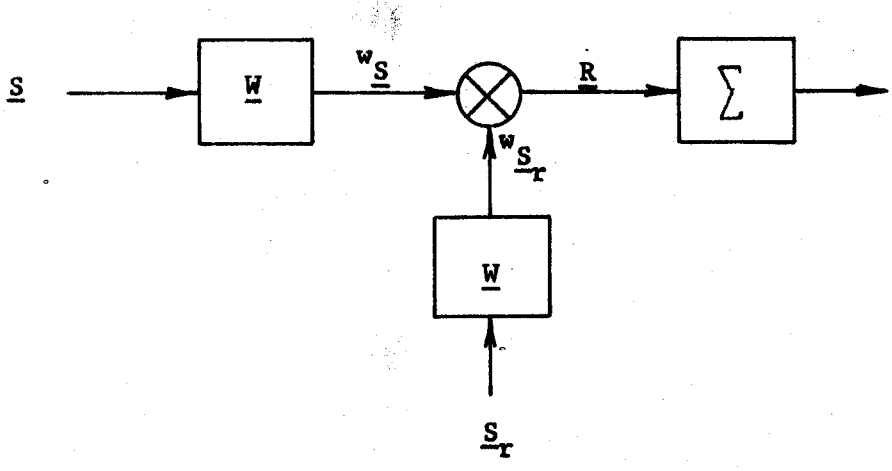

(b) Using the Factored Inverse Covariance Matrix

Figure 3-6 Block Diagram of Signal Processors

An equivalent expression is obtained if $\underline{K}^{-1}$ is factored into the upper triangular matrix and its transpose

$$\underline{K}^{-1} = \underline{W}\,\underline{W}^T = \underline{W}^T\,\underline{W} \tag{3-59}$$

which leads to the processor illustrated in Fig. 3-6(b).

It should be noted that the elements of ${}^{w}\underline{S}_r$ of Fig. 3-6(b) are uncorrelated and are equivalent to samples from a unit variance white noise process. This is shown by evaluating the covariance of ${}^{w}\underline{S}_r$; thus

$$E\left[{}^{w}\underline{S}_r\ {}^{w}\underline{S}_r^T\right] = E\left[\underline{W}\,\underline{S}_r\,(\underline{W}\,\underline{S}_r)^T\right] = \underline{W}\,E\left[\underline{S}_r\,\underline{S}_r^T\right]\underline{W}^T$$

$$= \underline{W}\,\underline{K}\,\underline{W}^T = \underline{W}(\underline{W}^T\underline{W})^{-1}\,\underline{W}^T = \underline{I} \tag{3-60}$$

The prewhitening of the observations of $\underline{S}_r$ is illustrated in Fig. 3-7. The scatter diagram exhibiting the correlation between adjacent elements of $\underline{S}_r$ is shown in part (a) of this figure. It is inferred from equation (3-60) that an equivalent representation of ${}^{w}\underline{S}_r$ is a vector consisting of samples from a unit variance process; the scatter diagram of adjacent elements of this processed vector is illustrated in Fig. 3-7(b). To be noted is that the variance along each coordinate axis is equal, resulting in a circular scatter diagram.

When the data become highly correlated the points in the scatter diagram tend to become concentrated along the unity correlation axis; thus the restructuring of the data into the circular scatter diagram requires a gain coefficient greater than unity along the axis perpendicular to the unity correlation axis. For values of data correlation approaching unity, it is reasonable to assume that the

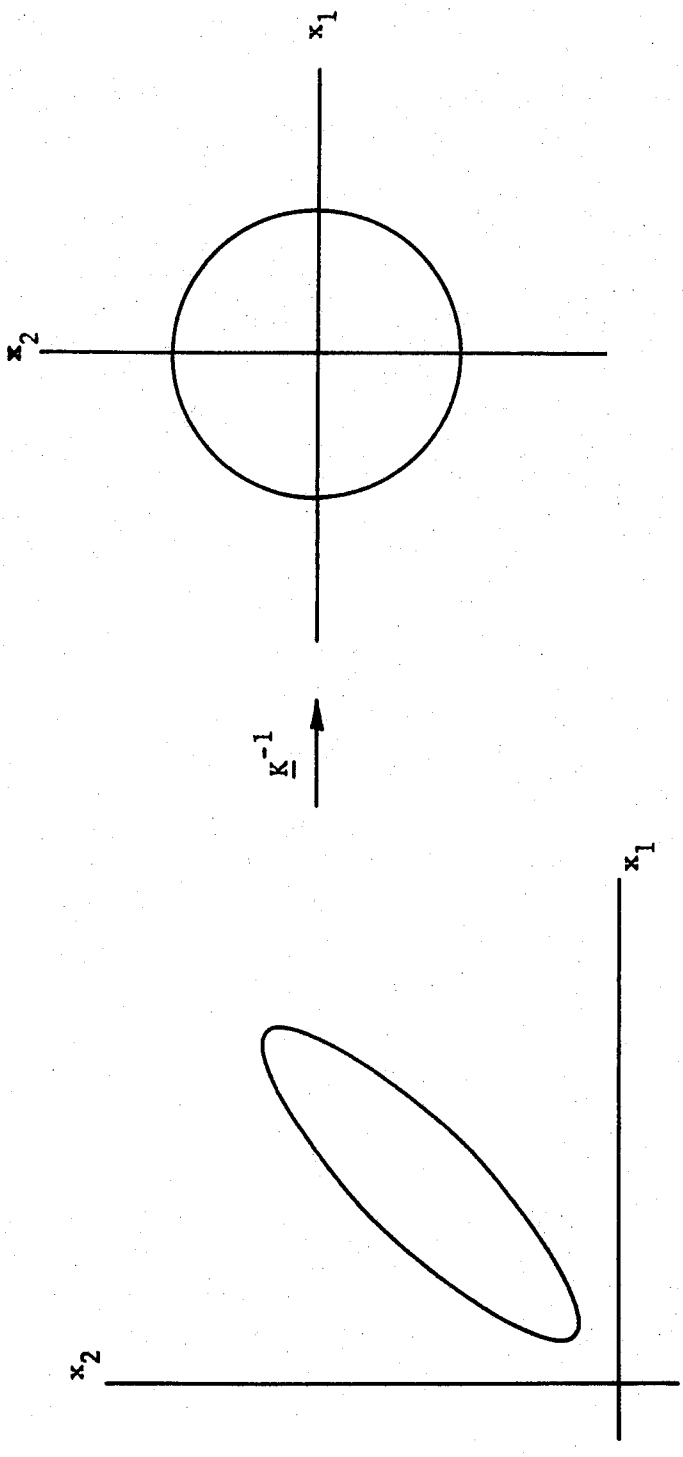

Figure 3-7. Signal Prewhitening.

algorithm will introduce serious numerical error into the processed vector and this resulting vector will be of little value.

Assuming that the covariance matrix of a data set is known, it is suggested that a measure suitable for determining if a vector from this data is amenable to prewhitening is the determinant of $\underline{K}$, or equivalently $\det(\underline{K}^{-1})$. For a unit variance process the value of $\det(\underline{K}^{-1})$ must always satisfy the relation.

$$\det(\underline{K}^{-1}) \geq 1 \tag{3-61}$$

To show this, first note that

$$\det(\underline{K}\,\underline{K}^{-1}) = \det(\underline{I}) = \det(\underline{K})\det(\underline{K}^{-1}) = 1 \tag{3-62}$$

thus,

$$\det(\underline{K}^{-1}) = \frac{1}{\det(\underline{K})} \tag{3-63}$$

A covariance matrix has the properties of being symmetric and positive definite. Thus the matrix $\underline{K}$ is diagonalizable by the similarity transformation [26].

$$\text{diag}(\underline{K}) = \underline{P}^{-1}\,\underline{K}\,\underline{P} \tag{3-64}$$

where $\underline{P}$ is the matrix whose columns are the eigenvectors of $\underline{K}$ and the resulting diagonal elements of $\text{diag}(\underline{K})$ are the eigenvalues λ_i of $\underline{K}$.

This matrix diagonalization is the well known principal component transformation [36], and in general the eigenvalues can be ordered

$$\lambda_1 \geq \lambda_2 \geq \cdots \geq \lambda_n > 0 \tag{3-65}$$

The energy in the process is represented by the sum of the eigenvalues

$$E = \sum_{i=1}^{n} \lambda_i \tag{3-66}$$

The determinant of the diagonal matrix is

$$\det [\text{diag } (\underline{K})] = \prod_{i=1}^{n} \lambda_i \tag{3-67}$$

and by the result derived in Appendix D

$$\det [\text{diag } (\underline{K})] \leq 1 \tag{3-68}$$

which implies that

$$\det [\underline{K}] \leq 1 \tag{3-69}$$

since the value of the determinant of the matrix $\underline{K}$ is invariant under the similarity transformation $\underline{P}^{-1}\ \underline{K}\ \underline{P}$.

Thus, it is concluded that

$$\det (\underline{K}^{-1}) \geq 1 \tag{3-70}$$

The equality holds only for the identity matrix which represents an uncorrelated process. As $\rho \rightarrow 1$ however, the value of $\det(\underline{K}^{-1})$ becomes large because at $\rho = 1$, $\underline{K}$ becomes singular and $\det(\underline{K}) = 0$.

From these considerations it is concluded that there must exist some range of $\det(K^{-1})$ such that

$$1 \leq \det(\underline{K}^{-1}) \leq M_1 < \infty \tag{3-71}$$

where the algorithm will work effectively. For those data sets where $\det(\underline{K}^{-1}) > M_1$, the data become too highly correlated to be of value and consequently should be rejected as a data set to be processed for obtaining registration. For the isotropic data sets this becomes a

matter only of rejecting those data for which the average adjacent cell correlation ρ is greater than some ρ_{max}.

3.5 Multitemporal Data Processor

In processing multitemporal data there must be available a minimum of two data sets; as these data sets are processed pairwise, the discussion will be phrased in terms of two sets. Subsets of data are selected from one set and are used as the processor reference signals. The background data are chosen from the second data set.

It is assumed that the reference signal $\underline{S}_r$ is noise free. It is further postulated that the approximate location of $\underline{S}_r'$, the corresponding data set in the background data set, is known, and that the differences in amplitude between $\underline{S}_r$ and $\underline{S}_r'$ are assumed to be due to additive noise These assumptions allow the development of the signal processor in an analogous manner to that done for the noise free case; the major difference is the addition of a covariance term reflecting the addition of the noise.

3.5.1 Filter Equations for the Multitemporal Processor

In a procedure analogous to that employed in section 3.3.1, the constrained problem is formed with

$$\underline{S}_s = \underline{S}_r + \underline{N} \tag{3-72}$$

The expected value of the output is constrained as

$$I_1 = E[z(r)] = E[\underline{H}^T(\underline{S}_r + \underline{N})] = \underline{H}^T \underline{S}_r = 1 \tag{3-73}$$

with $E[\underline{N}] = 0$. The filter is to have finite energy so that

$$I_2 = \underline{H}^T \underline{H} \leq M < \infty \tag{3-74}$$

The objective is to maximize the ratio given by equation (3-19) by minimizing the variance of the filter output

$$\text{Var}\,[\underline{Z}] = E\left\{ \left[\underline{H}\ (\underline{S} + \underline{N})\right]^T \underline{H}\ (\underline{S} + \underline{N})\right\} \tag{3-75a}$$

$$= \underline{H}^T E\left[(\underline{S}^T + \underline{N}^T)\ (\underline{S} + \underline{N})\right] \underline{H} \tag{3-75b}$$

$$= \underline{H}^T (\underline{K}_s + \underline{K}_n)\ \underline{H} \tag{3-75c}$$

where

$$E[\underline{S}^T \underline{S}] = \underline{K}_s \tag{3-75d}$$

$$E[\underline{N}^T \underline{N}] = \underline{K}_n \tag{3-75e}$$

$$E[\underline{S}^T \underline{N}] = E[\underline{N}^T \underline{S}] = 0 \tag{3-75f}$$

Thus all of the equations of subsection 3.3.1 are now modified by replacing $\underline{K}$ by $\underline{K}_s + \underline{K}_n$. Thus

$$I = \underline{H}^T(\underline{K}_s + \underline{K}_n)\underline{H} + \lambda_1\, \underline{H}^T\, \underline{S}_r + \lambda_2\, \underline{H}^T\underline{H}, \quad \lambda_2 \geq 0 \tag{3-76}$$

which has the solution for the stationary point

$$\underline{H} = -\frac{1}{2}\, \lambda_1\ (\underline{K}_s + \underline{K}_n\ + \lambda_2\, \underline{I})^{-1}\, \underline{S}_r \tag{3-77a}$$

with

$$\underline{H}^T\, \underline{S}_r = 1 \tag{3-77b}$$

$$\underline{H}^T\, \underline{H}\ \leq M \tag{3-77c}$$

As noted previously in the development of equation (3-21), the functional I is convex. Thus the solution for $\underline{H}$, equation (3-78), gives the stationary point of I and this solution is the minimum.

3.5.2 Multitemporal Algorithm Development

For the multitemporal processor both the reference and noise covariance matrices must be determined. Assuming there is sufficient data for computing these matrices, the reference covariance matrix, $\underline{K}_s$, is computed from the reference data as suggested in subsection 3.4.1. The additive noise component is taken to be the differences between the reference data $\underline{S}_r$ and the corresponding data set $\underline{S}'_r$ in the background data. The equation of this noise component is written

$$\underline{N} = \underline{S}'_r - (1 - k)\,\underline{S}_r \tag{3-78}$$

where a differential gain k has been considered. To determine the coefficient k, the stationary point of

$$e^2 = \underline{N}^T\underline{N} = [\underline{S}'_r - (1 - k)\,\underline{S}_r]^T\,[\underline{S}'_r - (1 - k)\,\underline{S}_r] \tag{3-79}$$

with respect to k is found. Thus

$$\frac{\partial e^2}{\partial k} = 2\,[\underline{S}'_r - (1 - k)\,\underline{S}_r]^T\,\underline{S}_r = 0 \tag{3-80}$$

which has the solution

$$k = 1 - \frac{\underline{S}_r^T\,\underline{S}_r}{\underline{S}_r^T\,\underline{S}_r} \tag{3-81}$$

This value of k yields the minimum of e^2 since this functional is convex.

The noise covariance matrix $\underline{K}_n$ can now be computed. With $\underline{K}=\underline{K}_s + \underline{K}_n$ the algorithms of section 3.4 are applicable to the multitemporal processor.

The difficulties encountered in the solution of equation (3-77) for the multitemporal processor include those requirements observed in subsection 3.4.1, the necessity for handling very large arrays. However, a more fundamental problem is the unavailability of a sufficiently large set of data, having similar statistical properties as the reference data, such that a useful estimate of $\underline{K}_s$ can be made. An additional difficulty is encountered in estimating the noise properties. With the noise defined as the differences between $\underline{S}_r$ and $\underline{S}_r'$, the determination of $\underline{K}_n$ requires that these data be essentially in registration such that the differences are due to scene changes and are not the result of misregistration error.

3.6 Correlator Signal-to-Noise Ratio

A signal-to-noise ratio for the processor is derived for the purpose of giving a measure of performance to the correlator. A dimensionless quantity is desired, thus define

$$\frac{S}{N} = \frac{z^2(r)}{\text{Var}\,[\underline{Z}]} \tag{3-82}$$

The result is derived for $\lambda_2 = 0$; thus from equations (3-73) and (3-75)

$$\frac{S}{N} = \frac{(\underline{H}^T \underline{S}_r)^2}{\underline{H}^T \underline{K}\, \underline{H}} \tag{3-83}$$

$$= \frac{\left[-\lambda_1 (\underline{K}^{-1}\underline{S}_r)^T \underline{S}_r\right]^2}{(-\lambda_1 \underline{K}^{-1} \underline{S}_r)^T \underline{K} (-\lambda_1 \underline{K}^{-1} \underline{S}_r)} \tag{3-84}$$

$$= \frac{(\underline{S}_r^T \underline{K}^{-1} \underline{S}_r)^2}{\underline{S}_r^T \underline{K}^{-1} \underline{S}_r} \tag{3-85}$$

$$= \underline{S}_r^T \underline{K}^{-1} \underline{S}_r \tag{3-86}$$

For the noise free case, $\underline{K}_n = \underline{0}$

$$\frac{S}{N} = \underline{S}_r^T \underline{K}_s^{-1} \underline{S}_r \tag{3-87a}$$

$$= \mathrm{Tr}\,(\underline{S}_r \underline{K}_s^{-1} \underline{S}_r^T) = N \tag{3-87b}$$

where N is the number of observations averaged. For $\underline{K}_n \neq \underline{0}$

$$\frac{S}{N} = \underline{S}_r^T (\underline{K}_s + \underline{K}_n)^{-1} \underline{S}_r \tag{3-88}$$

In the derivation of an equivalent result by Arcese *et al.* [6], there is an error in the derivation. A development such as suggested by these authors is given in Appendix C and the result is shown to be consistent with equation (3-87).

CHAPTER 4

EXPERIMENTAL RESULTS

4.0 Introduction

In this chapter certain of the algorithms developed in the previous chapters are applied to both ideal data sets and to imagery obtained with a line-scanning spectrophotometer mounted in an aircraft. The algorithms used with a specific data set, and taken collectively, are termed a processor. The results obtained using the ideal data are presented first, followed by the application of the processor to a scanner data set in which the reference data $\underline{S}_r$ is selected as a subimage of the background data. This, of course, yields a distortionless and noise free reference data set.

Multitemporal data sets are then considered. Search techniques utilizing the modulus of the Fourier transform of these data are used to estimate the regional geometric distortion, and results of the processor operating with these corrected data are obtained.

4.1 Ideal Data

The purpose of generating ideal data sets is to obtain picture functions with known statistical properties. These data are then used to both check for the correct operation of the computer codes as well as to evaluate the performance of the processing algorithms with variations in the data parameters. These ideal data were obtained by

convolving a two-dimensional array of computer generated random numbers, having a Gaussian distribution, with a two-dimensional low-pass filter having a specified impulse response.

Two sets of ideal data were generated, differing in the form of the filter used to smooth the set of random numbers. The impulse response of the first of these filters was chosen so as to obtain a data set with a covariance function modeled by equation (3-38); this data set exhibits a strong correlation of the data along the coordinate axes. An alternative data set having no preferential direction of data correlation was obtained with the second filter.

4.1.1 Separable Exponential Filter

The impulse response of the filter used in this subsection, termed the "separable exponential filter," is given by

$$h(\underline{x}) = k_1 \exp\left[-\frac{1}{R_o}(x_1 + x_2)\right] \qquad (4\text{-}1)$$

$$|x_i| \leq R, \quad i = 1,2$$

The normalization coefficient k_1, derived in Appendix B, is

$$k_1 = \left\{4 R_o \left[1 - \exp\left(\frac{R}{R_o}\right)\right]\right\}^{-2} \qquad (4\text{-}2)$$

where R_o is defined as the "characteristic length" of the filter. The variable R is the size of the truncated impulse response with both R and R_o being measured in units of picture elements. A plot of the impulse of this filter is shown in Fig. 4-1(a).

This filter was chosen so as to yield a data set with statistical properties closely approximating the isotropic exponential covariance matrix defined by equation (3-38). Thus the processor for this data

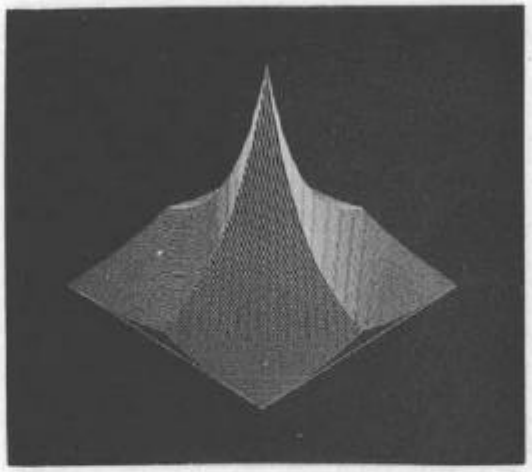

(a) Filter Impulse Response

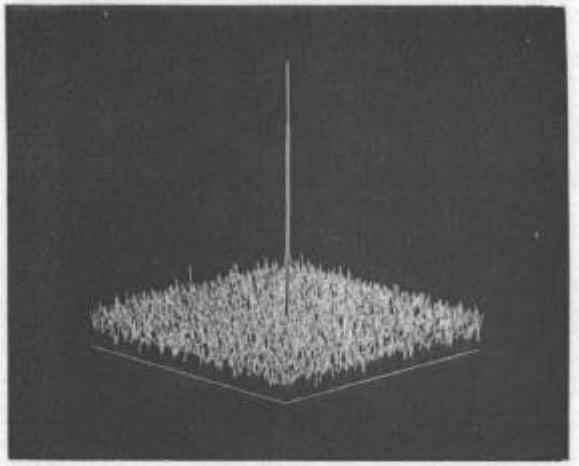

(b) $R_o = 0.0$

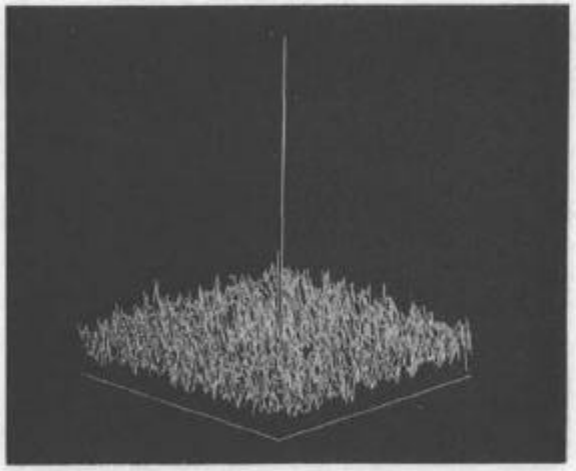

(c) $R_o = 0.5$

Figure 4-1 Correlator Outputs for Various Amounts of Data Correlation (Separable Exponential Filter)

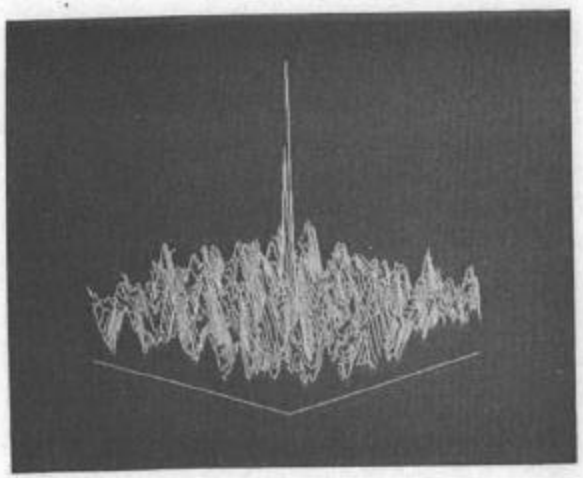

(d) $R_o = 1.0$

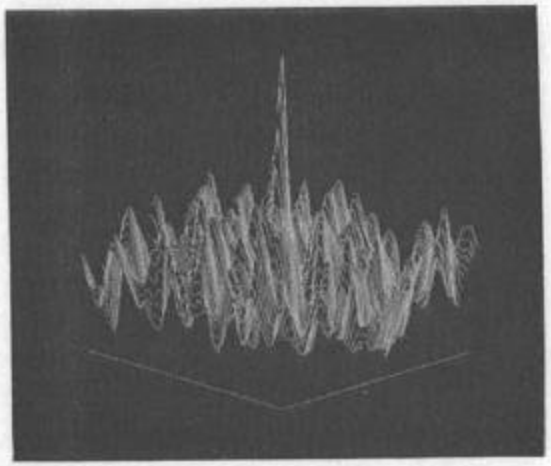

(e) $R_o = 2.0$

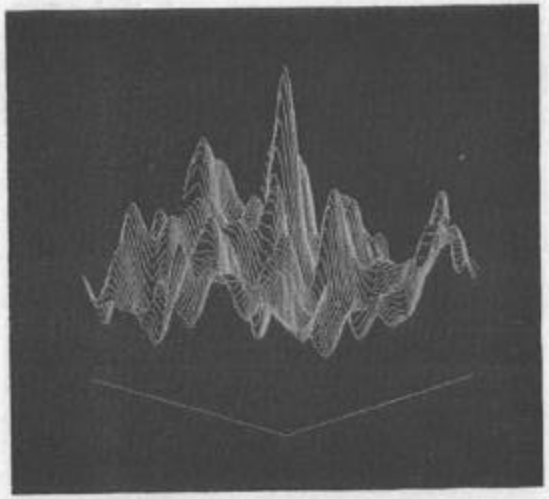

(f) $R_o = 4.0$

Figure 4-1 Cont.

set is the crosscorrelation of the background data with the template given by equation (3-46). This template is obtained by simply by convolving the grid operator G

$$\underline{G} = \begin{bmatrix} \rho^2 & -\rho(1+\rho^2) & \rho^2 \\ -\rho(1+\rho^2) & (1+\rho^2)^2 & -\rho(1+\rho^2) \\ \rho^2 & -\rho(1+\rho^2 & \rho^2 \end{bmatrix} \qquad (4\text{-}3)$$

with the subimage of the background data selected as the reference data set $\underline{S}_r$. The adjacent cell correlation coefficient ρ of the reference data $\underline{S}_r$ is used to determine the grid operator, and experimentally observed values of ρ for various values of R_o and template sizes are given in Table 4-1(a).

The processor outputs are shown in Figs. 4-1(b)-(f) for data sets having specified values of R_o and where the template is a subimage of the background data. The correlator template size for these results was 32 x 32 picture elements. There are several properties of these outputs which are of interest. The most obvious result is that the output function becomes smoother and the pedestal variance, relative to the central peak, increases as R_o increases; an increase in R_o decreases the spatial frequency bandwidth of the two-dimensional signal. Thus as the spatial-frequency bandwidth is reduced, there is both a loss in signal-to-noise ratio, as defined by equation (3-19), and a loss of resolution. In this application resolution is defined as the width of the central correlation peak at one-half its height.

It is also observed that the peak values of the output in the pedestal region appear to be distributed such that there are no large distinct peaks in this region. Thus, a unique central peak can be

Table 4-1. Experimental Values of the Average Adjacent Cell Correlation Coefficient (ρ).

(a) Separable Exponential Filtered Data

Template Size	Filter Characteristic Length (R_o) 0.0	0.5	1.0	2.0	4.0
32 x 32	.049	.309	.652	.868	.953
48 x 48	-.009	.296	.647	.874	.954
64 x 64	-.013	.297	.650	.887	.962

(b) Isotropic Exponential Filtered Data

Template Size	Filter Characteristic Length (R_o) 0.0	0.5	1.0	2.0	4.0
32 x 32	.049	.254	.658	.902	.972
48 x 48	-.009	.260	.676	.904	.964
64 x 64	-.013	.268	.699	.902	.967

unambiguously located.

Ideally the processor for the noise free signal given by equation (3-27) is the inverse of the filter used to obtain the data. Defining a parameter α with

$$0 \leq \alpha \leq 1 \tag{4-4}$$

as the prewhitening coefficient and choosing

$$p' = \alpha\, p \tag{4-5}$$

as the parameter for the grid operator, equation (4-3), yields the set of outputs shown in Fig. 4-2. The background data set used for this sequence of correlator outputs was obtained with a filter having the parameter $R_o = 2$, and the correlator template was 32 x 32 picture elements in size.

For the case of $\alpha = 0.0$, the processor reduces to a cross-correlation between the background data $\underline{S}_b$ and a template consisting of a subscene of $\underline{S}_b$. For $\alpha = 1.0$, the processor ideally implements the inverse filter. The effect of the prewhitening coefficient for $\alpha \leq 0.5$ is observed to be small. However for $\alpha \geq 0.7$, the processor template begins to significantly alter the correlator output.

Experimentally obtained curves giving the output signal-to-noise ratio as a function of the prewhitening coefficient are given in Fig. 4-3. This family of curves for various values of filter characteristic length was obtained by computing the processor output for each of the set of data parameters (R_o, α) where the processor template was 32 x 32 picture elements in size. The signal-to-noise ratio of each of these correlator outputs was then determined. The signal component

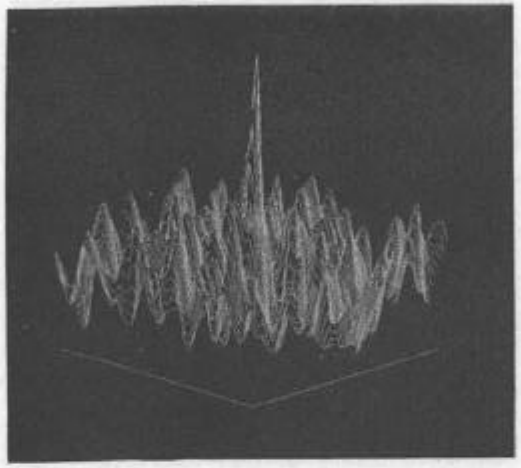

(a) $\alpha = 0.0$

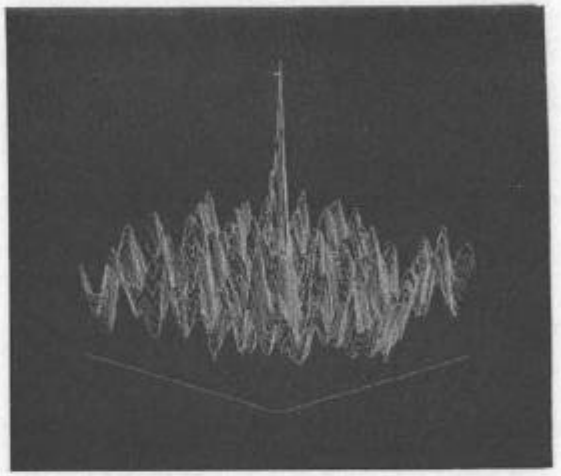

(b) $\alpha = 0$

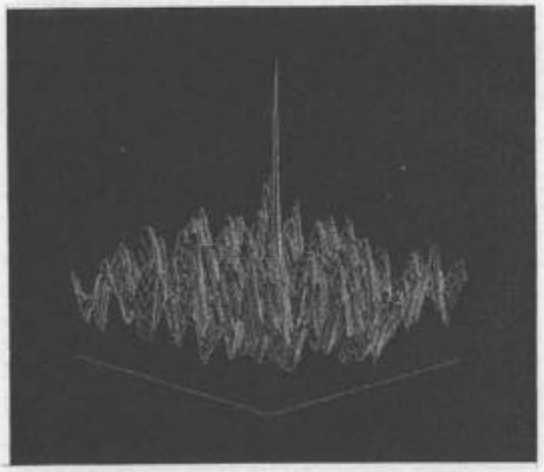

(c) $\alpha = 0.5$

Figure 4-2 Correlator Outputs for Various Prewhitening Coefficients (Separable Exponential Filter)

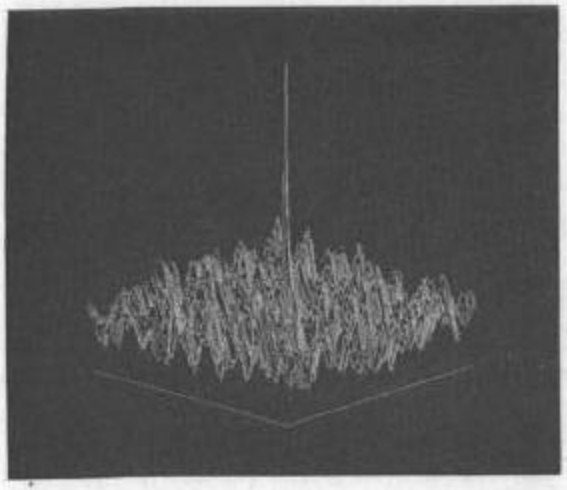

(d) $\alpha = 0.7$

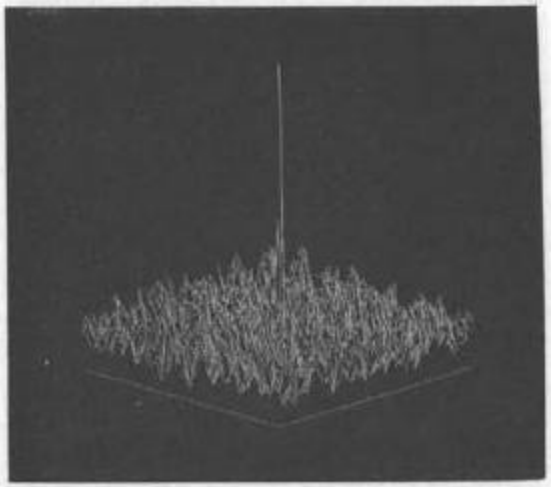

(e) $\alpha = 0.9$

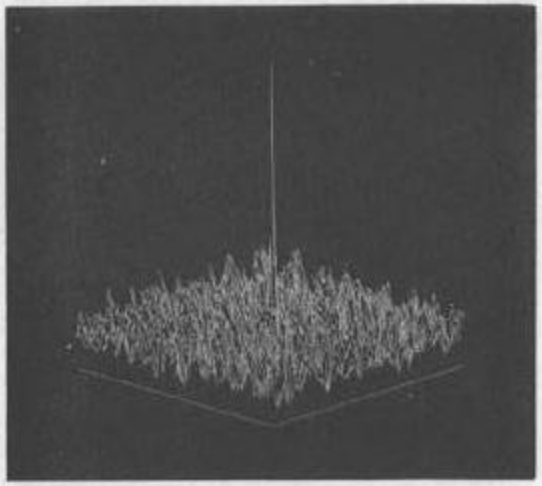

(f) $\alpha = 1.0$

Figure 4-2 Cont.

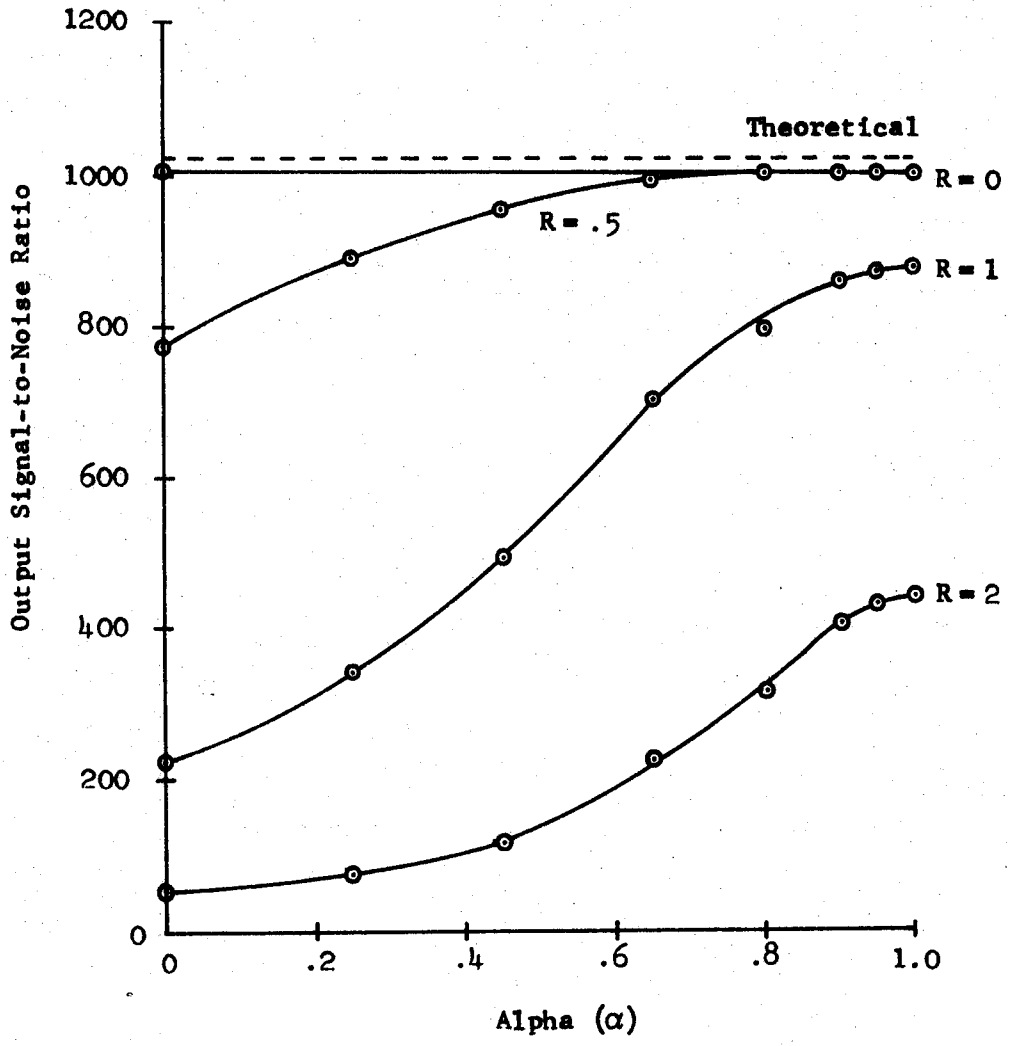

Figure 4-3 Correlator Output Signal-to-Noise Ratio as a Function of the Prewhitening Coefficient (Separable Exponential Filter)

is defined as the square of the difference of the amplitude of the central peak and the average value of the output in the pedestal region. Thus

$$S_c = \left[z(\underline{r}) - \langle z(\underline{u}) \rangle_{\underline{u} \neq \underline{r}} \right]^2 \tag{4-6}$$

The noise component is defined as the variance of the correlator in the pedestal

$$N_c = \frac{1}{N_p - 1} \sum_{u_1=1}^{N} \sum_{u_2=1}^{N} \left[z(\underline{u}) - \langle z(\underline{u}) \rangle_{\underline{u} \neq \underline{r}} \right]^2_{\underline{u} \neq \underline{r}} \tag{4-7}$$

where N_p is the number of points used in the summation. It should be noted that the condition $\underline{u} \neq \underline{r}$ used in equations (4-6) and (4-7) implies that the central peak was deleted and not just the point $\underline{u} = \underline{r}$. The average value $\langle \cdot \rangle$ was also taken of the set of points having the central peak deleted.

The significant results to be obtained from these plots are that the signal-to-noise ratio increased approximately 6 dB for reasonably correlated data and that the slope of each of the curves near $\alpha = 1.0$ is relatively small. This latter observation means that the processor is relatively insensitive to the choice of ρ for values of ρ near the correct value ρ_c. The performance of the processor for each value of R_o is given in Table 4-2.

The processor output signal-to-noise ratio, given by equation (3-88b), is theoretically independent of the adjacent cell correlation coefficient. However, for the class of data being considered in this section, as $\rho \rightarrow 1$ the amplitude of the data must approach a constant value. Curves giving experimental results of the output signal-to-noise

Table 4-2. Correlator Performance for the Separable Exponential Filtered Data.

R_o	ρ	$G_{\alpha=0}$	$G_{\alpha=1}$	Processor Gain (dB)
0	.049	1006	1001	0
0.5	.309	773	1001	1.1
1.0	.652	224	878	5.9
2.0	.868	52.6	441	9.2

ratio as a function of ρ are given in Fig. 4-4. It is observed that the correlator output signal-to-noise ratio decreases by approximately 3 dB at $\rho = 0.9$. For values of $\rho \geq 0.9$ the signal-to-noise drops precipitously. It is concluded that the processor yields acceptable results for the range $0 \leq \rho \leq 0.9$, and the value of the results for $\rho > 0.9$ is questionable.

4.1.2 Isotropic Exponential Filter

The experimental procedure of subsection 4.1.1 is repeated in this subsection where the data are obtained by convolving the two-dimensional array of random numbers with a circularly symmetrical exponential filter. The impulse response of this filter is of the form

$$h(\underline{x}) = k_2 \exp\left[-\frac{1}{R_o}(x_1^2 + x_2^2)^{1/2}\right] \qquad (4\text{-}8)$$

$$|x_i| \leq R, \quad i = 1,2,$$

where the normalization coefficient k_2, derived in Appendix B, is given by

$$k_2 = \left\{ 2\pi R_o \left[1 - (1 + \frac{R}{R_o}) \exp(-\frac{R}{R_o})\right] \right\}^{-1} \qquad (4\text{-}9)$$

The parameter R_o is defined as the characteristic length of the filter as was done earlier in equation (4-2). The variable R is the size of the filter, and both R and R_o are measured in terms of picture elements. A plot of the impulse response of this filter is shown in Fig. 4-5(a).

The data set used in subsection 4.1.1 had preferential correlation directions introduced by the filter defined by equation (4-1). The filter used in this section was selected so as not to introduce such

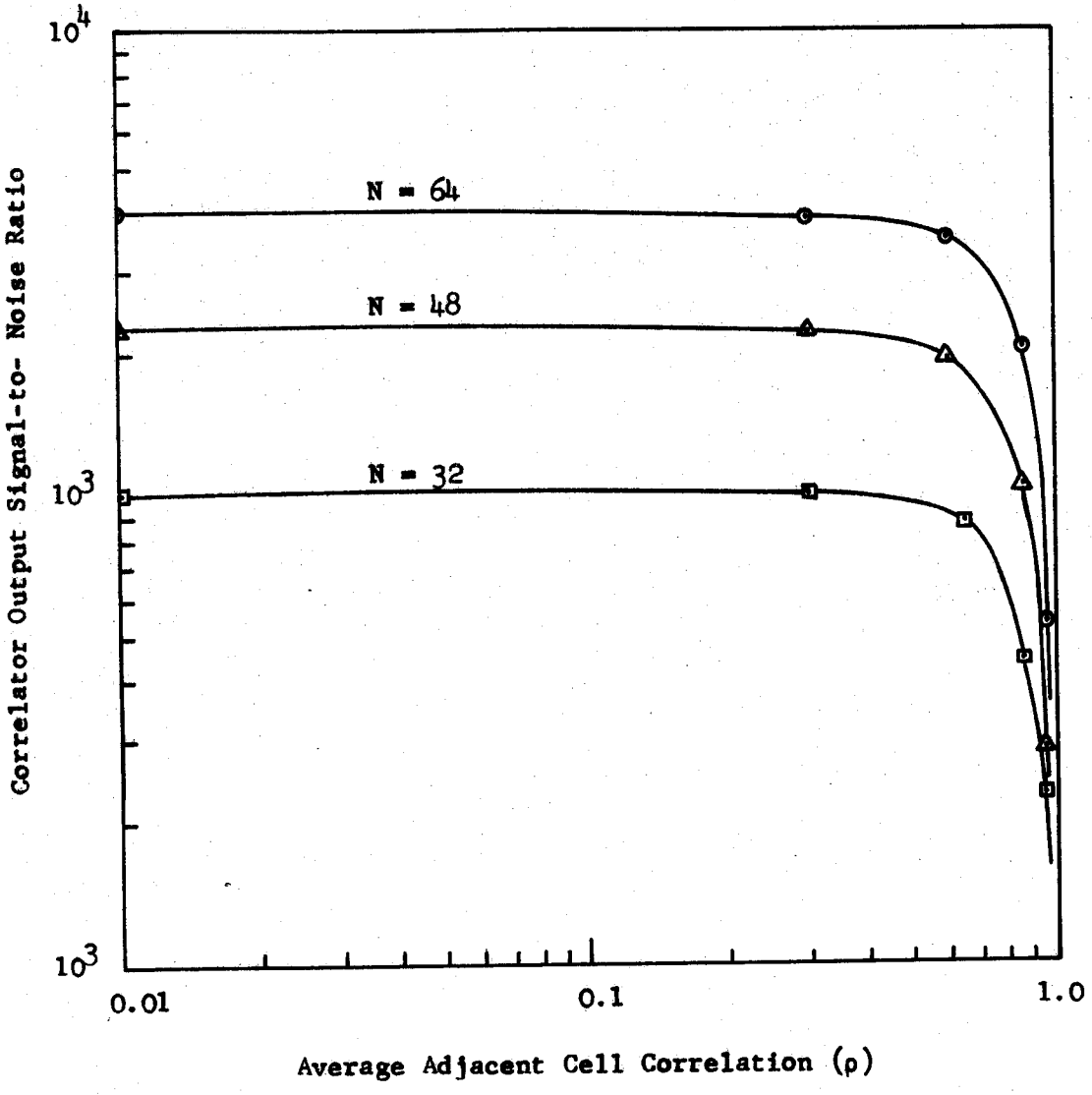

Figure 4-4 Correlator Output Signal-to-Noise Ratio as a Function of the Average Adjacent Cell Correlation (Separable Exponential Filter)

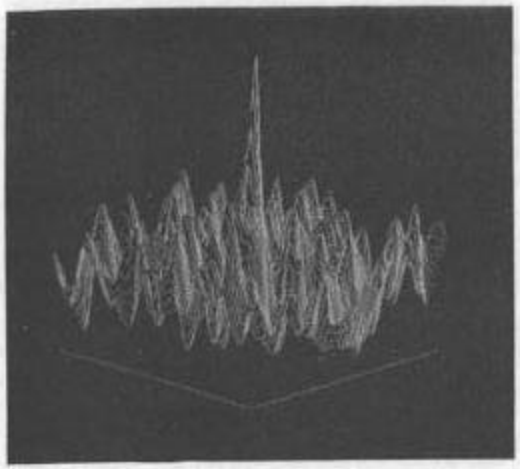

(a) $\alpha = 0.0$

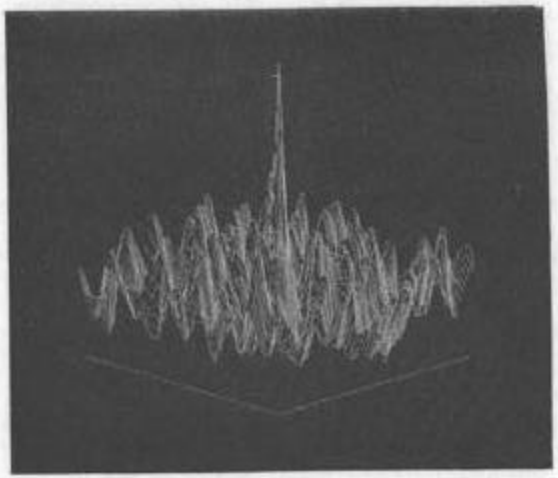

(b) $\alpha = 0$

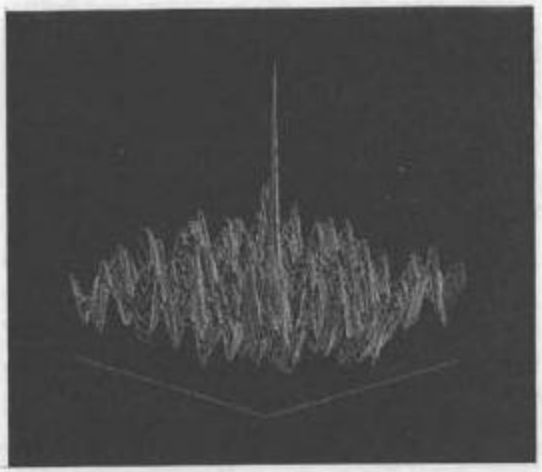

(c) $\alpha = 0.5$

Figure 4-2 Correlator Outputs for Various Prewhitening Coefficients (Separable Exponential Filter)

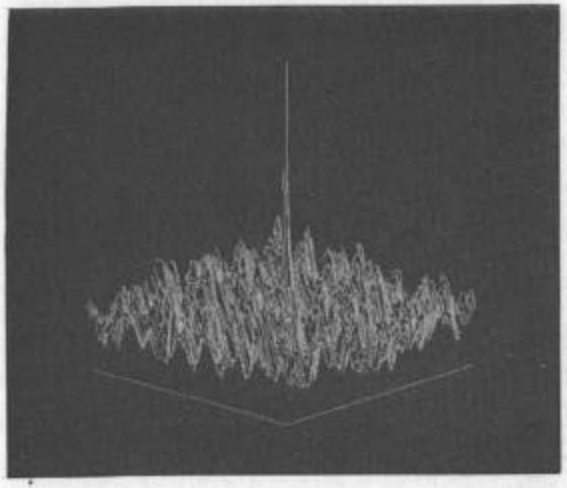

(d) $\alpha = 0.7$

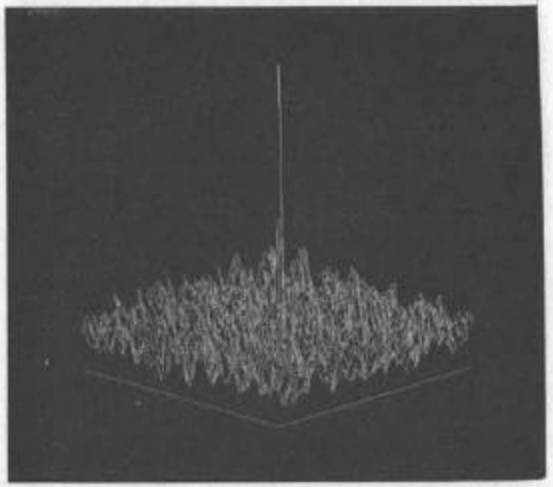

(e) $\alpha = 0.9$

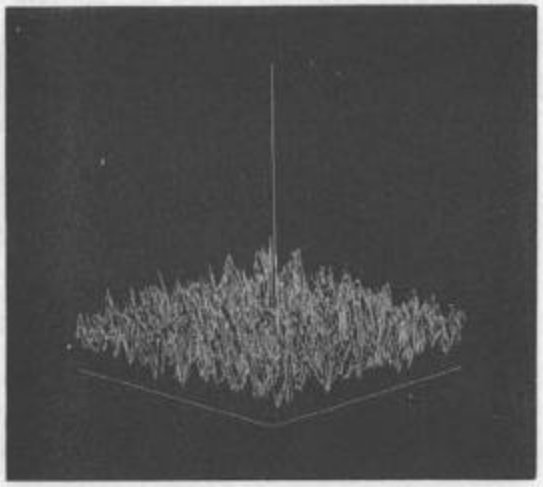

(f) $\alpha = 1.0$

Figure 4-2 Cont.

preferential directions into the correlation function; this filter is termed the "isotropic exponential filter." Observed values of ρ for various values of R_o and template sizes are given in Table 4-1(b).

The purpose of this experimental procedure is to compare the results of subsection 4.1.1 with the processor performance when the data set has statistical properties other than those given by equation (3-38). The correlator outputs for corresponding values of R_o as used in Fig. 4-1, but using this isotropic set of data as the input, are shown in Figs. 4-5(b)-(e). The template size was again 32 x 32 picture elements. Comparing the corresponding outputs in Figs. 4-1 and 4-5 shows that the outputs have very similar characteristics.

Defining ρ' and α as in the previous section, the sequence of processor outputs as the prewhitening coefficient α is varied, is given in Fig. 4-6. The data used in this sequence were obtained with the filter having $R_o = 2.0$ and the correlator template size was 32 x 32 elements.

The numerical results of the two sequences of experiments shown in Figs. 4-5 and 4-6 are summarized by the curves of Fig. 4-7. The identical procedure for determining the signal-to-noise ratios as used to obtain Fig. 4-3, was used to compute the curves of Fig. 4-7. The performance of the processor with the isotropic data set is summarized in Table 4-3.

Care must be used in comparing the results shown in Figs. 4-3 and 4-7 because the value of the average adjacent cell correlation coefficient differs between the data sets for the same value of R_o.

(a) $\alpha = 0.0$

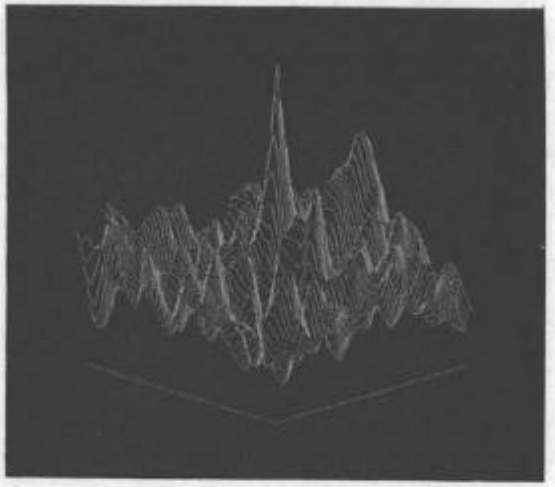

(b) $\alpha = 0.3$

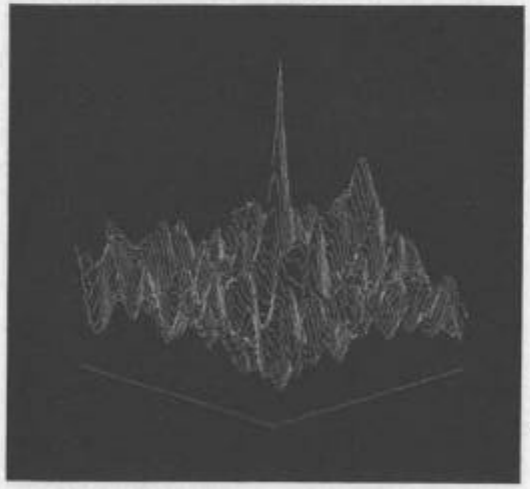

(c) $\alpha = 0.5$

Figure 4-6 Correlator Outputs for Various Prewhitening Coefficients (Isotropic Exponential Filter)

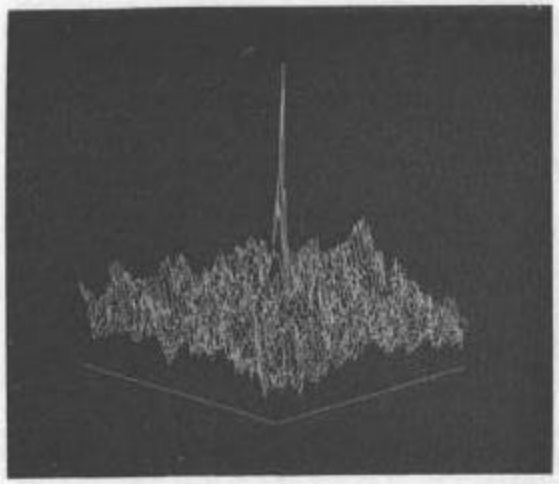

(d) $\alpha = 0.7$

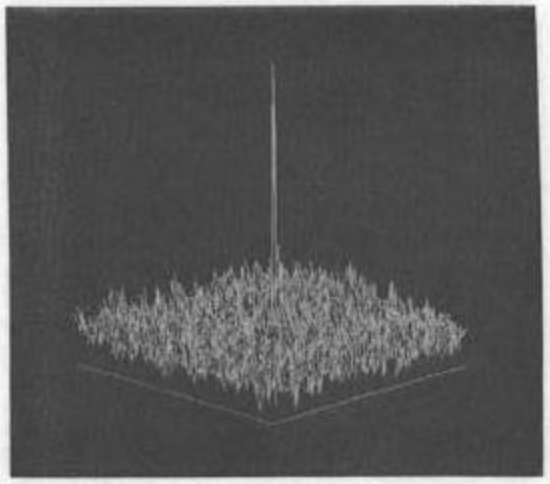

(e) $\alpha = 0.9$

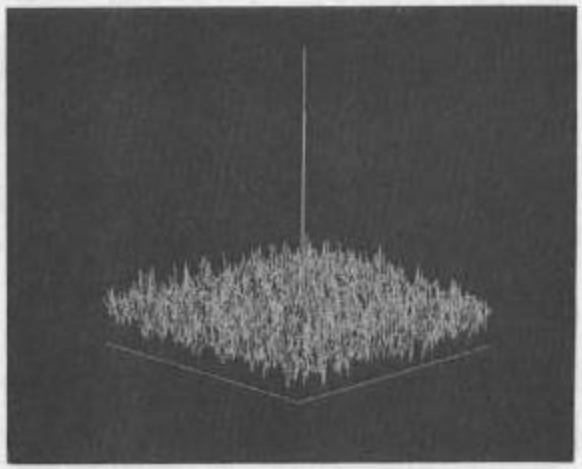

(f) $\alpha = 1.0$

Figure 4-6 Cont.

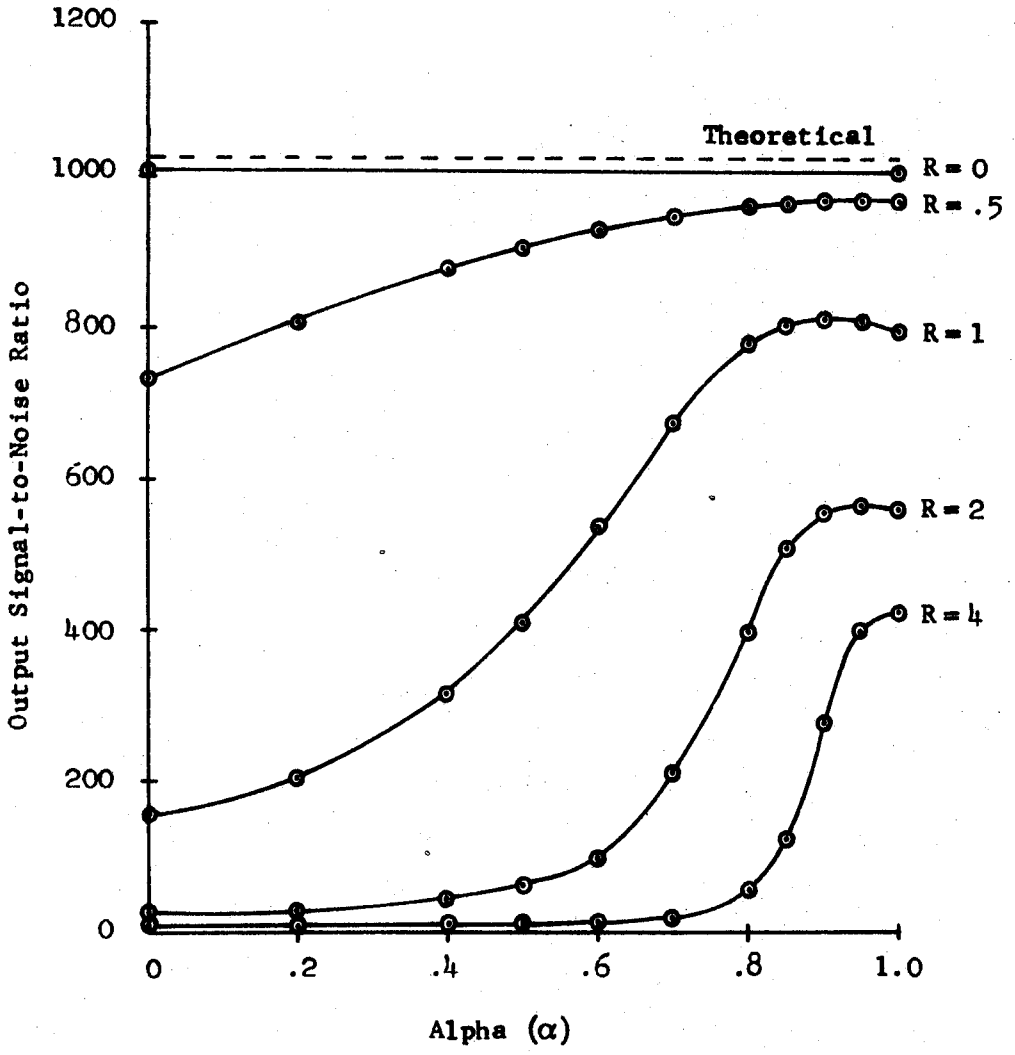

Figure 4-7 Correlator Output Signal-to-Noise Ratio as a Function of the Prewhitening Coefficient (Isotropic Exponential Filter)

Table 4-3. Correlator Performance for the Isotropic Exponential Filtered Data

R_o	ρ	$G_{\alpha=0}$	$G_{\alpha(MAX)}$	Processor Gain (dB)
0	0.049	1006	1005	0
0.5	.254	735	967	1.2
1.0	.654	153	813	7.2
2.0	.902	28.5	558	12.9
4.0	.972	9.58	423	16.6

However, it is readily observed that the curve for $R_o = 0.5$ of Fig. 4-7 does not reach the curve for $R_o = 0$. In addition the curves of Fig. 4-7 have their peak values at approximately $\alpha = 0.95$.

Fig. 4-9 gives the correlator output signal-to-noise ratio as a function of the average adjacent cell correlation for the family of curves generated by templates having N x N elements. Comparing Fig. 4-9 to the corresponding earlier result shown in Fig. 4-4 yields insignificant differences. Thus it is concluded that the processor is not critically dependent on the exact form of the covariance function of the data in order to give acceptable performance.

Certain additional results were computed using the data set obtained with the isotropic exponential filter. The correlator output for various sizes of templates is shown in Fig. 4-8. The data set used was obtained using the filter with $R_o = 2.0$ and the template sizes were N x N picture elements where the values of N were 32, 48 and 64. It is observed that the variance in the pedestal decreases as N increases; however, the width of the central peak remains essentially unchanged.

In Fig. 4-10 the processor output signal-to-noise ratio is plotted as a function of the template size; in these plots the independent variable was chosen as N where the number of picture elements in the template is N x N. Fig. 4-10(a) gives the results where the template is a subimage of the background whereas Fig. 4-10(b) gives the results where the template is obtained by the processor for the prewhitening coefficient $\alpha = 1.0$. It is of interest to note that the results of Fig. 4-10(b) are a series of linear loci and are approximately parallel.

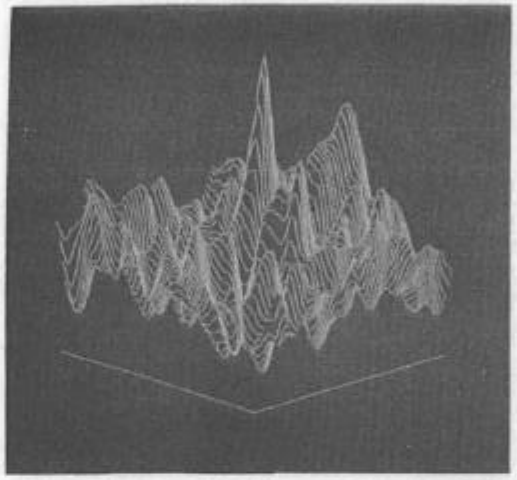

$N^2 = 1024$

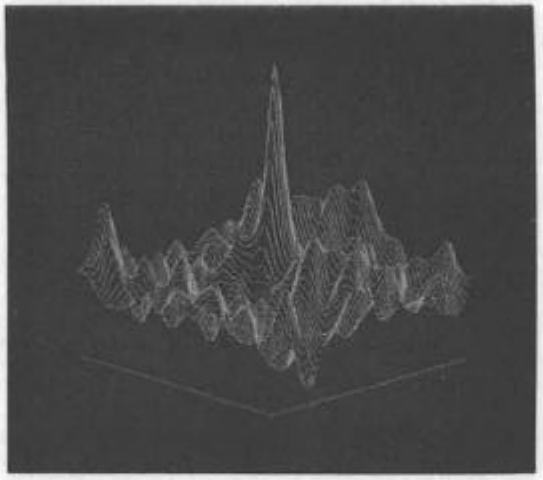

$N^2 = 2304$

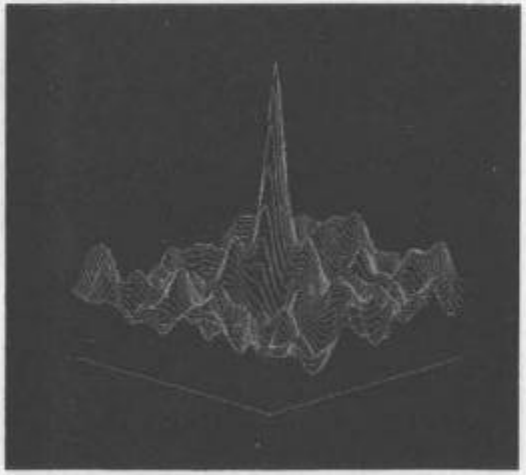

$N^2 = 4096$

Figure 4-8 Correlator Output for Various Template Sizes

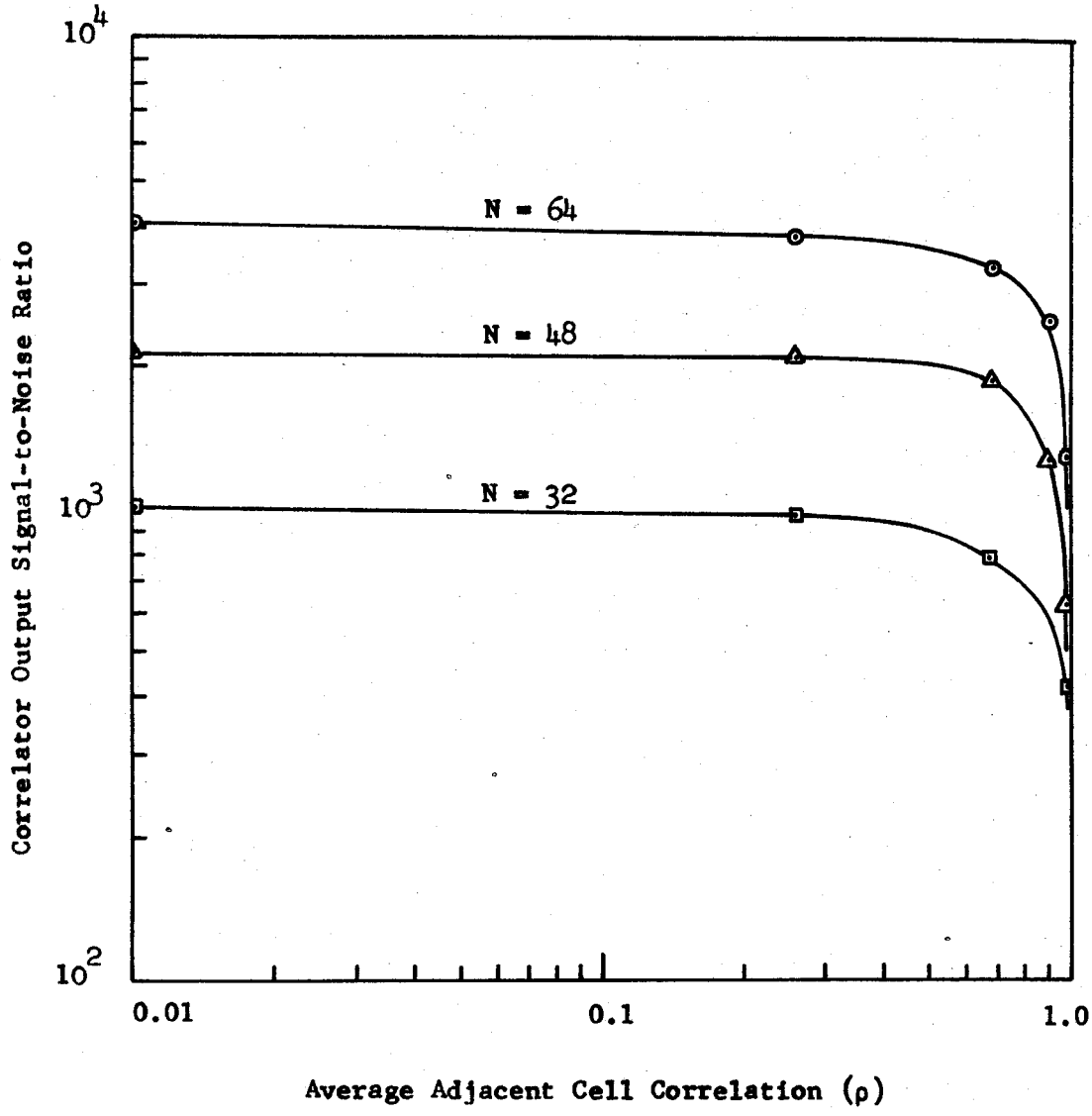

Figure 4-9 Correlator Output Signal-to-Noise Ratio as a Function of the Average Adjacent Cell Correlation (Isotropic Exponential Filter)

Figure 4-10 Correlator Output Signal-to-Noise Ratio as a Function of Template Size (Isotropic Exponential Filter)

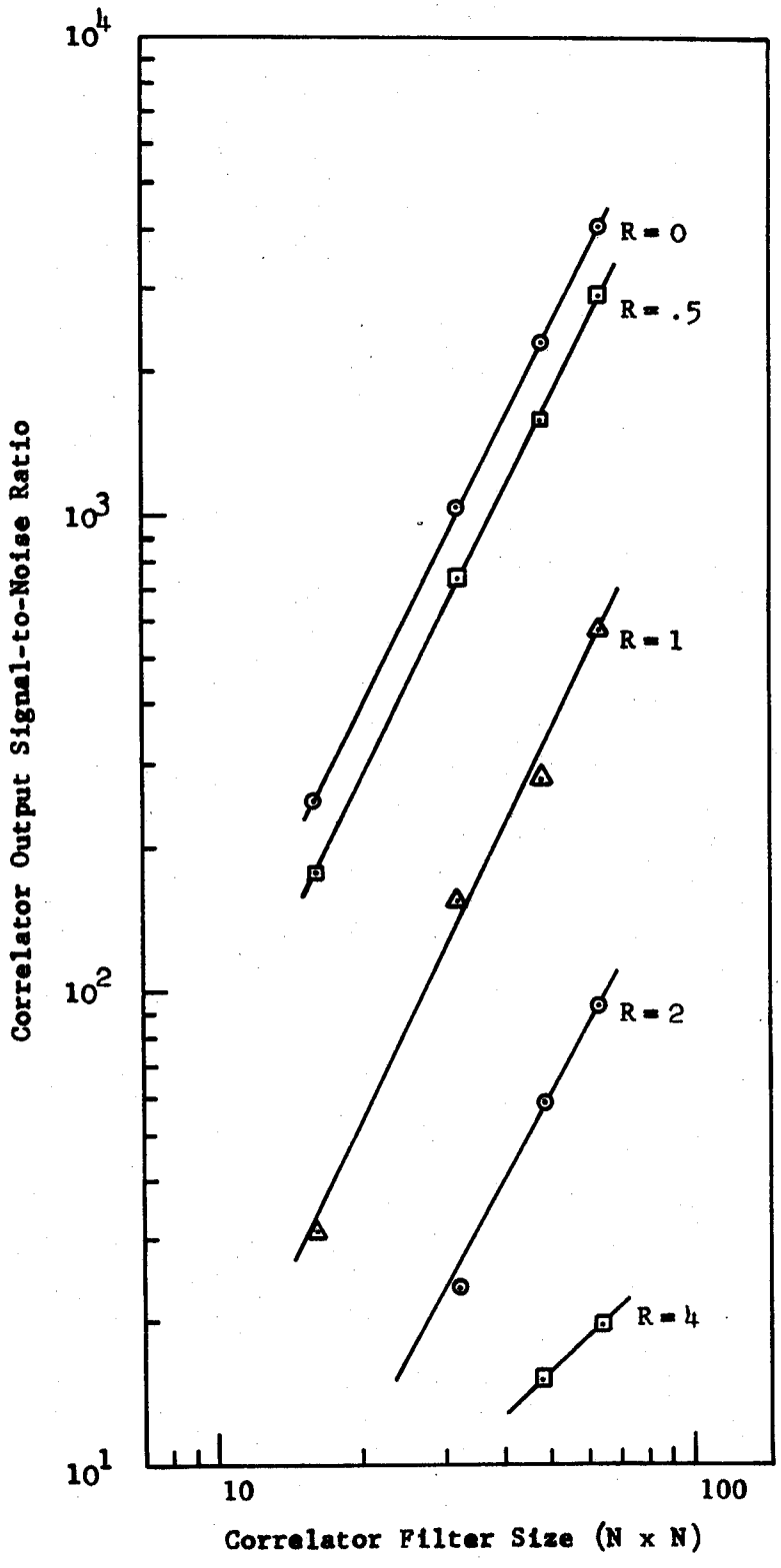

(a) Image Template

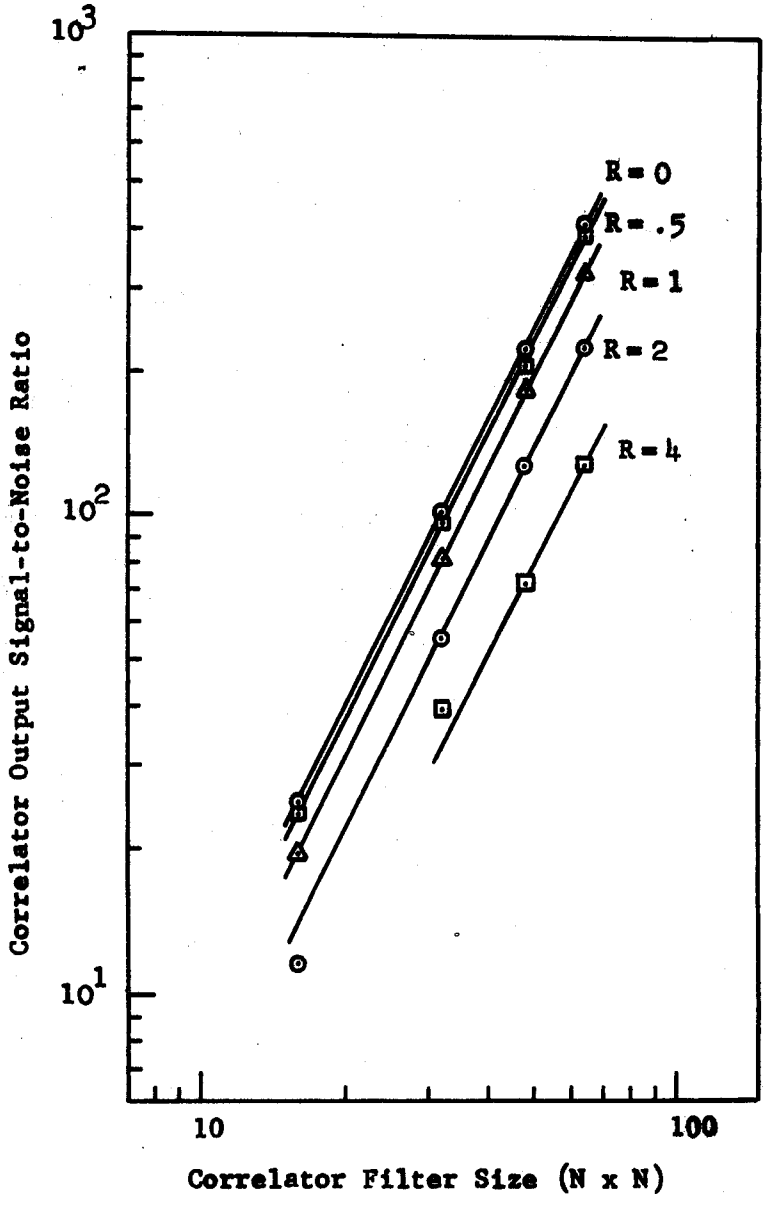

(b) Processor Template

Figure 4-10 Cont.

From the results of the two previous sections, it is observed that the differences which exist between corresponding processor outputs for the two data sets are not significant. Thus it is suggested that this processor which is developed for the class of data sets having isotropic exponential covariance may be applicable to data having different statistical properties. An additional result of interest is the smoothness of the curves of signal-to-noise ratio as a function of the prewhitening coefficient for values of α near $\alpha = 1$. This suggests that the choice of a value for ρ is not a critical factor for the processor to yield useful results.

4.1.3 Signal-to-Noise Ratios for Geometrically Distorted Data

If geometrical distortion exists between two corresponding sets of data, there results a loss in the correlator output signal-to-noise ratio compared to the value obtainable using undistorted data. An experimental verification of this statement was obtained and the results are shown in Figs. 4-11(a) through (c). These curves were computed using the ideal data discussed in section 4.1.

The distorted data were obtained by rotating the set of computer generated random numbers with a nearest-neighbor interpolation algorithm. Following this rotation these data were convolved with the isotropic exponential filter, equation (4-8), having the appropriate choice of characteristic length R_o. These data were then crosscorrelated with a similarly filtered set of undistorted data, and the resulting output signal-to-noise ratio was determined.

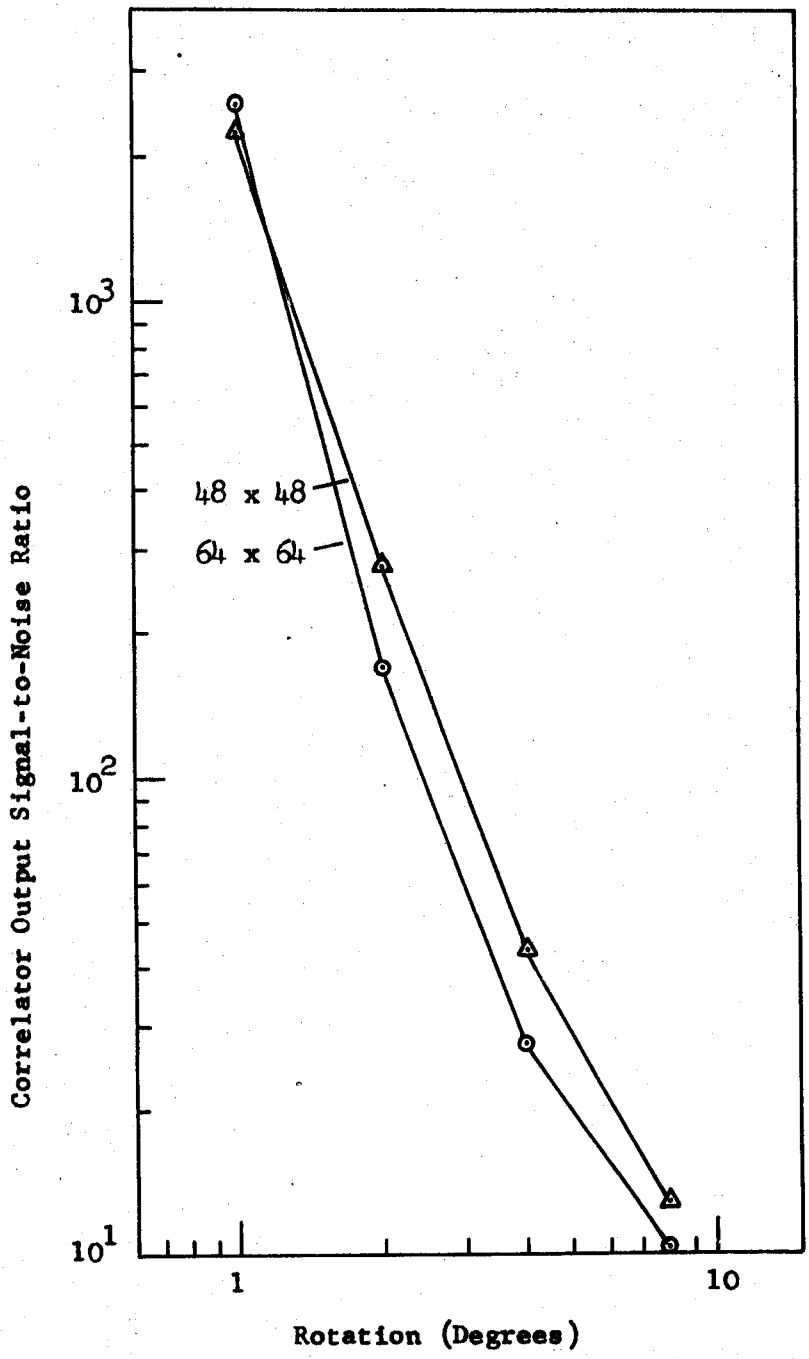

(a) $R_o = 0.0$

Figure 4-11 Correlator Output Signal-to-Noise Ratio as a Function of Rotational Misregistration (Isotropic Exponential Filter)

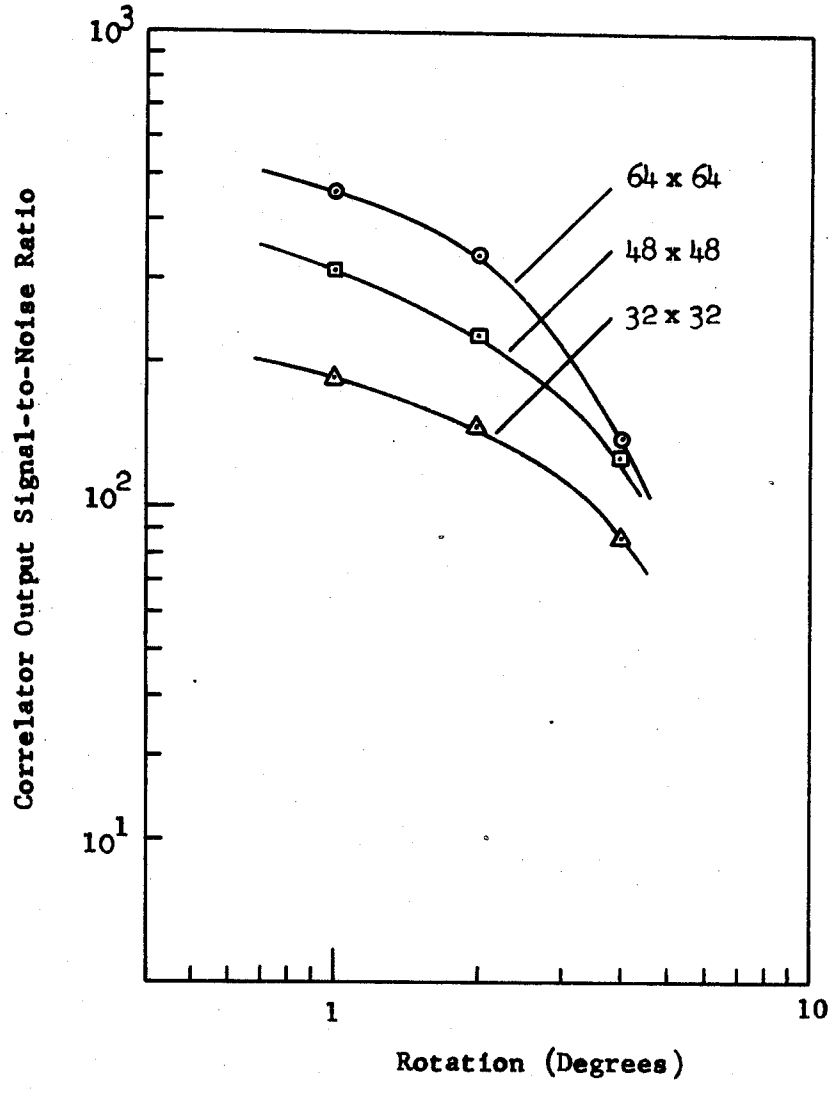

(b) $R_o = 1.0$

Figure 4-11 Cont.

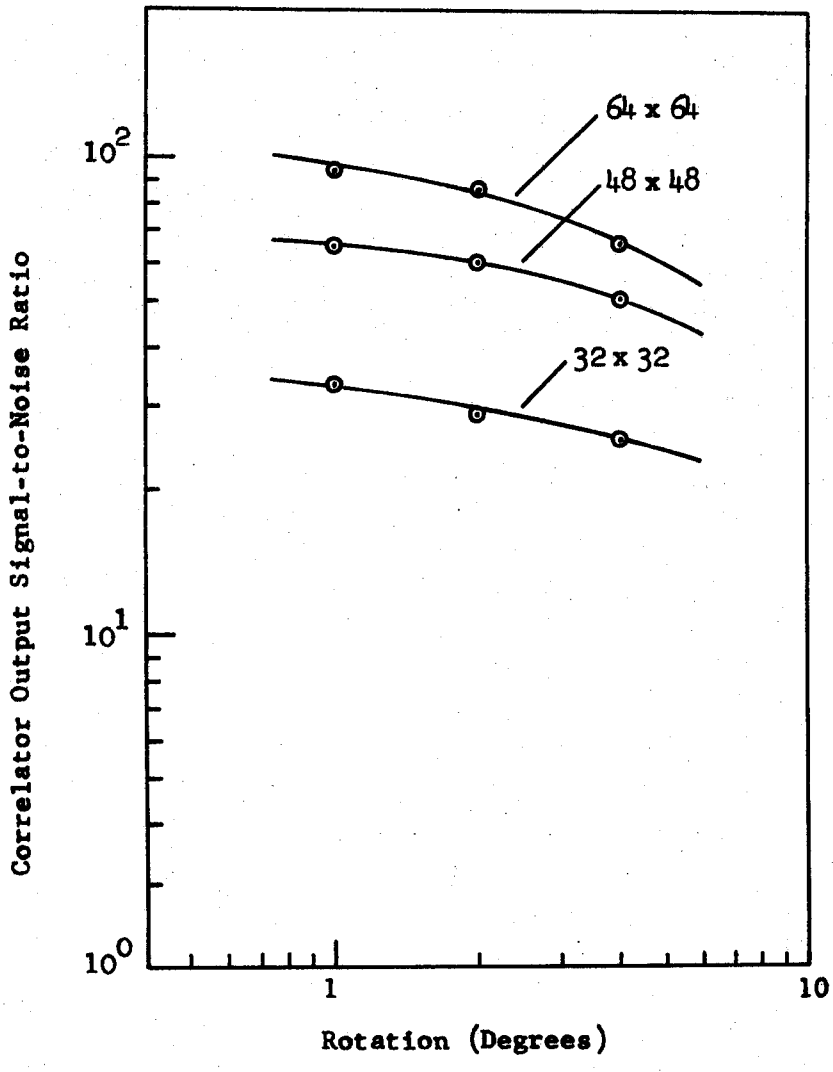

(c) $R_o = 2.0$

Figure 4-11 Cont.

The significant results shown by these curves is that as the data becomes more highly correlated, the correlator output signal-to-noise ratio, although less in magnitude, is less sensitive to the geometrical misregistration. This of course is an intuitively satisfying conclusion since the correlation distances become greater as the characteristic length of the filter increases.

4.2 Noise Free Experimental Data

The processor used in section 4.1 is now applied to line scanner data. In this section the reference data $\underline{S}_r$ is again selected from the background data, giving a reference signal which is both noise free and distortionless. The images processed in this section are typical of scenes observed in line scanner imagery.

In the results of this section, shown in Figs. 4-12 through 4-14, the title "image template" refers to the use of $\underline{S}_r$ itself as the correlator template, whereas the term "processor template" is taken to mean that $\underline{S}_r$ has been convolved with the grid operator $\underline{G}$, given by equation (4-3), to obtain the template for the correlator. In addition the number of picture elements in the template for a given correlator output is N^2.

A scene of an agricultural area is shown in Fig. 4-12(a); the outlined area represents the approximate area from which the reference data set $\underline{S}_r$ was selected. Fig. 4-12(b) shows the output of the cross-correlation of $\underline{S}_r$ with the background $\underline{S}_b$. It is noteworthy that Fig. 4-12(b) typifies the correlator output of those scenes consisting primarily of agricultrual fields. The correlation function is being viewed at an angle of $\pi/4$ radians, and it is readily apparent that the

(a) Agricultural Area

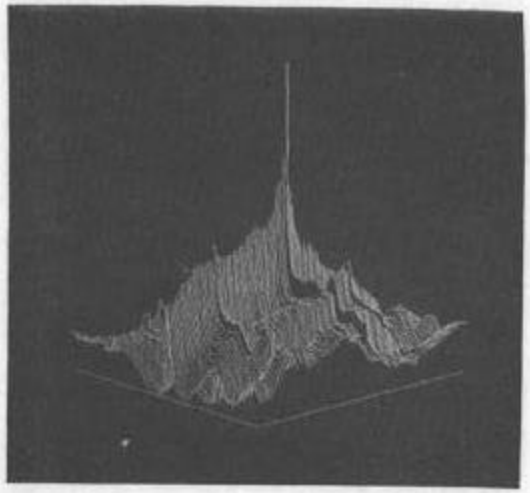

(b) Image Template
$N^2 = 4096$

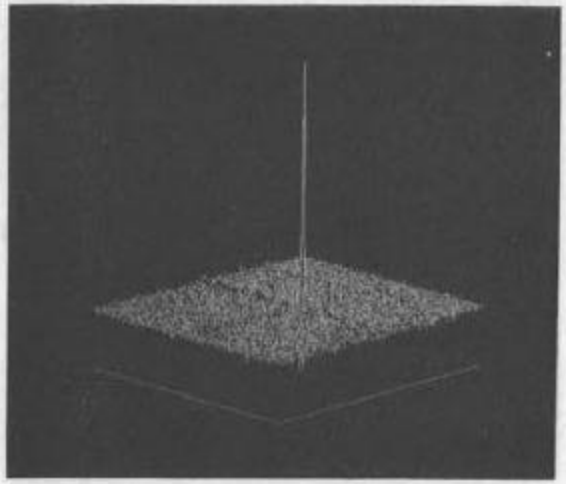

(c) Processor Template
$N^2 = 4096$

Figure 4-12 Correlator Output for an Agricultural Area

correlation distances along each of the orthogonal axes are significantly different.

The correlator output where the template was obtained by convolving the grid operator $\underline{G}$ with $\underline{S}_r$ is shown in Fig. 4-12(c). The peak of the correlation is readily identified as in the previous figure; however, this processor exhibits a significant suppression of the pedestal variance.

An urban scene is shown in the outlined area of Fig. 4-13(a) and the corresponding correlator outputs are shown in Figs. 4-13(b)-(e). As was previously observed for the agricultural area, the location of the peak in the correlator output using the image template is readily established. However, the pedestal variance in the correlator output using the processor template is significantly reduced.

The outlined area in Fig. 4-14(a) is an example of a natural area. The correlator outputs shown in Figs. 4-14(b) and (d) are significant because in each of the outputs the peak corresponding to the correct juxtaposition of $\underline{S}_r$ on the background appears as a narrow peak projecting from a larger bump. If a hill-climbing algorithm was being used to locate the correct juxtaposition of $\underline{S}_r$ and the step size was large, it is conceivable that an incorrect maximum would be found. However, in Figs. 4-14(d) and (e) these undesirable lobes have been reduced and the central peak is readily identified.

The significant numerical quantities associated with these results are tabulated in Table 4-4.

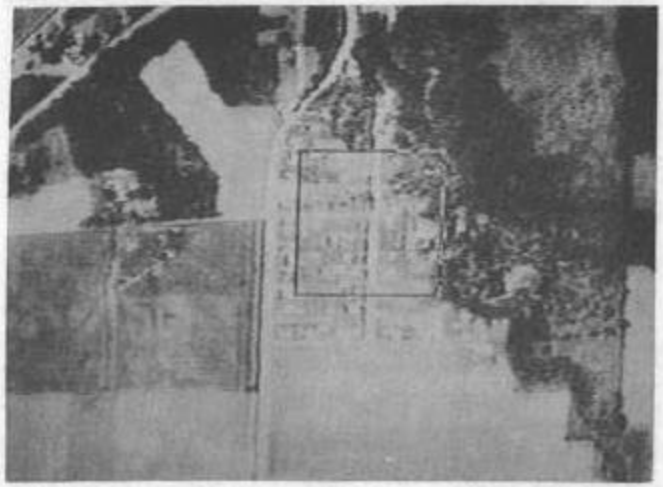

(a) Urban Area

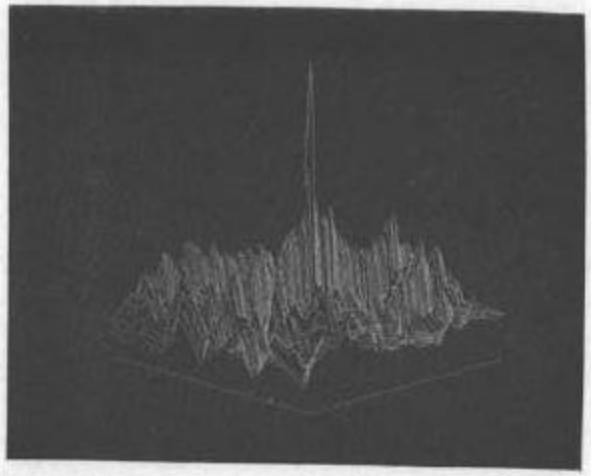

(b) Image Template
$N^2 = 1024$

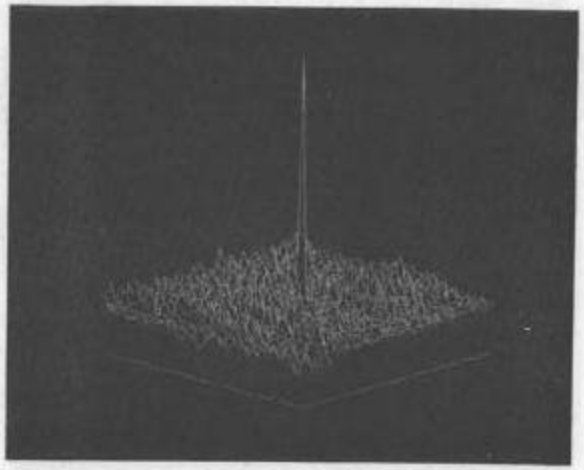

(c) Processor Template
$N^2 = 1024$

Figure 4-13 Correlator Output for an Urban Area

(d) Image Template
$N^2 = 4096$

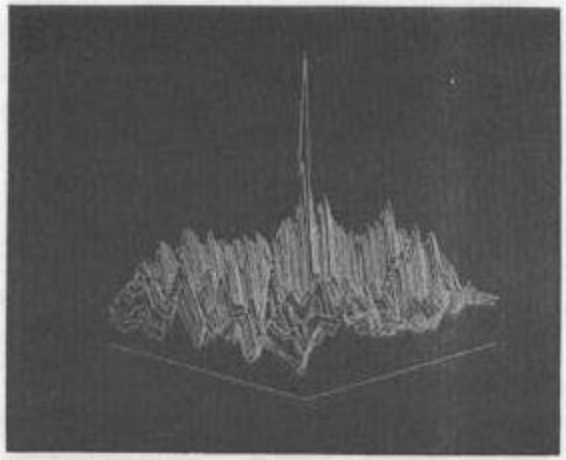

(e) Processor Template
$N^2 = 4096$

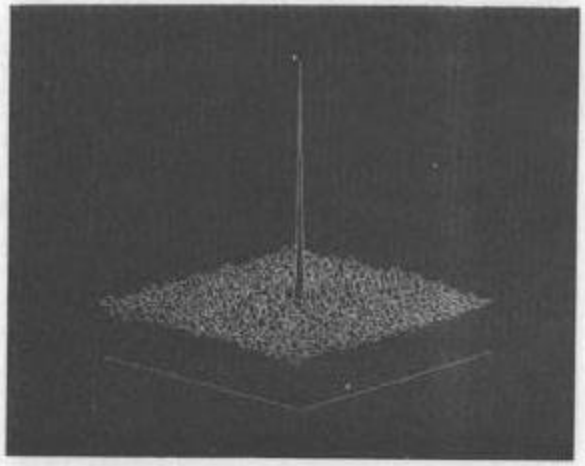

Figure 4-13 Cont.

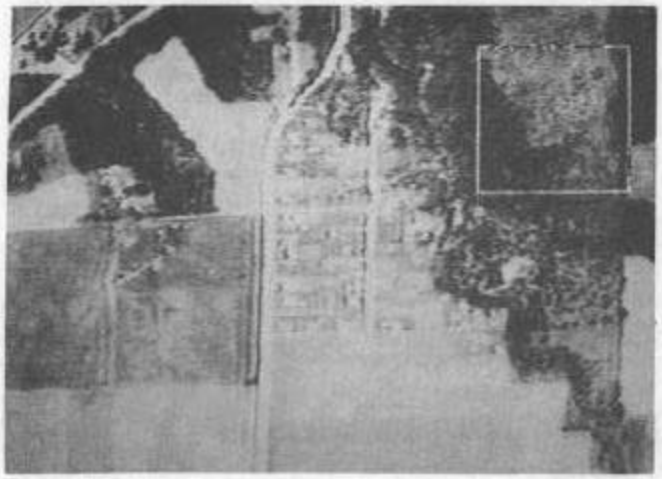

(a) Natural Area

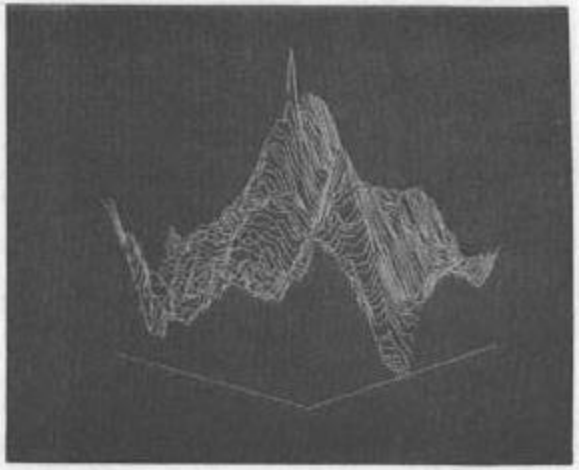

(b) Image Template $N^2 = 1024$

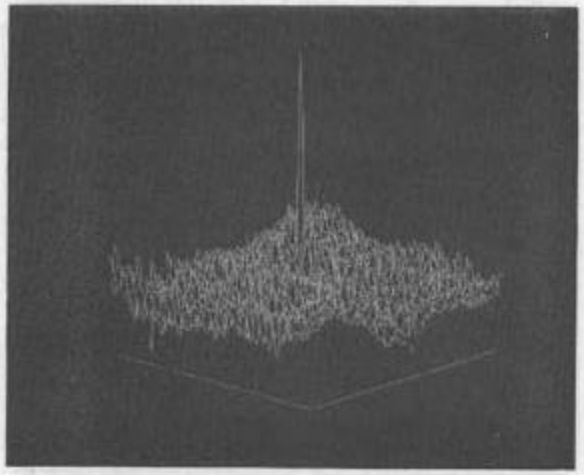

(c) Processor Template $N^2 = 1024$

Figure 4-14 Correlator Output for a Natural Area

(d) Image Template
$N^2 = 4096$

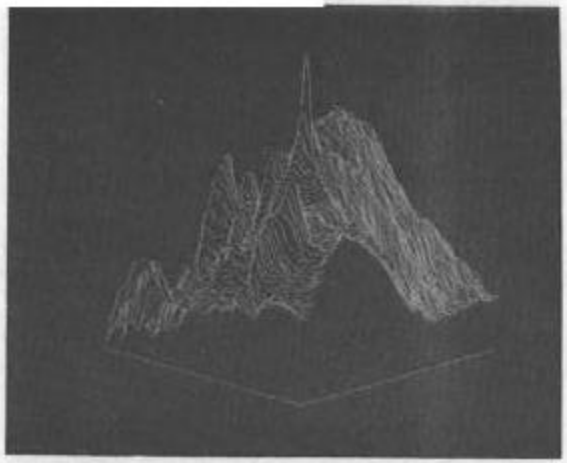

(e) Processor Template
$N^2 = 4096$

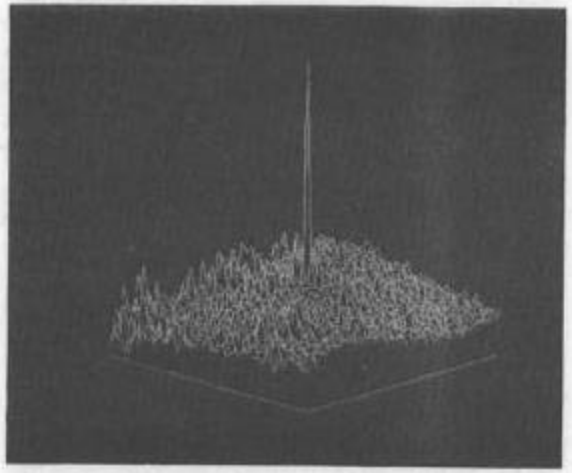

Figure 4-14 Cont.

Table 4-4. Significant Numerical Quantities in the Noise Free Line Scanner Data.

Figure	Template Size	Adjacent Cell Correlation	Signal-to-Noise Ratio
4-12(a)	64 x 64	.775	133
4-12(c)	64 x 64	.775	4510
4-13(b)	32 x 32	.629	106
4-13(c)	32 x 32	.629	664
4-13(d)	64 x 64	.690	234
4-13(e)	64 x 64	.690	1880
4-14(b)	32 x 32	.577	21.8
4-14(c)	32 x 32	.577	75.9
4-14(d)	64 x 64	.570	10.4
4-14(e)	64 x 64	.570	966

4.3 Multitemporal Data

Multitemporal data sets generally exhibit both misregistration and noise components. The processor template, given by equation (3-78), requires both the signal and noise covariance matrices. In the general case, these matrices must be estimated from the data, although for certain classes of data the form of the matrix is assumed and the parameters needed for determining the matrix elements are estimated from the data.

The difficulties in obtaining estimates of these covariance matrices were discussed in Chapter 3. Briefly, however, these difficulties arise from the requirements of large arrays of computer memory and the size of the data sets necessary to obtain meaningful statistical estimates of these matrices.

In view of these computational difficulties the development of the template given by equation (3-78) will not be carried out; instead, the processor used previously in this chapter will be used to experimentally evaluate its applicability to multitemporal data sets.

The data sets selected for multitemporal processing are shown in Fig. 4-15 with the reference data $\underline{S}_r$ selected from set A and the background data $\underline{S}_b$ chosen from set B. Four areas are selected from this data for processing, and the approximate locations of these areas are outlined in data set A. The following procedure is used in analyzing these data sets. The correlator outputs for these test areas for values of the prewhitening coefficient of 0.0 and 0.9 are computed. From these results it is concluded that the algorithm will not give meaningful results for geometrically uncorrected data regions.

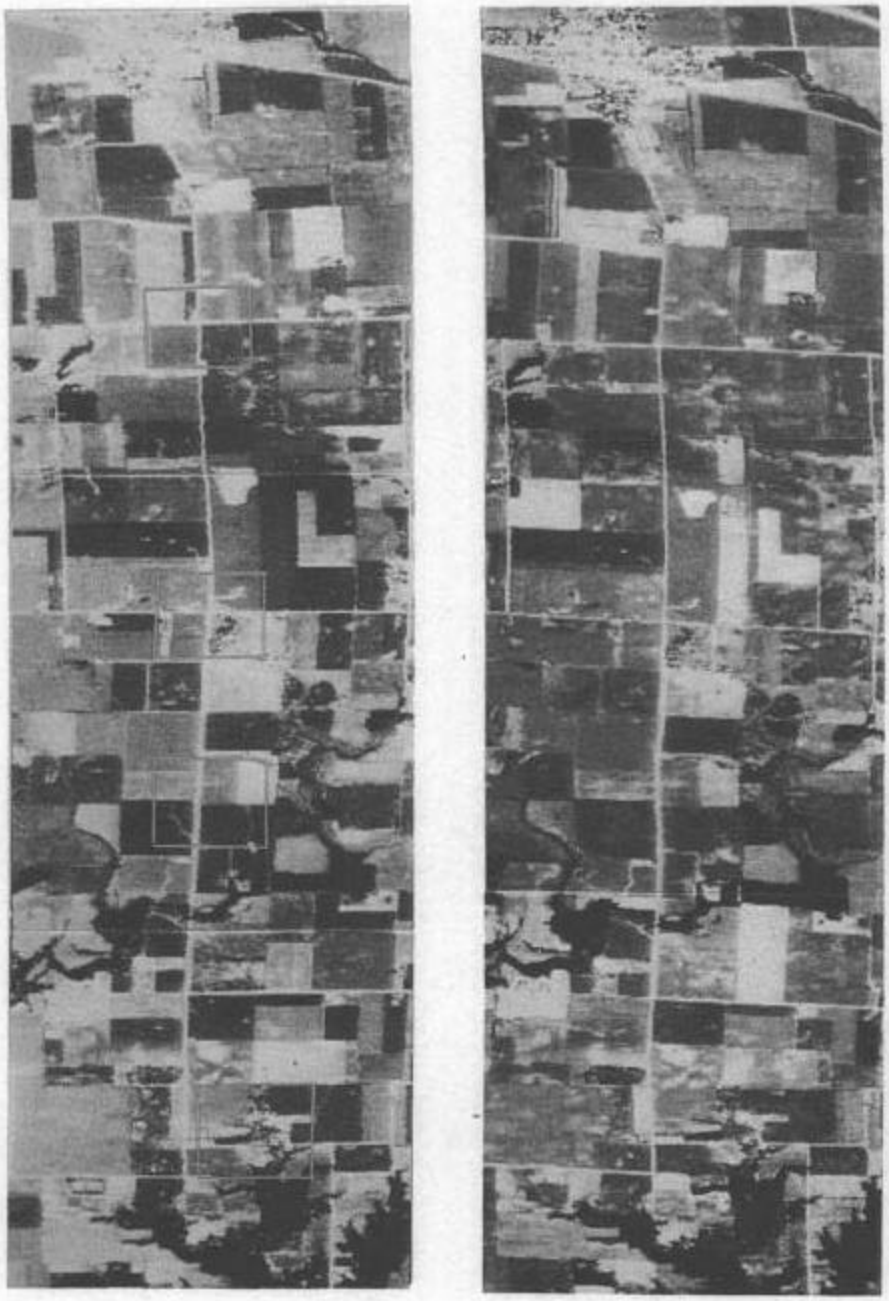

Region 1

Region 2

Region 3

Region 4

Data Set A

Data Set B

Figure 4-15 Multitemporal Data Sets

Table 4-5. Characteristics of the Experimental Multitemporal Data

Purdue Flight Line 210

	DATA SET A	DATA SET B
Run No.	71053900	71062900
Date	13 Aug 1971	30 Aug 1971
Time	1202	1229 hours
Altitude	5000	5000 feet
Heading	180	180 deg.
No. Samples/Line	222	222
Angular Resolution	6.06×10^{-3}	5.82×10^{-3} radian
Wavelength Band Used	.54 - .60	.54 - .60 μ

The moduli of the Fourier transforms of these data regions are then computed, and the data of Region 2 geometrically corrected. The section concludes with the crosscorrelator outputs where the corrected data are the crosscorrelator inputs.

4.3.1 Crosscorrelation of Misregistered Data

The outputs of the crosscorrelator for the data sets selected from the set of multitemporal imagery are shown in Fig. 4-16. For the results shown in this figure, the leftmost display is for a value of the prewhitening coefficient $\alpha = 0.0$. This corresponds to using the reference data set $\underline{S}_r$ as the correlator template. The outputs for $\alpha = 0.9$, a value chosen to approximate a nominally correct value of this coefficient for most previously observed data, are shown in the rightmost pictures.

The correlator outputs shown in Fig. 4-16 for regions 2 and 3 exhibit the typtically observed results for scenes consisting of rectangular fields. Observing the location of region 1 in Fig. 4-15, it is seen that this area too is composed of agricultural fields. However, data set B exhibits a non-linear distortion component in this area, suggesting that the aircraft began executing a maneuver during the period of time in which these data were being taken.

The correlator output shown in Fig. 4-16, region 4, shows a results obtained with input data selected from an area containing undeveloped terrain. This output exhibits a large, readily distinguishable unimodal peak. With data from a class exhibiting such a cross-correlation function, efficient algorithms can be developed such that

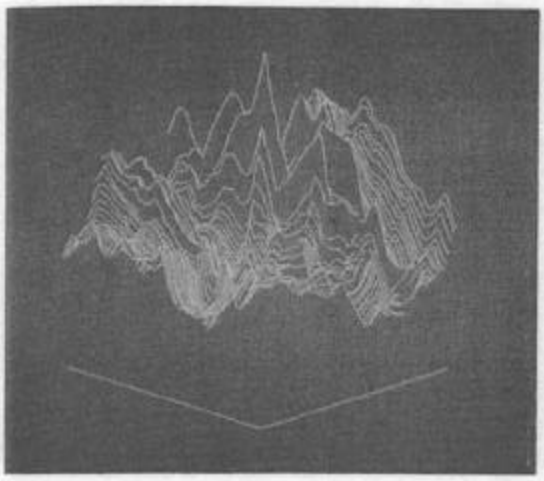

Region 1 , α = 0.0

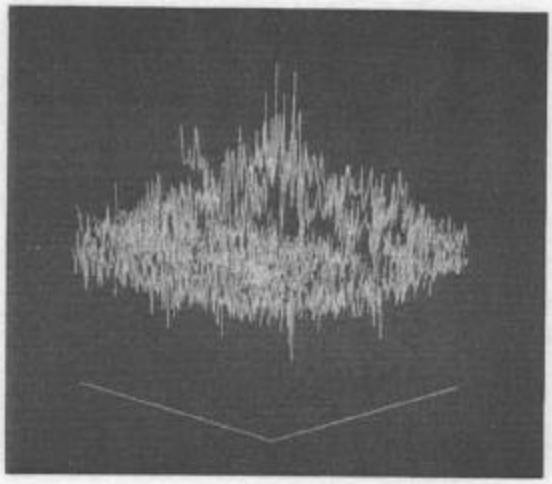

Region 1 , α = 0.9

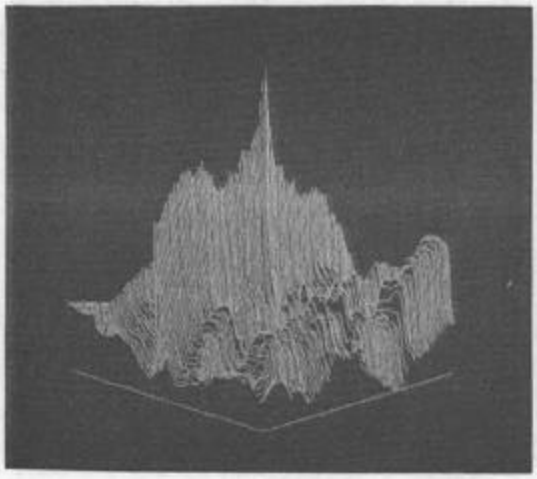

Region 2 , α = 0.0

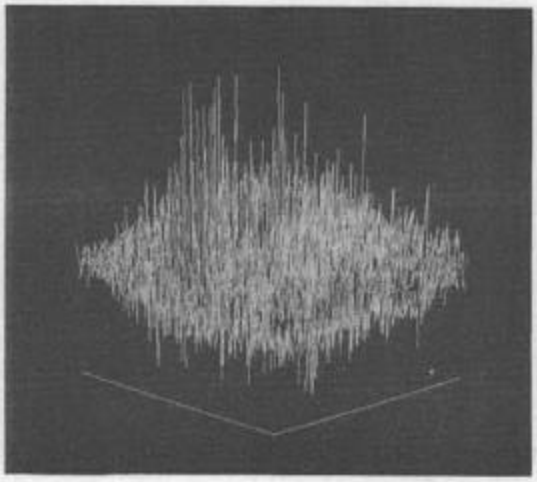

Region 2 , α = 0.9

Figure 4-16 Correlator Outputs for Multitemporal Data

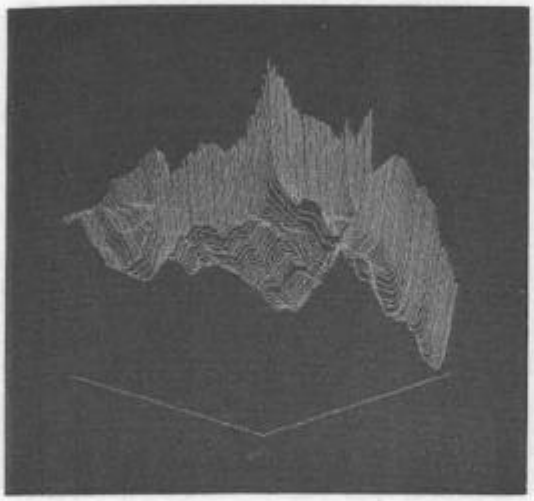

Region 3 , α = 0.0

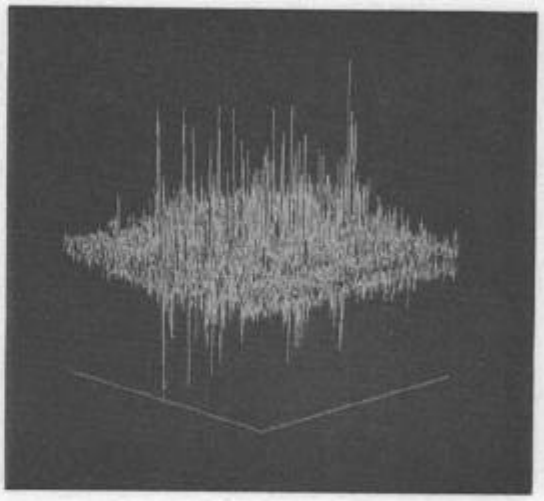

Region 3 , α = 0.9

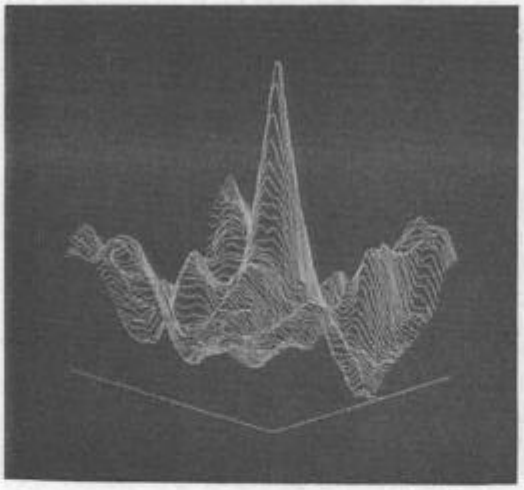

Region 4 , α = 0.0

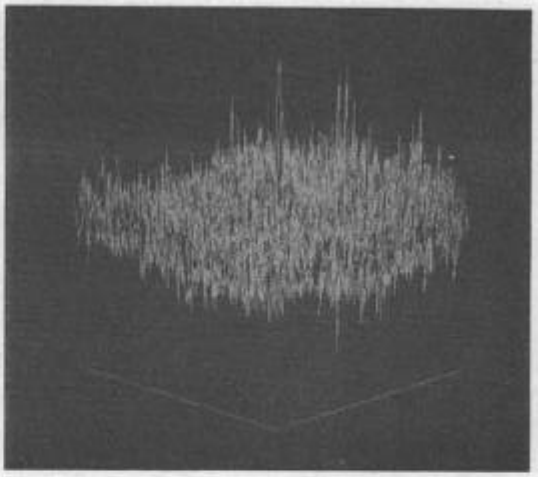

Region 4 , α = 0.9

Figure 4-16 Cont.

a complete search of a region of the correlation output plane for a maximum is not required. Rather a search procedure is implemented where successive steps move toward the peak.

The results for $\alpha = 0.9$ without exception are of little value. However, for the processor to yield useful results, it will be demonstrated that it is necessary to implement a geometrical correction of the data.

4.3.2 Regional Geometric Distortion

Regional geometrical distortion can, for certain classes of distortion and data, be estimated by determining the differences in the moduli of the two-dimensional Fourier transforms of the two approximately corresponding regions under consideration. Examples of moduli of Fourier transforms of line scanner data are shown in Fig. 4-17. The Fast Fourier Transform algorithm was used for computing the transform of these data. In each of these pictures the transformed data have a logarithmic amplitude scale, and the gray scale employed in the display system is linear. The size of the data set being transformed is 128 x 128 picture elements.

The transforms of regions 1 and 3 exhibit the concentration of spatial-frequency energy in the linear loci typical of structured data scenes, whereas the moduli of the transforms of region 4 exhibit unstructured characteristics. In each case it is of significance that most of the energy appears to be concentrated in the very low frequencies. The double lines in the moduli of the structured data are due to the aliased energy from the pattern located at the adjacent harmonics of the sampling frequency.

Data Set A
Region 1

Data Set B
Region 1

Data Set A
Region 3

Data Set B
Region 3

Data Set A
Region 4

Data Set B
Region 4

Figure 4-17 Moduli of Two-Dimensional Fourier Transforms

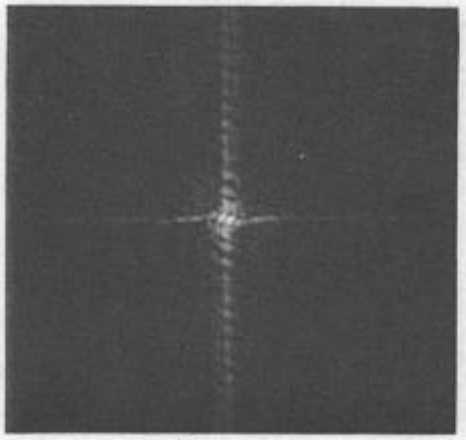

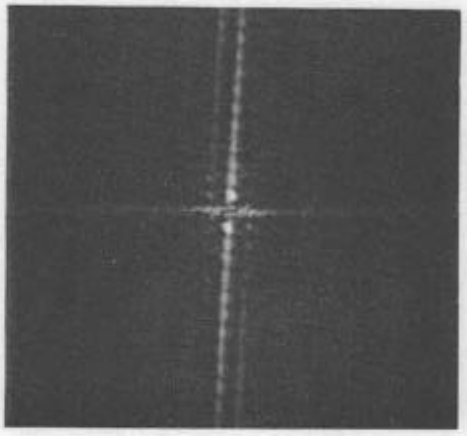

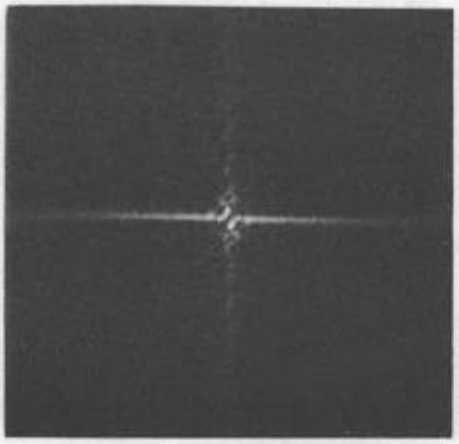

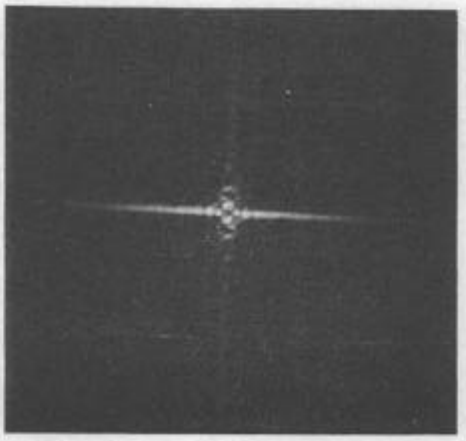

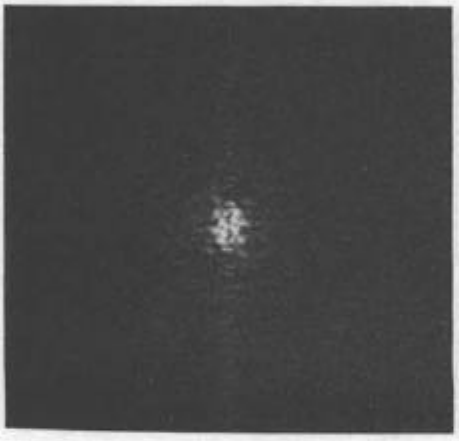

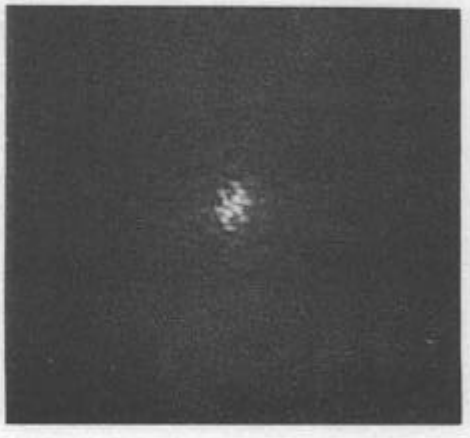

The data from region 2 were selected as the set to be geometrically corrected. The moduli of the transforms of these data are shown in Fig. 4-18. The algorithm for locating the loci of energy in the transform domain, which was developed in Chapter 2, was applied to these transformed data, and the angular quantities given by the algorithm, measured with respect to the u_1 axis, are as follows

data set A	-7.18×10^{-2} radian
	1.57 "
data set B	-3.30×10^{-2} "
	1.52 "

With a hypothetical transform coincident with the coordinate axes used as a reference data transform, the resultant angular quantities defined in Fig. 2-13 are

data set A	$\phi_1 = -4.1^\circ$
	$\phi_2 = 0^\circ$
data set B	$\phi_1 = -1.9^\circ$
	$\phi_2 = -3.3^\circ$

The two-dimensional polynomial given in equation (2-14) was used to implement the correction. Rather than mapping one data set into the other, it was chosen to rectify each data set assuming the reference data set was coincident with the coordinate axes. Examining the data sets in both the spatial and spatial-frequency domain, the angular quantities chosen for the rectification differed slightly from those above. The numerical values used for the rectification are

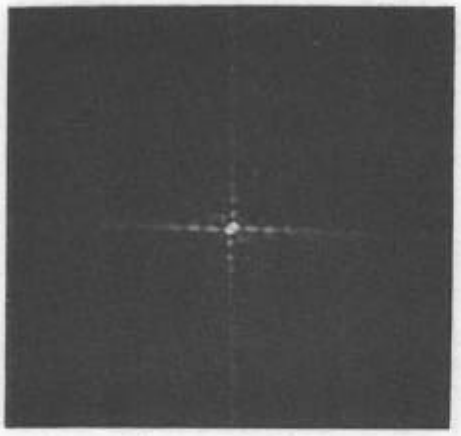

Data Set A

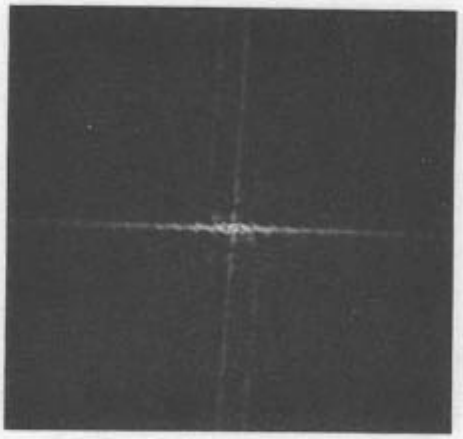

Data Set B

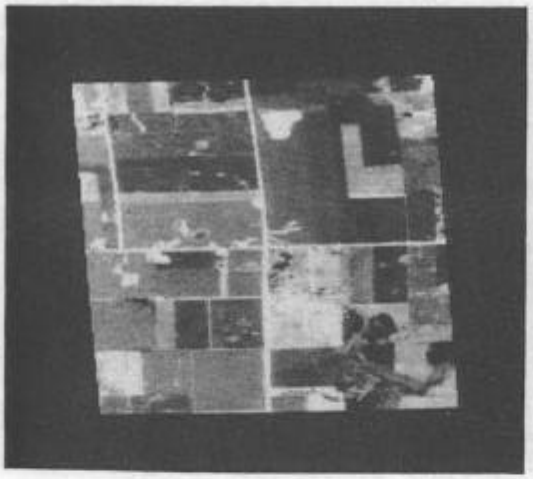

Data Set A

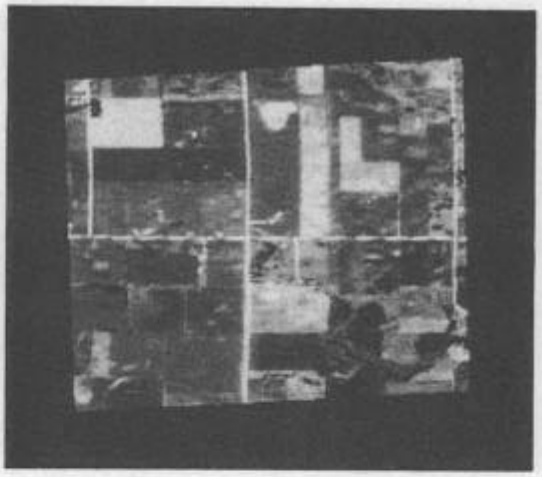

Data Set B

Figure 4-18 Modulus of Distorted Data and Geometrically Corrected Data for Region 2

data set A $\quad \phi_1 = -3.7^\circ$

$\phi_2 = 0^\circ$

data set B $\quad \phi_1 = -1.7^\circ$

$\phi_2 = -3.3^\circ$

with the reference transform angular quantities having the values

$\theta_1 = 0^\circ$

$\theta_2 = 90^\circ$

for each of the data sets.

Thus for data set A using equation (2-56) the value of the skew coefficient is

$$a_{21} \simeq \frac{1}{\tan\left[\frac{\pi}{2} - \frac{\pi}{180}(-3.7)\right]} = -\tan\left[\frac{\pi}{180}(3.7)\right] = -0.0647$$

The distortion matrix, defined by equation (2-58), is then

$$\underline{A}_1 = \begin{bmatrix} 0.9979 & -0.0645 \\ 0.0 & 1.002 \end{bmatrix}$$

The corresponding quantities for data set B are

$$a_{21} \simeq \frac{1}{\tan\left[\frac{\pi}{180}(86.7 + 1.7)\right]} = \tan\left[\frac{\pi}{180}(1.6)\right] = 0.0279$$

and the distortion matrix is

$$\underline{A}_2 = \begin{bmatrix} 0.9999 & -0.0297 \\ 0.0576 & 0.9987 \end{bmatrix}$$

The results of this geometrical correction on the spatial data are shown in Fig. 4-18. It is emphasized that the correction is applicable only in the center of each of these pictures as the distortion introduced by the aircraft motion is a dynamic quantity.

4.3.3 Correlator Output for Geometrically Corrected Data

The output of the crosscorrelator for the corrected data set is illustrated in Fig. 4-19 for various values of the prewhitening coefficient α. The template size for each of these outputs is 64 x 64 picture elements. Comparing the result of Fig. 4-19(a) to the corresponding output of region 2 of Fig. 4-16, it is seen that the geometrical correction has increased the sharpness of the peak at the correction justaposition of $\underline{S}_r$.

A significant result is that the pedestal variance is reduced while the central peak becomes more discriminable as the value of α approaches unity. A plot of the correlator output signal-to-noise ratio for these results is shown in Fig. 4-20.

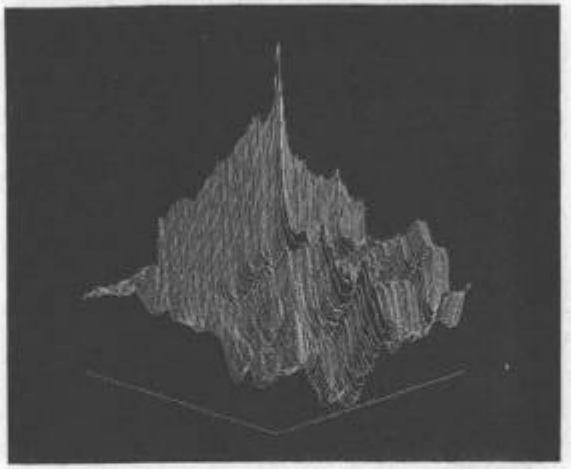

(a) $\alpha = 0.0$

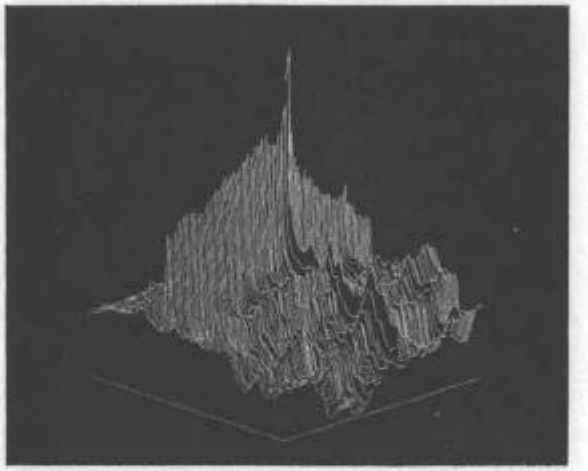

(b) $\alpha = 0.$

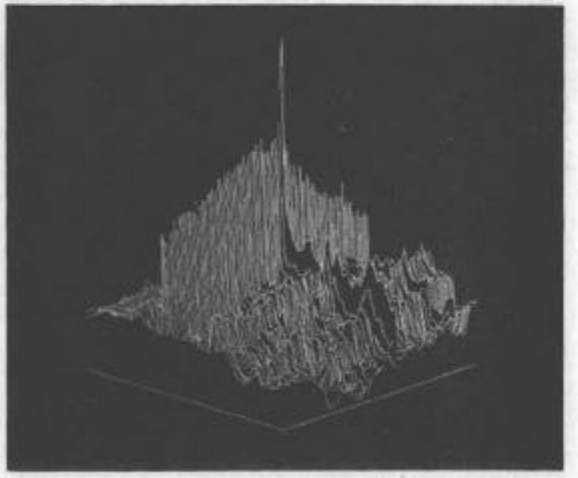

(c) $\alpha = 0.5$

Figure 4-19 Correlator Output for Corrected Multitemporal Data

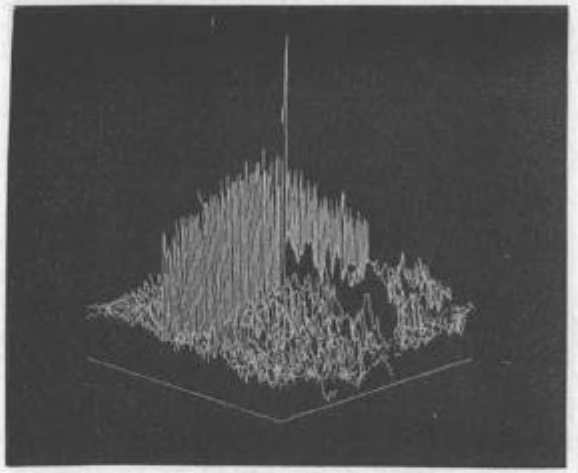

(d) $\alpha = 0.7$

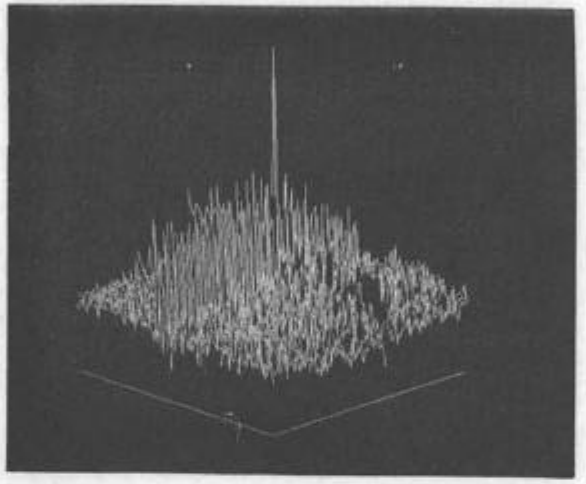

(e) $\alpha = 0.9$

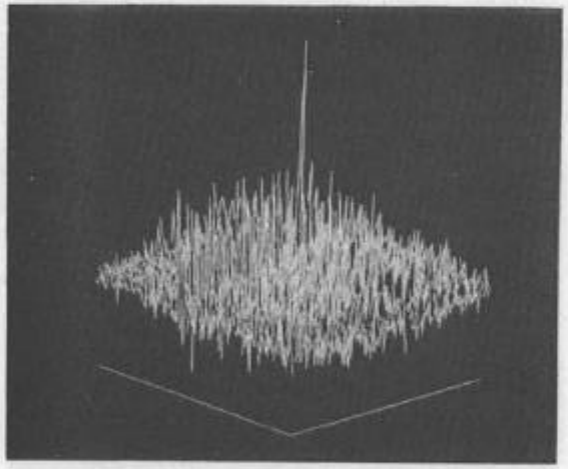

(f) $\alpha = 1.0$

Figure 4-19 Cont.

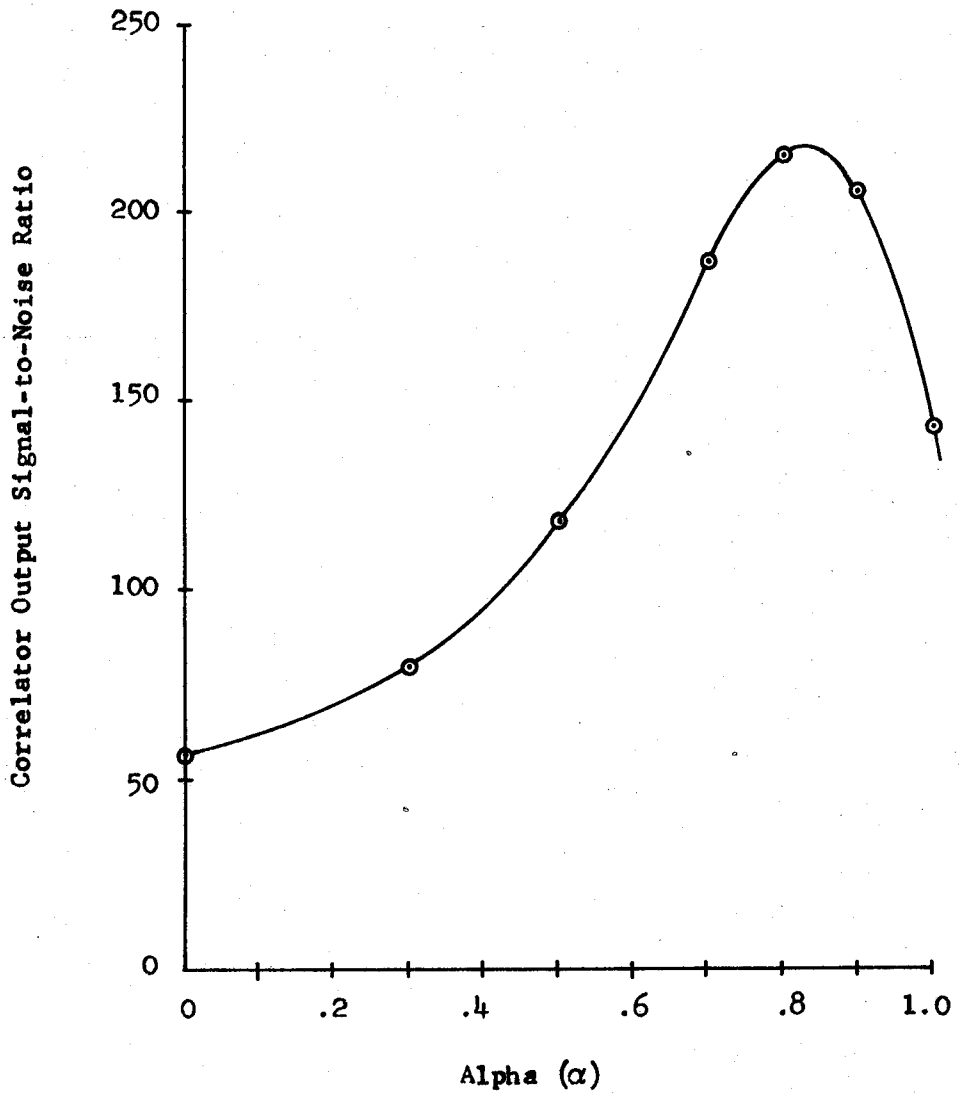

Figure 4-20 Correlator Output Signal-to-Noise Ratio as a Function of the Prewhitening Coefficient (Geometrically Corrected Multitemporal Data)

CHAPTER 5

SUMMARY

5.0 Summary

Given two sets of imagery of some common area taken at different times, it is observed that these data exhibit geometrical misregistration. The rectification of this imagery requires that the parameters be determined for the mathematical model assumed to characterize the misregistration. The problem studied in this investigation is the identification of conjugate, or corresponding, points in multitemporal imagery such that the coefficients of the misregistration model can be obtained.

Selecting a reference data subimage, denoted $\underline{S}_r$, from the first data set, these conjugate points are located by finding the corresponding subimage $\underline{S}_r'$ which is embedded in the background data $\underline{S}_b$. The measure of similarity between data sets is taken to be amplitude correlation. Assuming the misregistration between $\underline{S}_r$ and $\underline{S}_r'$ to be modeled by an affine transformation, a sequential procedure is implemented in which the geometrical distortion components are first estimated and removed. Algorithms utilizing the moduli of the two-dimensional Fourier transforms of the data $\underline{S}_r$ and its approximate corresponding subimage $\underline{S}_r'$ are developed for estimating the distortion model coefficients.

Following the geometrical correction, the displacement coefficients are estimated by determining the location of the peak of the correlation surface computed by crosscorrelating a template, generated from the reference data, with the background $\underline{S}_b$. The peak of this correlation surface is assumed to be the point of correct superposition of the reference data on the background data.

The algorithms reported in the literature for computing the correlation surface, or some equivalent quantity, do not give a surface on which the point of greatest correlation is maximally discriminable from the values at other points of the surface where the criterion of discrimination between points on the surface is as defined in Chapter 3. The one exception is the filter reported by Arcese et al. [6].

The filter derived in this investigation extends these previous results to data having a covariance matrix $\underline{K}_s$ and in which the background data contains an additive noise component with statistical properties characterized by the covariance matrix $\underline{K}_n$. The analytical expression of this filter is obtained under the constraints of both an output of unity at the correct superposition of the reference data on the background and for a bounded energy in the filter. With the removal of both constraints and for no additive noise components, this filter reduces to the result of Arcese et al. If in addition the correlation between adjacent picture elements is neglected, which yields the identity matrix for $\underline{K}_s$, the filter then becomes the reference image itself.

The application of this filter to noise free and distortionless data, with the covariance matrix of the image assumed to be of a simple exponential form, yields results which substantiate the theoretical development of the processor. In these results the correlation surfaces of the data sets processed with the filter exhibit narrow central peaks and have significantly decreased variance in the pedestal region of the surface.

The application of this algorithm to multitemporal data introduces some problems which at the present have no solution. Implementation of the general filter for this data requires knowledge of the covariance matrices of both the reference and noise processes; however, it is not possible to make meaningful estimates of these quantities at the present time. The difficulty in estimating these matrices arises from two sources. The first is the size of the arrays required for handling the matrices in the computer. It has been experimentally found that the useful sizes of reference data sets range between $2^5 \times 2^5$ to $2^7 \times 2^7$ picture elements, with the resulting sizes of the covariance matrices ranging between $2^{10} \times 2^{10}$ and $2^{14} \times 2^{14}$ elements. The second difficulty is the unavailability of a sufficiently large set of data having similar statistical properties to the reference such that a meaningful estimate of the covariance matrix of the reference data can be made. An additional difficulty in estimating the noise properties is that, with the noise defined as the difference between the data sets, the determination of $\underline{K}_n$ requires that the data be in registration to obtain the differences which are related to scene changes and are not due to misregistration error.

If it is possible to approximate the estimated covariance matrices with matrices having a Toplitz form, the requirement for computer storage can be reduced by a factor of 1/m where the number of elements in the reference data set is m x m. However, the requirement remains for the availability of data sets of sufficient size from which to make the initial covariance estimates.

The use of the algorithm derived for the noise free processor with both noise free and multitemporal data yields encouraging results in that the central peak of the correlator output indeed becomes more discriminable from the output in the pedestal region where discrimination is defined as the ratio of the correlator output signal-to-noise using the optimum filter to the corresponding correlator output quantity with the reference scene used as the filter. The increase in discrimination for the noise free data ranges between 3 to 15 dB and for the multitemporal data the corresponding increase is greater than 6 dB.

A requirement imposed on the data by the filter for the optimum discrimination of the correct superposition of $\underline{S}_r$ is that the geometrical distortion components of this misregistration model must be reduced below the magnitudes found to typically occur in the multitemporal data. It is demonstrated in this investigation that the linear geometrical distortion existing between two data sets can be determined from the moduli of the Fourier transforms of these data. Values of the skew and rotational distortion components were determined for a set of multitemporal imagery using the linear regression algorithms

developed in Chapter 2. These values of these distortion components were found to agree with numerical values obtained by independent methods to within a few tenths of a degree.

BIBLIOGRAPHY

BIBLIOGRAPHY

1. Alt, F. L., "Digital Pattern Recognition by Moments," JACM, Vol. 9, pp. 240-58, April, 1962.

2. Andrews, H. C., and K. L. Caspari, "Degrees of Freedom and Modular Structure in Matrix Multiplication," IEEE Trans. on Computers, Vol. CS-20, No. 2, pp. 133-41, February, 1972.

3. Anderson, G. B., and T. S. Huang, "Errors in Frequency-Domain Processing of Images," SJCC, Vol. 34, pp. 173-85, Spartan Book Co., Balitomore, 1969.

4. Anuta, P. E., "Digital Registration of Multispectral Video Imagery", JSPIE, Vol. 7, No. 6, September, 1969.

5. Anuta, P. E., "Spatial Registration of Multispectral and Multi-temporal Digital Imagery Using Fast Fourier Transform Techniques", IEEE Trans. G.E., Vol. GE-8, No. 4, pp. 353-67, October, 1970.

6. Arcese, A., P. H. Mengert, and E. W. Trombini, "Image Detection Through Bipolar Correlation," IEEE Trans. IT, Vol. IT-16, No. 5, pp. 534-41, September, 1970.

7. Barnea, D. I., and H. F. Silverman, "A Class of Algorithms for Fast Digital Image Registration," IEEE Trans. on Computers, Vol. C-21, No. 2, pp. 179-86, February, 1972.

8. Bednar, J. B., and C. H. Farmer, "An Algorithm for the Inversion of Finite Block Toglitz Matrices with Application to Spatial Digital Filters," presented at the Computer Image Processing and Recognition Conference, University of Missouri - Columbia, August 24-26, 1972.

9. Bergland, G. D., "A Guided Tour of the Fast Fourier Transform," IEEE Spectrum, Vol. 6, No. 7, pp. 41-52, July, 1969.

10. Bertram, S., "Application of Hybrid Analog and Digital Techniques in the Automatic Map Compilation System," Proc. SJCC, Vol. 23, Spartan Books, Baltimore, 1963.

11. Billingsley, F., "Applications of Digital Image Processing," Applied Optics, Vol. 9, No. 2, pp. 289-99, February, 1970.

12. Birkhoff and Maclane, "A Survey of Modern Algebra," Macmillan, New York, 1965.

13. Bracewell, R., "The Fourier Transform and its Application," McGraw-Hill, New York, 1965.

14. Buck, R. C., "Advanced Calculus," McGraw-Hill, New York, 1965.

15. Cathey, W. T., and G. Doidge, "Image Comparison by Interference," JOSA, Vol. 56, pp. 996-98, July, 1966.

16. Chapell, W. E., and J. J. Edmond, "The AS-11C Automatic System," Photogrammetric Engineering, Vol. 35, No. 10, pp. 1059-69, October, 1969.

17. Cochran, W. T., et al., "What is the Fast Fourier Transform?" Proc. IEEE, Vol. 55, No. 10, pp. 1664-74, October, 1967.

18. Cook, C. E., and M. Bernfeld, "Radar Signals," Academic Press, New York, 1967.

19. Cooper, G. R., and R. J. Purdy, "Detection, Resolution and Accuracy in the Random Signal Radar," TR-EE68-16, School of Electrical Engineering, Purdue University, Lafayette, Indiana.

20. Courant and Hilbert, "Methods of Mathematical Physics," Vol. 1, Interscience, New York, 1966.

21. Coxeter, H. S. M., "Introduction to Geometry," Wiley, New York, 1969.

22. Cutrona, L. J., et al., "Optical Data Processing and Filtering Systems," IRE Trans. IT, Vol. IT-6, pp. 386-400, June, 1960.

23. Deutsch, R., "Estimation Theory," Prentice Hall, Englewood Cliffs, 1965.

24. Diamantides, N. D., "Correlation Measure of Contrast for Map Matching," JOSA, Vol. 58, No. 7, pp. 996-98, July, 1968.

25. Dietz, R. S., and W. P. Sprall, "Fit Between Africa and Antartica: A Continental Drift Reconstruction," Science, Vol. 167, pp. 1612-14, March 20, 1970.

26. Franks, L. E., "Signal Theory," Prentice Hall, Englewood Cliffs, 1969.

27. Friedman, B., "Principles and Techniques of Applied Mathematics," Wiley, New York, 1965.

28. Fu, K. S., D. A. Landgrebe, and T. L. Phillips, "Information Processing of Remotely Sensed Data," Proc. IEEE, Col. 57, No. 4, pp. 639-53, April, 1969.

29. Fu, K. S., and P. J. Min, "A Feature Selection in Multiclass Pattern Recognition," Technical Report TR-EE68-17, Purdue University, July, 1968.

30. Goodman, J. W., "Introduction to Fourier Optics," McGraw-Hill, New York, 1968.

31. Grenander, U., and G. Szego, "Toplitz Forms and Their Application," Univ. of Calif. Press, Berkeley, 1958.

32. Hadley, G., "Linear Algebra," Addison Wesley, Reading, 1961.

33. Hall, J. D., et al., "Objective Methods for Registering Landmarks and Determining Cloud Motions from Satellite Data," IEEE Trans. on Computers, Vol. CS-21, No. 7, pp. 768-76, July, 1972.

34. Hamming, R. W., "Numerical Methods for Scientists and Engineers," McGraw-Hill, New York, 1962.

35. Hardy, J., H. Johnson, and J. Godfrey, "Electronic Correlator for the Planimat," Photogrammetric Engineering, Vol. 35, No. 8, pp. 780,88, August, 1969.

36. Harger, R. O., "Signal Sequence Detection Given Noisy, Common Background Image Sets," IEEE Trans. AES, Vol. AES-8, No. 2, pp. 174-185, March, 1972.

37. Harman, H. H., "Modern Factor Analysis," University of Chicago Press, Chicago, 1967.

38. Hobrough, G. L., "Automation in Photogrammetric Instruments," Photogrammetric Engineering, Vol. 31, No. 4, pp. 595-603, July, 1965.

39. Hu, M. K., "Visual Pattern Recognition by Moment Invariants," IRE Trans. IT, Vol. IT-8, pp. 170-87, February, 1962.

40. Huang, T. S., W. F. Schreiber, and O. J. Tretiak, "Image Processing," Proc. IEEE, Vol. 59, No. 11, pp. 1586-1609, November, 1971.

41. Kozma, A., and D. L. Kelly, "Spatial Filtering for Detection of Signals Submerged in Noise," Applied Optics, Vol. 4, No. 4, pp. 387-92, April, 1965.

42. Landgrebe, D. A., "Data Analysis and Remotely Sensed Data," presented at the AIAA Earth Resources Observations and Information Systems Meeting, Annapolis, Maryland, March 2-4, 1970.

43. Lendaris, G., and G. Stanley, "Diffraction-Pattern Sampling for Automatic Pattern Recognition," Proc. IEEE, Vol. 58, No. 1, pp. 198-216, February, 1970.

44. Levine, M. D., "Feature Extraction; a Survey," Proc. IEEE, Vol. 57, No. 8, pp. 1391-1407, August, 1969.

45. Levinson, N., "The Weiner RMS (Root Mean Square) Error Criterion in Filter Design and Prediction," Appendix B of N. Weiner, Extrapolation, Interpolation and Smoothing of Stationary Time Series, Wiley, New York, 1948.

46. Lillestrand, R. L., "Techniques for Change Detection," IEEE Trans. on Computers, Vol. CS-21, No. 7, pp. 654-59, July, 1972.

47. Luenberger, D. G., "Optimization by Vector Space Methods," Wiley, New York, 1969.

48. Nathan, P.,"Picture Enhancement for the Moon, Mars and Man," in G. Chang, et al., Pictoral Pattern Recognition, Thompson Book Co., Washington, D.C., 1968. (See also VPL Technical Report No. 32-877, Digital Video Data Handling, January, 1966.)

49. Proceeding of the IEEE, Special Issue on Detection Theory, Vol. 58, No. 5, May 1970.

50. Pratt, W. K., "Generalized Weiner Filtering Computation Techniques," IEEE Trans. on Computers, Vol. CS-21, No. 7, pp. 636-41, July, 1972.

51. Papoulis, A., "Systems and Transforms with Applications in Optics," McGraw-Hill, 1968.

52. Ready, P. J., and P. A. Wintz, "Multispectral Data Compression Through Transform Coding and Block Quantization," LARS Information Note 050572, Laboratory for Applications of Remote Sensing, Purdue University, Lafayette, Indiana.

53. Robinson, E. A., "Statistical Communication and Detection," Charles Griffin, London, 1967.

54. Robinson, E. A., "Multichannel Time Series Analysis with Digital Computer Programs," Holden-Day, San Francisco, 1967.

55. Robinson, E. A., "Mathematical Development of Discrete Filters for the Detection of Nuclear Explosions," Journal of Geophysical Research, Vol. 68, pp. 5559-67, 1963.

56. Rosenfeld, A., "Picture Processing by Computer," Academic Press New York, 1969.

57. Stakgold, I., "Boundary Value Problems of Mathematical Physics," Vol. 1, MacMillan, New York, 1967.

58. U. S. Office of Naval Research, Handbook of Military Infared Technology, Washington, D. C., U. S. Gov't. Printing Office, 1965.

59. Urkowitz, H., "Filters for Detection of Small Radar Signals in Clutter," J. Appl. Phys., Vol. 24, pp. 1024-31, 1953.

60. Vander Lugt, A., "Signal Detection by Complex Spatial Filtering," IEEE Trans. IT, Vol. IT-10, No. 4, pp. 139-45, April, 1964.

61. Van Trees, H. L., "Detection, Estimation, and Linear Modulation Theory," Vol. 1, John Wiley, 1968; Vol. 2, John Wiley, 1971.

62. Wiggins, R. A., and E. A. Robinson, "Recursive Solution to the Multichannel Filtering Problem," Journal of Geophysical Res., Vol. 70, pp. 1886-91, 1965.

63. Woods, J. W., "Two-dimensional Discrete Markonian Fields," IEEE Trans. IT, Vol. IT-18, No. 2, pp. 232-40, March, 1972.

64. Zhan, C. T. and R. Z. Roskies, "Fourier Descriptors for Plane Closed Curves," IEEE Trans. on Computers, Vol. CS-21, No. 3, pp. 269-281, March, 1972.

65. Zangwill, W. I., "Nonlinear Programming, A Unified Approach," Prentice-Hall, Inc., Englewood Cliffs, 1967.

APPENDICES

APPENDIX A

THE TWO-DIMENSIONAL FOURIER TRANSFORM

The properties of the two-dimensional Fourier transform of the function $f(\underline{x})$ under an affine transformation

$$\underline{H} = \underline{A}\,\underline{x} + \underline{t} \tag{A-1}$$

where $\underline{A}$ is a [2 x 2] nonsingular matrix and

$$\underline{x} = \begin{bmatrix} x_1 \\ x_2 \end{bmatrix}, \quad \underline{t} = \begin{bmatrix} t_1 \\ t_2 \end{bmatrix}$$

are of interest in this study. In the following, expressions for both cartesian and polar coordinate systems are derived and the symmetry between the spatial and spatial-frequency domains is discussed.

The two-dimensional Fourier transform of the function $f(\underline{x})$ is defined as

$$F(\underline{u}) = \int_{-\infty}^{\infty} \int f(\underline{x}) \exp\left[-j2\pi\ (\underline{u},\underline{x})\ \right] d\underline{x} \tag{A-2}$$

and the inverse is

$$f(\underline{x}) = \int_{-\infty}^{\infty} \int F(\underline{u}) \exp\left[\ j2\pi\ (\underline{u},\underline{x})\ \right] d\underline{u} \tag{A-3}$$

where

$$\underline{u} = \begin{bmatrix} u_1 \\ u_2 \end{bmatrix}$$

is the spatial frequency and $(\underline{u},\underline{x})$ is the inner product

$$(\underline{u},\underline{x}) = \underline{u}^T \underline{x} = u_1 x_1 + u_2 x_2 .$$

(a) The Affine Mapping

The Fourier Transform of the function

$$f(\underline{x}) \xrightarrow{H} f(\underline{H}\,\underline{x}) = g(\underline{y}) \tag{A-4}$$

is

$$F(\underline{u}) = \int_{-\infty}^{\infty}\int f(\underline{H}\,\underline{x}) \exp\left[-j2\pi(\underline{u},\underline{x})\right] d\underline{x} \tag{A-5}$$

$$= \frac{1}{|J|}\int_{-\infty}^{\infty}\int g(\underline{y}) \exp\left\{-j2\pi\left[(\underline{u},\underline{A}^{-1}\underline{y} - \underline{A}^{-1}\underline{t})\right]\right\} d\underline{y} \tag{A-6}$$

$$= \frac{1}{|J|} \exp\left[\, j2\pi(\underline{u},\, \underline{A}^{-1}\, \underline{t})\right]$$

$$\cdot \int_{-\infty}^{\infty}\int g(\underline{y}) \exp\left[-j2\pi(\underline{u}\,,\, \underline{A}^{-1}\, \underline{y})\right] d\underline{y} \tag{A-7}$$

$$= \frac{1}{|J|} \exp\left[\, j2\pi\, (\underline{u},\, \underline{A}^{-1}\, \underline{t})\right]$$

$$\cdot \int_{-\infty}^{\infty}\int g(\underline{y}) \exp\left\{-j2\pi\left[(\underline{A}^{-1\,T}\, \underline{u},\, \underline{y})\right]\right\} d\underline{y} \tag{A-8}$$

$$= \frac{1}{|J|} \exp\left[\, j2\pi\, (\underline{u},\underline{t})\right] \mathcal{F}\left[(\underline{A}^{-1}\underline{t})\, \underline{u}\right] \tag{A-9}$$

$$= G(\underline{v}) \tag{A-10}$$

where J is the Jacobian of the transformation

$$J = \begin{bmatrix} \frac{\partial y_1}{\partial x_1} & \frac{\partial y_1}{\partial_{x_2}} \\ \frac{\partial y_2}{\partial x_1} & \frac{\partial y_2}{\partial x_2} \end{bmatrix}$$

The relation between these coordinate variables is

$$\begin{array}{ccc} f(\underline{x}) & \longleftrightarrow & g(\underline{y}) \\ \Updownarrow & & \Updownarrow \\ F(\underline{u}) & \longleftrightarrow & G(\underline{v}) \end{array}$$

where $\Longleftrightarrow$ denotes a Fourier transform pair.

(b) The Two-Dimensional Fourier Transform in Polar Coordinates

To obtain the equation analogous to equation (A-10) in polar coordinates, let

$$x_1 = r \cos \theta \qquad \text{(A-11)}$$

$$x_2 = r \sin \theta$$

and

$$u_1 = \rho \cos \phi$$

$$u_2 = \rho \sin \phi \qquad \text{(A-12)}$$

Substituting equation (A-12) into equation (A-2)

$$F(\underline{u}) = \int_0^\infty \int_0^{2\pi} r\, f[\underline{x}(r,\theta)] \exp\left[-j2\pi\, (\underline{u},\underline{x})\right] d\theta\, dr \qquad \text{(A-13)}$$

$$= \int_0^\infty \int_0^{2\pi} r\, g(r,\theta) \exp\left[-j2\pi(u_1 r \cos\theta + u_2 r \sin\theta)\right] d\theta\, dr \qquad \text{(A-14)}$$

Now using equation (A-11) in (A-14)

$$F[\underline{u}(\rho,\phi)] = G(\rho,\phi)$$

$$= \int_0^\infty \int_0^{2\pi} r\, g(r,\theta) \exp\left[-j2\pi r\rho \cos(\theta-\phi)\right] d\theta\, dr. \qquad \text{(A-15)}$$

(c) Scale and Rotation in Polar Coordinates

Uniform scale changes or rotations of the function $g(r,\theta)$ are related by the coordinate mapping.

$$g(r,\theta) \xrightarrow{T} g(ar, \theta + \theta_o) \tag{A-16}$$

Substituting equation (A-16) into equation (A-15) yields

$$G'(\rho,\phi) = \int_o^\infty \int_o^{2\pi} r\, g(ar, \theta + \theta_o) \exp\left[-j2\pi r\rho \cos(\theta-\phi)\right] d\theta\, dr \tag{A-17}$$

Letting $\xi = ar$

$$\lambda = \theta + \theta_o$$

$$G'(\rho,\phi) = \int_o^\infty \int_o^{2\pi} \left(\frac{\xi}{a}\right) g(\xi,\lambda) \exp\left[-j2\pi \left(\frac{\xi}{a}\right)\rho \cos(\lambda-\theta_o-\phi)\right] d\lambda\, d\left(\frac{\xi}{a}\right) \tag{A-18}$$

$$= \frac{1}{|a|^2} \int_o^\infty \int_o^{2\pi} \xi\, g(\xi,\lambda) \exp\left\{-j2\pi\xi \left(\frac{\rho}{a}\right) \cos\left[\lambda - (\phi + \theta_o)\right]\right\} d\lambda\, d\xi \tag{A-19}$$

$$= \frac{1}{|a|^2} G(\rho/a, \phi + \theta_o) \tag{A-20}$$

(d) Spatial and Spatial-Frequency Domain Symmetries

For the affine transformation defined by equation (A-1) the resultant transform was given by equation (A-9) as

$$G(\underline{r}) = \frac{1}{|J|} \exp\left[\, j2\pi(\underline{u},\underline{t})\right] \mathcal{F}\left[(\underline{A}^{-1}\underline{t})\ \underline{u}\right] \tag{A-21}$$

Thus the coordinates are related as

$$\underline{v} = (\underline{A}^{-1})^T\, \underline{u} \tag{A-22}$$

The energy density spectrum of $f(\underline{x})$ is

$$S(\underline{u}) = |F(\underline{u})|^2 \tag{A-23}$$

and the linear phase term cancels. Thus the coordinates of the energy density spectrum (or equivalently the modulus) are related to the linear distortion matrix in the spatial domain, whereas any spatial shift results in a linear phase term in the spatial frequency domain.

For real signals it follows immediately from equation (A-2) that

$$F(-\underline{u}) = F^*(\underline{u}) \tag{A-24}$$

where the asterisk denotes the complex conjugate. Thus the energy density spectrum (or modulus) is symmetric about any line passing through the origin in the spatial frequency domain.

APPENDIX B

FILTER NORMALIZATION COEFFICIENTS

The normalization coefficients for the filters used to smooth the random number ideal data are derived assuming a continuous functional form. These weighting coefficients are then used with the discrete two-dimensional convolution expression to implement the smoothing filter. As a check for the correctness of these coefficients, the gain (volume) of each filter was experimentally verified by convolving each filter impulse response with an array, each element of which was unity.

Separable Exponential Filter

The filter impulse response is given by

$$h_1(\underline{x}) = k_1 \exp\left[-\frac{1}{R_o}\ (x_1 + x_2)\right] \tag{B-1}$$

$$R_o \geq 0, \quad |x_1|,\ |x_2| \leq R < \infty\ .$$

The gain of $h_1(x)$ is

$$G_1 = 4 \int_o^R \int_o^R k_1 \exp\left[-\frac{1}{R_o}\ (x_1 + x_2)\right] dx_1\ dx_2 \tag{B-2a}$$

$$= 4\ k_1\ R_o^2 \left[1 - \exp\left(\frac{R}{R_o}\right)\right]^2 \tag{B-2b}$$

For unity gain

$$k_1 = \left\{ 2\, R_o \left[1 - \exp\left(\frac{R}{R_o} \right) \right] \right\}^{-2} \tag{B-3}$$

Isotropic Exponential Filter

The isotropic filter impulse response is given by

$$h_2(\underline{x}) = k_2 \exp\left(- \frac{r}{R_o} \right) \tag{B-4}$$

$$r = (x_1^2 + x_2^2)^{1/2} \geq 0, \quad 0 \leq R_o \leq R < \infty.$$

The gain of $h_2(\underline{x})$ is then given by

$$G_2 = \int_o^R \int_o^{2\pi} k_2\, r \exp\left(- \frac{r}{R_o} \right) d\theta\, dr \tag{B-5a}$$

$$= 2\pi\, k_2 \int_o^R r \exp\left(- \frac{r}{R_o} \right) dr \tag{B-5b}$$

let

$$\lambda = \frac{r}{R_o}, \qquad R_o\, d\lambda = dr \tag{B-6}$$

Thus

$$G_2 = 2\pi\, k_2 \int_o^{R/R_o} R_o^2\, \lambda \exp(-\lambda)\, d\lambda \tag{B-7}$$

and integrating by parts

$$G_2 = 2\pi\, k_2\, R_o^2 \left[-\lambda \exp(-\lambda) \Big|_o^{R/R_o} + \int_o^{R/R_o} \exp(-\lambda)\, d\lambda \right] \tag{B-8a}$$

$$= 2\pi\, k_2\, R_o^2 \left[- \frac{R}{R_o} \exp\left(- \frac{R}{R_o} \right) - \exp\left(- \frac{R}{R_o} \right) + 1 \right] \tag{B-8b}$$

$$= 2\pi\, R_o^2\, k_2 \left[1 - \left(1 + \frac{R}{R_o} \right) \exp\left(- \frac{R}{R_o} \right) \right] \tag{B-8c}$$

For unity gain

$$k_2 = \left\{ 2\pi R_o^2 \left[1 - \left(1 + \frac{R}{R_o} \right) \exp\left(- \frac{R}{R_o} \right) \right] \right\}^{-1} \qquad \text{(B-9)}$$

Test of Gain

For each filter the convolution

$$C(u,v) = \sum_i \sum_j h(u-i,\ v-j)\ a(i,j) \Big|_{u,v=0} \qquad \text{(B-10)}$$

was computed with the filter having characteristic length $R_o = 1.0$ and an a(i,j) consisting of a 100 x 100 array of element each element having a value of unity. The values obtained are

$$k_1 = 1.0006$$

$$k_2 = 0.9998 \ .$$

APPENDIX C

CORRELATOR OUTPUT SIGNAL TO NOISE RATIO

In the absence of uncorrelated additive noise the correlator output signal-to-noise ratio was shown in Chapter 3 to be given by

$$\frac{S}{N} = \underline{S}_r^T \underline{K}^{-1} \underline{S}_r \tag{C-1}$$

where $\underline{S}_r$ is the reference signal and $\underline{K}$ is the covariance matrix of the unit variance process of which $\underline{S}_r$ is a finite realization. It is assumed that the covariance matrix has the form

$$\underline{K} = \begin{bmatrix} \underline{k} & \rho\underline{k} & \rho^2\underline{k} & \cdots & \rho^{n-1}\underline{k} \\ \rho\underline{k} & \underline{k} & \rho\underline{k} & & \\ \vdots & & & & \\ \rho^{n-1}\underline{k} & \cdots & & & \underline{k} \end{bmatrix} \tag{C-2}$$

where

$$\underline{k} = \| \rho_{ij} \| \tag{C-3}$$

and

$$\rho_{ij} = \begin{cases} 1 & , \ i=j \\ \rho^{|i-j|} & , \ i \neq j \ . \end{cases} \tag{C-4}$$

where ρ is the correlation between adjacent cells.

The covariance matrix then has the explicit inverse

$$\underline{K}^{-1} = \frac{1}{1-\rho^2}\begin{bmatrix} \underline{k}^{-1} & -\rho\underline{k}^{-1} & 0 & \cdots & 0 \\ -\rho\underline{k}^{-1} & (1+\rho^2)\underline{k}^{-1} & -\rho\underline{k}^{-1} & & \\ 0 & -\rho\underline{k}^{-1} & (1+\rho^2)\underline{k}^{-1} & & \\ \vdots & & & \ddots & \\ 0 & & & & \underline{k}^{-1} \end{bmatrix} \qquad \text{(C-5)}$$

where

$$\underline{k}^{-1} = \frac{1}{1-\rho^2}\begin{bmatrix} 1 & -\rho & 0 & \cdots & 0 \\ -\rho & 1+\rho^2 & -\rho & & \\ 0 & -\rho & 1+\rho^2 & & \\ \vdots & & & \ddots & \\ 0 & & & & 1 \end{bmatrix} \qquad \text{(C-6)}$$

To evaluate equation (C-1), substitute equation (C-5) into (C-1) and expand, noting that the r subscript has been deleted.

$$\frac{S}{N} = \frac{1}{1-\rho^2}\,(\underline{S}^T(1),\ldots,\underline{S}^T(m))\begin{bmatrix} \underline{k}^{-1} & -\rho\underline{k}^{-1} & 0 & \cdots & 0 \\ -\rho\underline{k}^{-1} & (1+\rho^2)\underline{k}^{-1} & -\rho\underline{k}^{-1} & & \\ 0 & -\rho\underline{k}^{-1} & (1+\rho^2)\underline{k}^{-1} & & \\ \vdots & & & \ddots & \\ 0 & & & & \underline{k}^{-1} \end{bmatrix}\begin{bmatrix} \underline{S}(1) \\ \vdots \\ \underline{S}(m) \end{bmatrix}$$

(C-7)

$$= \frac{1}{1-\rho^2}\,(\underline{S}^T(1)\underline{k}^{-1} - \rho\underline{S}^T(2)\underline{k}^{-1},\ -\rho\underline{S}^T(1)\underline{k}^{-1} + (1+\rho^2)\underline{S}^T(2)\underline{k}^{-1} - \rho\underline{S}^T(3)\underline{k}^{-1},$$

$$\ldots,\ -\rho\underline{S}^T(m-1)\underline{k}^{-1} + \underline{S}^T(m)\underline{k}^{-1})\begin{bmatrix} \underline{S}(1) \\ \vdots \\ \underline{S}(m) \end{bmatrix} \qquad \text{(C-8)}$$

$$\frac{S}{N} = \frac{1}{1-\rho^2}\left[\underline{S}^T(1)\underline{k}^{-1}\,\underline{S}(1) - \rho\underline{S}^T(2)\underline{k}^{-1}\,\underline{S}(1) - \rho\underline{S}^T(1)\underline{k}^{-1}\,\underline{S}(2)\right.$$

$$+ (1+\rho^2)\,\underline{S}^T(2)\underline{k}^{-1}\,\underline{S}(2) - \rho\underline{S}^T(3)\underline{k}^{-1}\,\underline{S}(2) - \rho\underline{S}^T(2)\underline{k}^{-1}\,\underline{S}(3)$$

$$+ (1+\rho^2)\,\underline{S}^T(3)\underline{k}^{-1}\,\underline{S}(3) - \rho\underline{S}^T(4)\underline{k}^{-1}\,\underline{S}(3) -$$

$$\left.\ldots - \rho\underline{S}^T(m-1)\underline{k}^{-1}\,\underline{S}(m) + \underline{S}^T(m)\underline{k}^{-1}\,\underline{S}(m)\right] \qquad \text{(C-9)}$$

Now each term is a scalar, thus

$$\underline{S}^T(i)\underline{k}^{-1}\,\underline{S}(j) = [\underline{S}^T(i)\underline{k}^{-1}\,\underline{S}(j)]^T = \underline{S}^T(j)\underline{k}^{-1}\,\underline{S}(i) \qquad \text{(C-10)}$$

since $(\underline{k}^{-1})^T = \underline{k}^{-1}$, $\underline{k}^{-1}$ symmetric.

$$\frac{S}{N} = \frac{1}{1-\rho^2}\left[\underline{S}^T(1)\underline{k}^{-1}\,\underline{S}(1) - 2\rho\underline{S}^T(1)\underline{k}^{-1}\,\underline{S}(2) + \rho^2\underline{S}^T(2)\underline{k}^{-1}\,\underline{S}(2)\right.$$

$$\left. + \underline{S}^T(2)\underline{k}^{-1}\,\underline{S}(2) + \ldots + \underline{S}^T(m)\underline{k}^{-1}\,\underline{S}(m)\right] \qquad \text{(C-11)}$$

$$= \frac{1}{1-\rho^2}\left[\sum_{i=1}^{m}\underline{S}(i)\underline{k}^{-1}\,\underline{S}(i) - 2\rho\sum_{i=1}^{m-1}\underline{S}(i)\underline{k}^{-1}\,\underline{S}(i+1)\right.$$

$$\left. + \rho^2\sum_{i=1}^{m-2}\underline{S}^T(i)\underline{k}^T\,\underline{S}(i)\right] \qquad \text{(C-12)}$$

Expanding a term of equation (C-12)

$$\underline{S}^T(i)\underline{k}^{-1}\,\underline{S}(i) = \frac{1}{1-\rho^2}\,(s_{i1},\ldots,s_{in})\begin{bmatrix} 1 & -\rho & 0 & \ldots. & 0 \\ -\rho & 1 & -\rho & & \\ 0 & -\rho & 1 & & \\ \vdots & & & \ddots & \\ 0 & & & & 1 \end{bmatrix}\begin{bmatrix} s_{i1} \\ \vdots \\ s_{in} \end{bmatrix}$$

(C-13)

$$\frac{S}{N} = \frac{1}{1-\rho^2}\Big[s_{i1} - \rho s_{i2},\ -\rho s_{i1} + (1+\rho^2)\, s_{i2} - \rho s_{i3},$$

$$-\rho s_{i2} + (1+\rho^2) s_{i3} - \rho s_{i4}, \ldots, -\rho s_{i,n-1} + s_{in}\Big] \begin{bmatrix} s_{i1} \\ \vdots \\ s_{in} \end{bmatrix} \tag{C-14}$$

$$= \frac{1}{1-\rho^2}\Big[s_{i1}^2 - 2\rho\, s_{i1}s_{i2} + (1+\rho^2)s_{i2}^2 - 2\rho\, s_{i2}s_{i3}$$

$$+ (1+\rho^2)\, s_{i3}^2 - \ldots - \rho\, s_{i,n-1}\, s_{in} + s_{in}^2\Big] \tag{C-15}$$

$$= \frac{1}{1-\rho^2}\Big[\sum_{j=1}^{N} s_{ij}^2 - 2\rho \sum_{j=1}^{N-1} s_{ij}s_{i,j+1} + \rho^2 \sum_{j=1}^{N-2} s_{ij}^2\Big] \tag{C-16}$$

$$= \frac{1}{1-\rho^2}\Big[N - 2\rho(N-1) + \rho^2(N-2)\Big] \tag{C-17}$$

$$= \Big[N\Big] \tag{C-18}$$

where $N\left(\frac{1}{N}\sum_{j=1}^{N} s_{ij}^2\right) = N$, since $\underline{S}$ is assumed to be from a unit variance process and $(N-1)\left(\frac{1}{N-1}\sum_{j=1}^{N-1} s_{ij}\, s_{i,j+1}\right) = \rho(N-1)$ where ρ is the correlation between adjacent cells.

Substituting equation (C-18) into equation (C-12) yields

$$\frac{S}{N} = \frac{1}{1-\rho^2}\Big[\sum_{i=1}^{M} N - 2\rho \sum_{i=1}^{M-1} \rho N + \rho^2 \sum_{i=1}^{M-2} N\Big] \tag{C-19}$$

$$\frac{S}{N} = \frac{1}{1-\rho^2}\left[MN - 2\rho^2(M-1)N + \rho^2(M-2)N\right] \qquad \text{(C-20)}$$

$$= \left[\ MN\ \right] \qquad \text{(C-21)}$$

Thus the processing gain of the two-dimensional crosscorrelator theoretically is equal to the total number of samples processed and is independent of the adjacent cell correlation ρ.

APPENDIX D

THE MAXIMUM PRODUCT OF A CONSTRAINED SUM

If the sum of a set of real numbers λ_i is constrained to have the fixed value

$$\sum_{m=1}^{n} \lambda_m = K \tag{D-1}$$

then the product

$$P = \prod_{m=1}^{n} \lambda_m \tag{D-2}$$

is maximized for all λ_i equal.

Solving for λ_j

$$\lambda_j = K - \sum_{\substack{m=1 \\ m \neq j}}^{n} \lambda_m \tag{D-3}$$

$$P = \left(K - \sum_{\substack{m=1 \\ m \neq j}}^{n} \lambda_m\right) \lambda_1 \cdots \lambda_{j-1} \lambda_{j+1} \cdots \lambda_n \tag{D-4}$$

$$= K(\lambda_1 \cdots \lambda_{j-1} \lambda_{j+1} \cdots \lambda_n) \tag{D-5}$$

$$- \sum_{\substack{m=1 \\ m \neq j}}^{n} \lambda_m (\lambda_1 \cdots \lambda_{j-1} \lambda_{j+1} \cdots \lambda_n)$$

$$\frac{\partial P}{\partial \lambda_{j+1}} = K(\lambda_1 \cdots \lambda_{j-1}\lambda_{j+2}\cdots\lambda_n) - \sum_{\substack{m=1 \\ m \neq j}}^{n} \lambda_m(\lambda_1\cdots\lambda_{j-1}\lambda_{j+2}\cdots\lambda_n) \tag{D-6}$$

$$- (\lambda_1\cdots\lambda_{j-1}\lambda_{j+1}\cdots\lambda_n) = 0$$

But

$$K = \sum_{m=1}^{n} \lambda_m$$

therefore,

$$\sum_{m=1}^{n} \lambda_m - \sum_{\substack{m=1 \\ j \neq m}}^{n} \lambda_m - \lambda_{j+1} = 0 \qquad \text{(D-7)}$$

$$\lambda_j - \lambda_{j+1} = 0 \qquad \text{(D-8)}$$

$$\lambda_j = \lambda_{j+1} \qquad \text{(D-9)}$$

for all $j = 1, \ldots, n-1$.

Thus all λ_j must be equal and have the value

$$\lambda_j = \frac{K}{n} . \qquad \text{(D-10)}$$

APPENDIX E

THE AFFINE TRANSFORMATION

The affine transformation is defined as

$$\underline{y} = \underline{A}\,\underline{x} + \underline{t} = \underline{B}\,\underline{x} \qquad \text{(E-1)}$$

where for a real two-dimensional space

$$\underline{y} = \begin{bmatrix} y_1 \\ y_2 \end{bmatrix}, \quad \underline{x} = \begin{bmatrix} x_1 \\ x_2 \end{bmatrix}, \quad \underline{t} = \begin{bmatrix} t_1 \\ t_2 \end{bmatrix}$$

and

$$\underline{A} = \begin{bmatrix} a_{11} & a_{12} \\ a_{21} & a_{22} \end{bmatrix}$$

is a non-singular matrix.

Two properties of this transformation are of importance in this study; these are proved in the following.

(1) Any non-singular affine transformation maps lines into lines.

Proof: In any affine space the vector $\underline{x}$ lying on the line passing through $\underline{u}$, $\underline{v}$ can be represented as

$$\underline{x} = (1 - \lambda)\,\underline{u} + \lambda\,\underline{v}, \quad \lambda \text{ real} \qquad \text{(E-2)}$$

Then

$$\underline{B}\,\underline{x} = \underline{A}\left[(1-\lambda)\,\underline{u} + \lambda\,\underline{v}\right] + \underline{t} \qquad \text{(E-3)}$$

$$= (1-\lambda)\,(\underline{A}\,\underline{u} + \underline{t}) + \lambda\,(\underline{A}\,\underline{v} + \underline{t})$$

$$= (1-\lambda)\,\underline{B}\,\underline{u} + \lambda\,\underline{B}\,\underline{v}$$

Thus $\underline{B}$ maps the line passing through $\underline{u},\underline{v}$ into the line passing through $\underline{Bu}$, $\underline{Bv}$.

(2) Ratios of lengths of line segments are invariant under an affine transformtion.

Proof: $\underline{u}$, $\underline{u}_o$, $\underline{v}$, $\underline{v}_o$ are elements in the real n-dimensional Euclidean space E_n. The distance between vectors is defined as

$$||\underline{u} - \underline{v}|| = \left[\sum_i (u_i - v_i)^2\right]^{1/2} \qquad \text{(E-4)}$$

Consider the mapping

$$\underline{u} \xrightarrow{\underline{B}} \underline{B}\,\underline{u} \qquad \text{(E-5)}$$

with

$$\underline{B}\,\underline{u} = \underline{A}\,\underline{u} + \underline{t}$$

where $\underline{A}$ is an n x n nonsingular matrix and $\underline{t}$ is the n x 1 displacement vector.

Now the ratio of line segments in the affine space is

$$R = \frac{\|\underline{H}(\underline{u} - \underline{u}_o)\|}{\|\underline{H}(\underline{v} - \underline{v}_o)\|} = \frac{\|\underline{H}\,\underline{u} - \underline{H}\,\underline{u}_o\|}{\|\underline{H}\,\underline{v} - \underline{H}\,\underline{v}_o\|} \qquad \text{(E-6)}$$

$$= \frac{\|\underline{A}\,\underline{u} + \underline{t} - \underline{A}\,\underline{u}_o - \underline{t}\|}{\|\underline{A}\,\underline{v} + \underline{t} - \underline{A}\,\underline{v}_o - \underline{t}\|} = \frac{\|\underline{A}(\underline{u} - \underline{u}_o)\|}{\|\underline{A}(\underline{v} - \underline{v}_o)\|}$$

$$= \frac{\|\underline{A}\|\ \|\underline{u} - \underline{u}_o\|}{\|\underline{A}\|\ \|\underline{v} - \underline{v}_o\|} = \frac{\|\underline{u} - \underline{u}_o\|}{\|\underline{v} - \underline{v}_o\|}$$

where $\|\underline{A}\|$ is the norm of the operator $\underline{A}$.

UNCLASSIFIED

Security Classification

DOCUMENT CONTROL DATA - R & D

(Security classification of title, body of abstract and indexing annotation must be entered when the overall report is classified)

1. ORIGINATING ACTIVITY *(Corporate author)*

School of Electrical Engineering

Purdue University

2a. REPORT SECURITY CLASSIFICATION

UNCLASSIFIED

2b. GROUP

3. REPORT TITLE

Conjugate Point Determination in Multitemporal Data Overlay

4. DESCRIPTIVE NOTES *(Type of report and inclusive dates)*

scientific report

5. AUTHOR(S) *(First name, middle initial, last name)*

Richard A. Emmert and Claire D. McGillem

6. REPORT DATE	7a. TOTAL NO. OF PAGES	7b. NO. OF REFS
December, 1972	188	

8a. CONTRACT OR GRANT NO.	9a. ORIGINATOR'S REPORT NUMBER(S)
NASA Grant No. NGL 15-005-112	TR-EE 73-5
b. PROJECT NO.	
c.	9b. OTHER REPORT NO(S) *(Any other numbers that may be assigned this report)*
d.	LARS Information Note # 111872

10. DISTRIBUTION STATEMENT

UNLIMITED

11. SUPPLEMENTARY NOTES	12. SPONSORING MILITARY ACTIVITY
	National Aeronautics and Space Administration

13. ABSTRACT

The machine processing of spatially variant multitemporal data such as imagery obtained at different times requires that these data be in geometrical registration. The processor may then identify the datum for a specified ground resolution element in each of the sets of imagery being analyzed.

Misregistration between corresponding subsets of imagery contains both a displacement and a geometrical distortion component consisting of rotation, skew and scale change. The affine transformation is postulated to characterize this misregistration between data subsets. Search techniques utilizing the moduli of the the Fourier transforms of these data are developed for estimating the coefficients of geometrical distortion components of this model. After correction of the distortion components, the displacement is located by the crosscorrelation of a template obtained from one set of data, termed the reference, with the second, or background data. This template, derived for the optimum discrimination of the reference data embedded in the background, is determined by the solution of a system of equations involving the reference data, the covariance matrix of these data, and constraints on the magnitude and energy of the filter response.

An experimental evaluation of the registration technique is carried out for artificially generated images and for multispectral scanner images taken at different times.

DD FORM 1 NOV 65 1473

UNCLASSIFIED

Security Classification

14. KEY WORDS	LINK A		LINK B		LINK C	
	ROLE	WT	ROLE	WT	ROLE	WT